PHOTOTHERMAL AND PHOTOACOUSTIC INVESTIGATIONS ON CERTAIN POLYMERS AND SEMICONDUCTING MATERIALS

Thesis submitted to
COCHIN UNIVERSITY OF SCIENCE AND TECHNOLOGY
in partial fulfillment of the requirements for the award of the degree of
DOCTOR OF PHILOSOPHY

By

JYOTSNA RAVI

LASER AND SPECTROSCOPY LABORATORY
DEPARTMENT OF PHYSICS
COCHIN UNIVERSITY OF SCIENCE AND TECHNOLOGY
KOCHI-682 022
INDIA

APRIL 2003

Photothermal and photoacoustic investigations on certain polymers and semiconducting materials

Ph.D. thesis in the field of material characterization using photothermal techniques

Author
Jyotsna Ravi
Research Fellow, Department of Physics
Cochin University of Science and Technology, Cochin-682 022, India
Jyotsna@cusat.ac.in; jyotsnaravi2004@yahoo.co.in.

Research Supervisors
Dr.T.M.Abdul Rasheed & Prof. K.P.Rajappan Nair
Department of Physics
Cochin University of Science and Technology, Cochin 682 022, India.

Laser and Spectroscopy Lab
Department of Physics
Cochin University of Science and Technology, Cochin 682 022, India.

APRIL 2003

Department of Physics
Cochin University of Science and Technology
Cochin - 682 022, India

CERTIFICATE

Certified that the work presented in this thesis entitled **"PHOTOTHERMAL AND PHOTOACOUSTIC INVESTIGATIONS ON CERTAIN POLYMERS AND SEMICONDUCTING MATERIALS"** based on the bonafide research work done by Miss. Jyotsna Ravi is an authentic record of research work done by her under my guidance in the Department of Physics, Cochin University of Science and Technology, Cochin 682 022 and has not been included in any other thesis submitted previously for the award of any degree.

Dammam-31451
(Saudi Arabia)

Date: 15-03-2003

Dr.T.M.Abdul Rasheed
(Supervising Guide)
Reader,
Department of Physics,
CUSAT, KOCHI-22

Present affiliation:
Department of Physics
King Faisal University
P.B.2114, Dammam-31451
Kingdom of Saudi Arabia

Department of Physics

Cochin University of Science and Technology
Cochin - 682 022, INDIA.

CERTIFICATE

Certified that the work presented in this thesis entitled **"PHOTOTHERMAL AND PHOTOACOUSTIC INVESTIGATIONS ON CERTAIN POLYMERS AND SEMICONDUCTING MATERIALS"** based on the bonafide research work done by Miss. Jyotsna Ravi is an authentic record of research work done by her under my guidance in the Department of Physics, Cochin University of Science and Technology, Cochin 682 022 and has not been included in any other thesis submitted previously for the award of any degree.

K.P. Rajappan Nair

Date: 7th April 2003

Prof. K. P. Rajappan Nair
(Co-Guide)
Dean, Faculty of Science, CUSAT.

Prof. Dr. K.P. RAJAPPAN NAIR
Dean, Faculty of Science
Cochin University of
Science and Technology
Cochin 682 022, India
Ph : 0484-575588

DECLARATION

I hereby declare that the present work entitled **"PHOTOTHERMAL AND PHOTOACOUSTIC INVESTIGATIONS ON CERTAIN POLYMERS AND SEMICONDUCTING MATERIALS "** which will be submitted is based on the original work done by me under the guidance of Dr. T.M.Abdul Rasheed, Department of Physics, and the co-guidance of Prof. K.P.Rajappan Nair, Department of Physics, Cochin University of Science and Technology, has not been included in any other thesis submitted previously for the award of any degree.

Kochi – 22

Date: 7th April 2003

Jyotsna Ravi.

ACKNOWLEDGEMENT

karmany evadhikaras te
ma phalesu kadacana
ma karma-phala-hetur bhur
ma te sango 'stv akarmani

-- The Bhagavad Gita 2.47

A journey is comfortable, swift and easy when you travel together. Interdependence is certainly more valuable than independence. I am delighted to express my gratitude to those people who supported and accompanied me in the successful conduct as well as for the critical appraisal of this inquiry.

I am greatly indebted to my supervising guide Dr.T. M. Abdul Rasheed, Reader, Department of Physics, Cochin University of Science and Technology, for his efficient guidance through out the course of my work. His enthusiasm and integral view on research together with the strict and extensive comments had a direct impact on the final form and quality of the thesis.

I extend sincere thanks to my guide –in-charge, Prof. K.P. Rajappan Nair, Dean, Faculty of Science, Cochin University of Science and Technology, for not only being an excellent guide but also for providing a friendly and comfortable atmosphere in laboratory. He always kept an eye on the progress of my work and was available whenever I needed his advice.

I wish to thank the Head, Department of Physics, Cochin University of Science and Technology, Prof K.P. Vijayakumar and former Heads, Prof.M.Sabir and Prof. Elizabeth Mathai for their attention and assistance.

I would like to acknowledge Dr. T. Ramesh Babu for lending a helping hand in developing the theoretical aspects of my work and Dr. M.K.Jayaraj for providing me with adequate samples for performing experiments.

I am thankful to Raghavan Master for the help received in repairing the RF oscillator that played a key role in the preparation of samples studied in this work. Dr. A A Sudhakaran and Mr.Aboobecker (Department of Physics) are acknowledged here for providing the necessary accessories for this work. I am grateful to Mr.Casimir, Mr.A.B. Muraleedharan, Mr.Jose and Mr.Sukumaran, (USIC) for their immense help in fabricating the instrumentation part of this project. Mr.Vinod Kumar P P (Dept. of Computer Science) who has always been a helping hand is gratefully acknowledged. I am extremely thankful to the administrative and library staff of the Physics Department.

This work would not have been possible without the involvement of Dr. Nibu A George, Sebu Thomas K and Thomas Lee S. I take this opportunity to express my deep sense of gratitude for their invaluable support and suggestions. I would like to thank B.Aneeshkumar for his timely help rendered to me whenever required.

The senior colleagues of my lab Shaji S and Shibu M Eapen have always been with me and helped me a lot in sorting out the official and academic problems. Their brotherly affection and friendly nature added flavour to the good working environment in the laboratory. The wonderful experience of working with a few enthusiastic and energetic teachers B.Syamalakumari, T. Nandini, Sunny Kuriakose, K.K. Vijayan, Usha John, Thomas P. Zacharia and K Raveendranath from various prestigious colleges is unforgettable. I am extremely thankful to each and every one of them for the various bits of knowledge and wisdom which they imparted to me.

My profound thanks to the research scholars S. Saravanan, Joseph Mathai, Santhosh D Shenoy, Santhosh Kumar M.C., Saji Augustine, Bindu K, Paulraj M, Aldrin Antony, Ratheeshkumar P.M., Abraham V. S., Alex Mathew, Prasanth Ravi, Sajan D.George and Unnikrishnan K.P. for all the help and co-operation extended to me during my work. I also acknowledge the positive attitude of all the other fellow research scholars of the Department of Physics.

The unconditional support rendered by my room mate Pravitha Ramanand in personal as well as academic matters is gratefully acknowledged from the bottom of my heart. The fun we had together with Iswarya Mathew, Kochutheressia S, Santhi A, Rekha Mathew, Sr. Ritty J Nedumpara, Anisha T.K., Roshini R.S., T. Radhika T, Jasmine C., Vrinda S, Sheeba, Lekshmi V. and Lekshmi S in the famous room No.7 of Athulya Hostel, relieved and eased the tensions faced during the course of the work. It is a pleasant aspect that I now have the opportunity to express my gratitude to all of them.

I had the pleasure to work with and supervise projects of several M.Sc students Dinish U S, Rajmohan S, Jyothilakshmi J K, Vinod Kumar , Denny Mathew, Anija T, Mohammad Shafi, Shanavas M, Lekshmi S, Agie Antony, Teena K James and M.Phil student Priya which has been beneficial in one way or the other for the presented work in the thesis.

I thank Cochin University of Science and Technology and Department of Science and Technology (DST), India for the financial assistance.

I am extremely grateful to the love, support, encouragement and patience of my parents and brother helping me to complete my work successfully.

Jyotsna

LIST OF PUBLICATIONS:

1. Mirage detection applied to low thermal diffusivity measurements of weakly absorbing thermally thin plasma polymerized film
   Jyotsna Ravi, B.Syamalakumari, T. Nandini, K.P.R.Nair and T.M.A Rasheed
   Nondestructive Testing and Evaluation (in press)
2. A simple theoretical extension to the analysis of photothermal deflection signal for low thermal diffusivity evaluation
   Jyotsna Ravi, S.Lekshmi, K.P.R.Nair, T.M.A.Rasheed
   Journal of Quantitative Spectroscopy and Radiative Transfer. (in press)
3. Photothermal Investigations on weakly absorbing plasma polymerized diethyl aniline thin film.
   Jyotsna Ravi, B.Syamalakumari, Usha John, K.P.R. Nair, T.M.A Rasheed
   Journal of Material Science Letters (in press)
4. Effect of Te doping and electron irradiation on thermal diffusivity of Bi2Se3 thin films by photothermal technique
   A.Saji, **Jyotsna Ravi,** K.P.R.Nair, T.M.A Rasheed, Tamio Endo, Elizabeth Mathai
   Journal of Physics D: Applied Physics (in press)
5. Photoacoustic studies on thermal diffusivity of $CuGa_{1-x}Fe_xO_2$
   Jyotsna Ravi, M.K.Jayaraj, K.A.Vanaja, K.P.R. Nair, T.M.A. Rasheed
   Semiconductor Science and Technology (communicated)
6. Photothermal investigations on plasma polymerized o-toluidine thin film
   Jyotsna Ravi, B. Syamalakumari, Rajmohan S. Dinish U.S., K.P.R. Nair, T.M A. Rasheed
   Physica Status Solidi A (communicated)

PAPERS PRESENTED IN SEMINARS/CONFERENCES:

1. Photothermal investigations on plasma polymerized o-toluidine thin film
   Jyotsna Ravi, B. Syamalakumari, Rajmohan S. Dinish U.S., K.P.R. Nair, T.M A. Rasheed
   Photonics Asia 2002, 14-18 October 2002, Shanghai, China. Proceedings of SPIE - International society for Optical Engineering, Vol 4913 -70 (2002)
2. Optical and thermal characterization of plasma polymerized m-toluidine,
   Jyotsna Ravi, B.Syamalakumari, T.Nandini, K.P.R.Nair, T.M.A Rasheed
   Nineteenth Austin Symposium 2002, March2-March 5, Austin, U.S.A
3. Comparative study of the optical and thermal properties of plasma-polymerized benzyl amine and N-methyl aniline
   B.Syamalakumari, **Jyotsna Ravi**, T.Nandini, T.M.A Rasheed, K.P.R.Nair
   Nineteenth Austin Symposium 2002, March2-March 5, Austin, U.S.A.
4. Optical and thermal characterization of plasma polymerized N-methyl aniline by probe beam deflection technique
   B.Syamalakumari, **Jyotsna Ravi**, T.Nandini, T.M.A Rasheed, K.P.R.Nair
   National Symposium on Atomic , Molecular Structure, Interactions and Laser spectroscopy, February 22-24, 2002.
5. Optical and thermal characterization of plasma polymerized benzyl amine
   B.Syamalakumari, **Jyotsna Ravi**, T.M.A. Rasheed, K.P.R.Nair
   National Laser Symposium 2002, November 14-16.
6. Thermal characterization of plasma polymerized thin film using mirage technique
   Jyotsna Ravi, B.Syamalakumari, T.Nandini, S.Rajmohan, K.P.R Nair and T.M.A Rasheed
   National Laser Symposium 2001,December 19-21, CAT Indore.
7. Determination of thermal diffusivity of plasma polymerized poly m-toluidine by probe beam deflection

Jyotsna Ravi, B.Syamalakumari, T.Nandini, K.P.R Nair and T.M.A Rasheed
Second International Conference and XXVII Annual Convention of the optical society, August 27-29, Trivandrum, Kerala, India (2001)

8. Determination of thermal diffusivity of PAN films using probe beam deflection.
   Jyotsna Ravi, Dinish U.S and T.M.A Rasheed.
   CTIMS-2001, March23-24, M.G University, Kottayam.
9. Thermal diffusivity measurement in cross-linked polymer films using mirage effect
   Thomas P.Zacharia, **Jyotsna Ravi**, U.Manju and T.M Abdul Rasheed
   National Laser Symposium 2000, December 13-15, Lastec, Delhi.

CONTENTS

Preface

CHAPTER I INTRODUCTION TO PHOTOTHERMAL EFFECTS

CHAPTER II ANALYSIS OF PHOTOTHERMAL DEFLECTION SIGNAL FOR DETERMINATION OF THERMAL DIFFUSIVITY: THEORETICAL EXTENSION TO AMPLITUDE METHOD

CHAPTER III PREPARATION AND OPTICAL CHARACTERIZATION OF CERTAIN R.F. PLASMA POLYMERIZED THIN FILMS

PREFACE

Material synthesizing and characterization has been one of the major areas of scientific research for the past few decades. Various techniques have been suggested for the preparation and characterization of thin films and bulk samples according to the industrial and scientific applications. Material characterization implies the determination of the electrical, magnetic, optical or thermal properties of the material under study. Though it is possible to study all these properties of a material, we concentrate on the thermal and optical properties of certain polymers. The thermal properties are determined using photothermal beam deflection technique and the optical properties are obtained from various spectroscopic analyses. In addition, thermal properties of a class of semiconducting compounds, copper delafossites, are determined by photoacoustic technique.

Photothermal technique is one of the most powerful tools for non-destructive characterization of materials. This forms a broad class of technique, which includes laser calorimetry, pyroelectric technique, photoacoustics, photothermal radiometric technique, photothermal beam deflection technique etc. However, the choice of a suitable technique depends upon the nature of sample and its environment, purpose of measurement, nature of light source used etc. The polymer samples under the present investigation are thermally thin and optically transparent at the excitation (pump beam) wavelength. Photothermal beam deflection technique is advantageous in that it can be used for the determination of thermal diffusivity of samples irrespective of them being thermally thick or thermally thin and optically opaque or optically transparent. Hence of all the above-mentioned techniques, photothermal beam deflection technique is employed for the successful determination of thermal diffusivity of these polymer samples. However, the semiconducting samples studied are thermally thick and optically opaque and therefore, a much simpler photoacoustic technique is used for the thermal characterization.

The production of polymer thin film samples has gained considerable attention for the past few years. Different techniques like plasma polymerization, electron bombardment, ultra violet irradiation and thermal evaporation can be used for the preparation of polymer thin films from their respective monomers. Among these, plasma polymerization or glow discharge polymerization has been widely used for polymer thin film preparation. At the earlier stages of the discovery, the plasma polymerization technique was not treated as a standard method for preparation of polymers. This method gained importance only when they were used to make special coatings on metals and began to be recognized as a technique for synthesizing polymers. The well-recognized concept of conventional polymerization is based on molecular processes by which the size of the molecule increases and rearrangement of atoms within a molecule seldom occurs. However, polymer formation in plasma is recognized as an atomic process in contrast to the above molecular process. These films are pinhole free, highly branched and cross linked, heat resistant, exceptionally dielectric etc. The optical properties like the direct and indirect bandgaps, refractive indices etc of certain plasma polymerized thin films prepared are determined from the UV-VIS-NIR absorption and transmission spectra. The possible linkage in the formation of the polymers is suggested by comparing the FTIR spectra of the monomer and the polymer. The thermal diffusivity has been measured using the photothermal beam deflection technique as stated earlier. This technique measures the refractive index gradient established in the sample surface and in the adjacent coupling medium, by passing another optical beam (probe beam) through this region and hence the name probe beam deflection. The deflection is detected using a position sensitive detector and its output is fed to a lock-in-amplifier from which the amplitude and phase of the deflection can be directly obtained. The amplitude and phase of the deflection signal is suitably analyzed for determining the thermal diffusivity.

Another class of compounds under the present investigation is copper delafossites. These samples in the form of pellets are thermally thick and optically opaque. Thermal diffusivity of such semiconductors is investigated using the photoacoustic technique, which measures the pressure change using an electret microphone. The output of the microphone is fed to a lock-in-amplifier to obtain the amplitude and phase from which the thermal properties are obtained. The variation in thermal diffusivity with composition is studied.

The whole work described in the thesis is divided into six chapters.

CHAPTER I gives a general outline of all the photothermal effect and their applications.1-dimensional as well as 3-dimensional theory of periodic temperature distribution which forms the basis of photoacoustic and photothermal beam deflection technique respectively is given in this chapter. Application of the periodic temperature distribution to the photoacoustics and photothermal beam deflection is also discussed.

In *CHAPTER II* different methods in the analysis of the probe beam deflection signal like the zero crossing detection method, phase method, modified phase method, amplitude method, thermal wave coupling method, multiparameter fitting method etc are discussed. The advantages and disadvantages of each of these methods are briefed when applied to materials of different category - thermally thick, thermally thin, optically opaque and optically transparent. A theoretical piece of work extending the amplitude method for determination of low thermal diffusivity of materials is included. We have proved that while dealing with low thermal diffusivity i.e. when the thermal diffusivity of the sample is less than the thermal diffusivity of the coupling medium, the height of the probe beam above the sample surface need be taken into account.

General discussion of different plasma polymerization techniques with emphasis on r.f. plasma polymerization is given in ***CHAPTER III***. It deals with various aspects like difference between plasma polymerization and conventional polymerization, properties of plasma polymerized thin films etc. This chapter also includes the preparation and optical characterization of three different plasma polymerized thin films namely poly *o*-toluidine, poly *m*-toluidine and poly diethyl aniline. Optical characterization consists of determination of direct and indirect bandgaps from the UV-VIS-NIR absorption spectrum, refractive index from transmission spectrum and possible linkage in the polymerization process by comparing the FTIR spectra of the monomer and the corresponding polymer.

Design and fabrication of transverse PBD setup for the determination of thermal diffusivity of the samples is given in ***CHAPTER IV***. The experimental setup is standardized using InP. The measurement of thermal diffusivity of the three r.f. plasma polymerized thin film samples using two different methods of analysis viz the phase method and the amplitude method in two different coupling media, carbontetrachloride and liquid paraffin is given in this chapter. It is found that there is no contribution from the thermal properties of coupling media to the photothermal signal from the sample. Since the substrate is non-absorbing at the pump wavelength, there is no photothermal signal from the substrate too.

CHAPTER V describes the design and fabrication of an open Photoacoustic cell. The experimental setup has been standardized using silicon wafer and InP. Determination of the thermal diffusivity of certain copper delafossites is included. The effect of changing composition on thermal diffusivity is also studied.

CHAPTER VI gives the conclusions and brief summary of the thesis.

CHAPTER I

INTRODUCTION TO PHOTOTHERMAL EFFECTS

1.1 INTRODUCTION

Interaction of electromagnetic radiation with matter causes absorption, emission and inelastic scattering of light. Except for emission, absorbed energy results in production of several forms of energy like luminescence, photochemical energy, photoelectrical energy or heat (figure.1). Heat can be produced promptly or at various time delays. This heating induces changes in the sample as well as in the

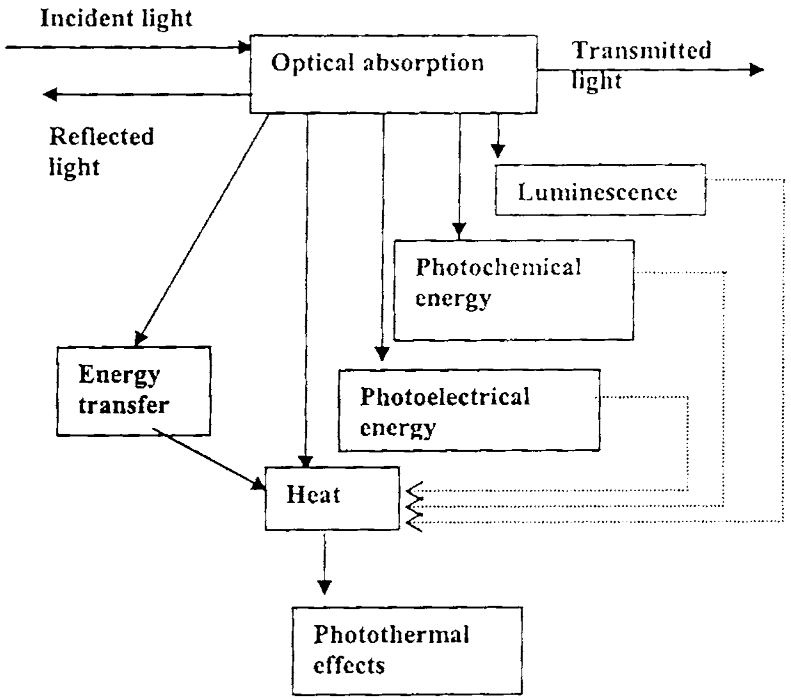

Figure 1: Block diagram indicating the consequences of optical absorption leading to prompt or delayed heat production

surrounding medium. These changes are referred to as photothermal effects [1,2]. Although it may seem counterintuitive to pursue phenomena based on the transformation of energy to the most chaotic form, heat, these techniques have many advantages for applications in low absorption environments and in the domain of materials characterization and nondestructive testing.

The discovery of photothermal effects dates back to Graham Bell's observation in 1880, of the generation of acoustic waves in a sample resulting from the absorption of photons. In his experiment, sunlight was focussed on to the sample contained in a cell connected to a listening tube. When the sunlight was repeatedly blocked and unblocked, sound could be heard through the listening tube at the sunlight chopping frequency. Unfortunately, this technique found only a few applications due to non-availability of good light sources. In 1968, there was an upsergence in its use, after the invention of laser sources.

Photothermal effects are observed commonly in nature. A concrete example of the photothermal effect observed in nature is the optical mirage effect. A hot highway sometimes look like a reflective surface and appears as if it were a puddle. This apparent shiny surface is not due to reflection but is just a mirage. Mirage effect is one of the photothermal effects that have been exploited for physical and chemical analysis. The phenomena can be explained as follows: radiation from the sun is absorbed by the concrete or asphalt resulting in the surface heating. Energy is transferred to the air above the surface and hence a temperature gradient is developed between the air near the surface and bulk air above. Since the temperature of air near the surface is high, it expands resulting in a decrease in its density. The decreased density results in decreased refractive index. Since light travels fast in low refractive index media, light incident at an acute tangent angle is refracted upwards. Hence an observer looking at the surface at an acute tangent angle does not see the surface but rather see rays coming from the sky above the surface.

In short PT generation is an example of energy conversion and has in general three kinds of applications. a) PT material probing: do not cause any sample modification. b) PT material processing: causes the sample to change to another useful form. c) PT material destruction: makes the sample useless.

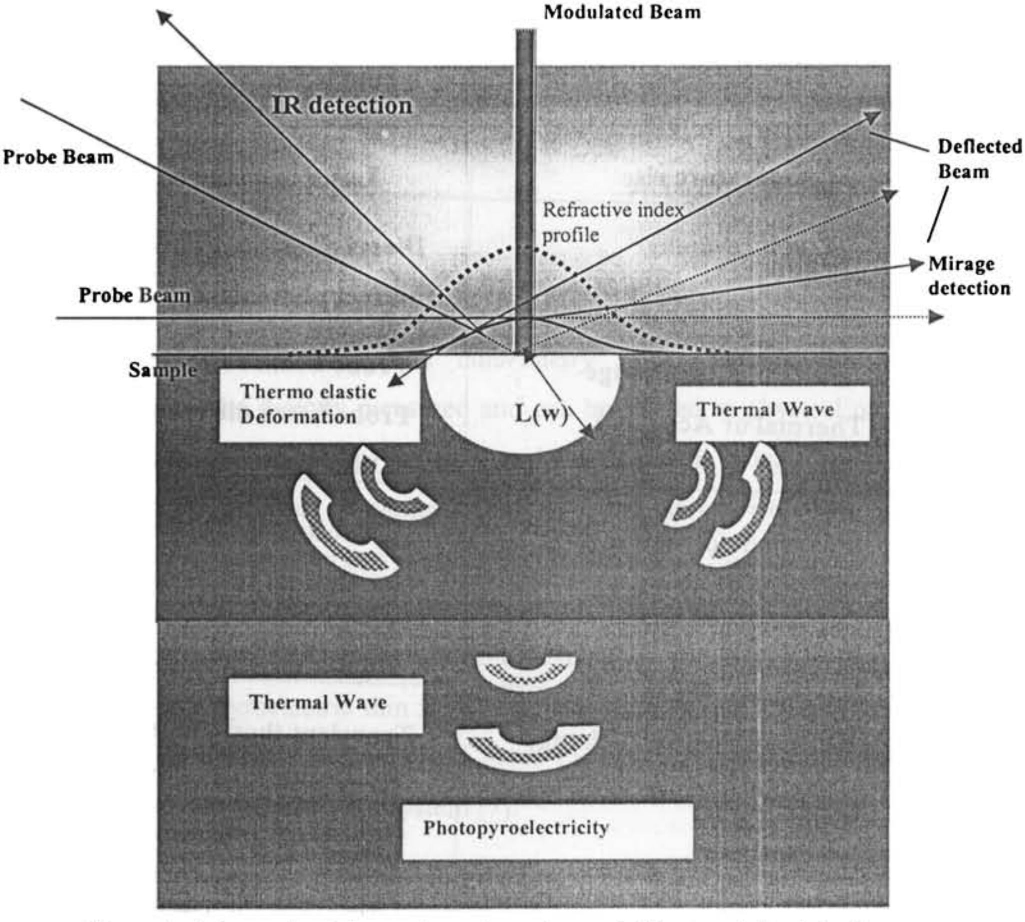

Figure 2: Schematic of the various photothermal effects and the detection mechanisms

Of the above three, PT material probing is the most important in making significant contribution to the field of science and technology. Photothermal material characterization relies on high sensitivity detection techniques to monitor the effects caused by PT material heating of a sample. The effects are illustrated in figure 2. Most of the photothermal effects occur simultaneously. The choice of a suitable PT effect for detection depends on the nature of the sample and its environment, the light source used and the purpose of measurement.

Photothermal Effects	**Detection methods (applicable to sample S or adjacent coupling medium F)**
Temperature rise	**Laser calorimetry (S or F)**
Pressure change	**Direct photoacoustic detection (S)** **Indirect photoacoustic detection (F)**
Refractive index change (Thermal or Acoustic)	**Probe beam refraction (S or F)** **Probe beam diffraction (S or F)** **Other optical probes (S or F)**
Surface deformation (Thermal or acoustic)	**Probe beam deflection (S)** **Optical Interference (S)**
Thermal emission change	**Photothermal radiometry (S)**
Reflectivity/Absorptivity change	**Transient thermal reflectance (S)** **Transient piezo reflectance (S)** **Optical transmission monitoring (S or F)**

Table I : various photothermal effects and the corresponding detection schemes detection methods for the various photothermal effects are classified generally into two depending on whether the detection methods are applied to sample itself or to the surrounding media. The former one is the *direct detection* scheme and the latter is the *indirect detection* scheme. Table I shows various photothermal effects and the corresponding detection schemes. It is to be noted that all the PT detection schemes require a modulation in the excitation light. The modulation can be in the form of continuous train of pulses at nearly 50% duty cycle (continuous modulated PT detection) or in the form of short intense pulses (pulsed PT detection) The continuous modulated PT detection is in the frequency domain (lock-in-detection) and pulsed PT detection is in the time domain. Brief descriptions of the various PT methods are given below.

Temperature rise: Temperature rise can be directly measured using thermocouples, thermistors, or pyroelectric detectors and is called laser *calorimetry* or *optical calorimetry* or *photothermal calorimetry* [3,4]. Though the observed temperature rise can be directly measured and can be related to physical parameters like absorption co-efficients, the response and sensitivity is low. Moreover, heat leakage from the sample must be minimized by elaborate thermal isolation. However, it was shown that fast rise time and high sensitivity for a thin film sample is possible if it is directly coated on to a thin film pyroelectric detector [5,6]. Heat produced within the solid due to the non-radiative de-excitation process can give rise to electrical signal in a pyroelectric thin film in contact with the sample and analysis of the dependence of the pyroelectric signal gives the optical, thermal and geometric parameters of the solid/pyroelectric system [7].

Pressure change: Another temperature dependent parameter exploited is the pressure change. Pressure variations or modulations resulting from the absorption of modulated light by the sample are referred to as *optoacoustic* or *photoacoustic* generation [8,9,10]. The pressure wave generated after light excitation contains contributions from various sources such as radiation pressure, electrostriction, thermoelastic expansion (by non radiative transition or thermal energy of chemical reaction), photoinduced volume change, gas evolution, boiling, ablation and dielectric breakdown. The acoustic wave can be detected in the sample itself (i.e. direct photoacoustic detection) or it can be detected via coupling fluid medium adjacent to the sample.

Refractive index gradient: The majority of studies addressing the use of photothemal spectroscopy for chemical analysis have been based on the refractive index measurements. The refractive index change produced upon light absorption may be induced by the pressure wave, density change, a temperature change (by radiationless transition or chemical reaction), molecular alignment, vibration excitation, rotational excitation, electronic excitation, concentration change, photoinduced volume change, creation of electric field (charge creation), clustering and so on. In transparent samples, the temperature dependent changes in refractive index of the sample itself are probed. For opaque samples, the temperature dependent changes in refractive index of the fluid that couples heat out of the sample are measured. Two types of refractive index gradient are produced- *Thermal RIG* and *Acoustic RIG*. The thermal RIG is produced by the decreased density of the medium caused by the local temperature rise, decays in time following the diffusional decay of the temperature profile and remains near the initially optically excited region. The acoustic RIG is associated with the density fluctuation of the medium caused by the propagation of PA wave, decays in propagation distance following attenuation of the PA wave and travels at acoustic velocity away from initially optically excited region. The thermal RIG generated by the excitation beam affects the propagation of an optical beam in its viscinity, including its own propagation resulting in a well-known effect of *self-defocusing or thermal blooming* [11]. In other words, spatial dependent refractive index profiles can also result in focussing and defocusing of light. The thermally perturbed sample acts as lens. Light transmitted through an aperture placed beyond the photothermal lens will vary with the strength of the lens. Photothermal methods based on the measurement of the strength of the lens are known as *Photothermal lensing spectroscopy*[12,13]. The thermal RIG also affects the propagation of another weak beam in the viscinity of the excitation beam. Thus, as light exits the medium, with a refractive index gradient, at an angle relative to the incident ray. The detection of bending of light path is utilized in *Photothermal deflection method* [14,15,16,17,18]. Some experimental apparatus measure a signal that is due the combined effects of deflection and lensing. These can be generally classified as *Photothermal refraction methods* [19] and take advantage of the effects of the temperature distribution on the probe beam propagation. The optical path length changes that occur due to the Photothermal induced refractive index change can be measured with *interferometry*. A periodic refractive index modulation results in a volume phase diffraction grating. The grating will diffract light at an angle that meets requirements from Bragg's law. The amount of light diffracted is proportional to the refractive index change. The diffracted light is measured with a photoelectric detector. Methods used to measure spectroscopic signals based on volume phase grating formed by the photothermal heating are called *Photothermal diffraction spectroscopy* [20,21]. The various configurations dealing with the different measurements cited above are depicted in Figure 3.

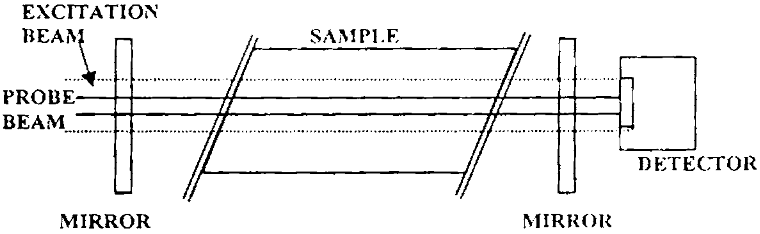

Figure 3a: Interferometry

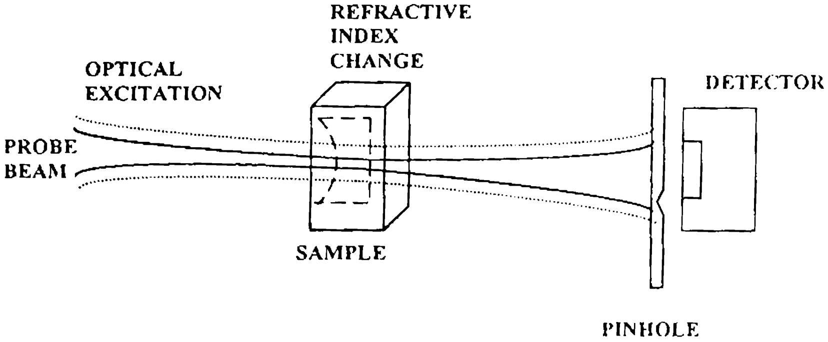

Figure 3b: thermal lensing

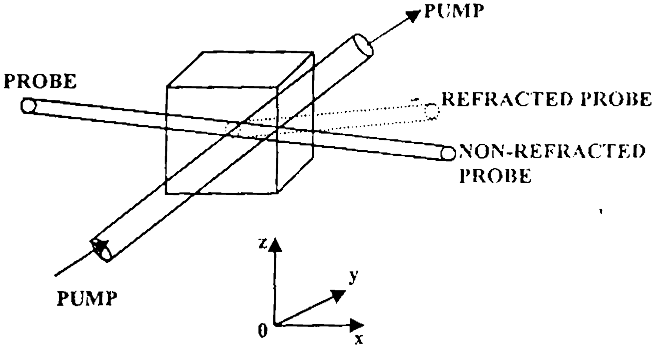

Figure 3c: Perpendicular probe beam deflection through the sample

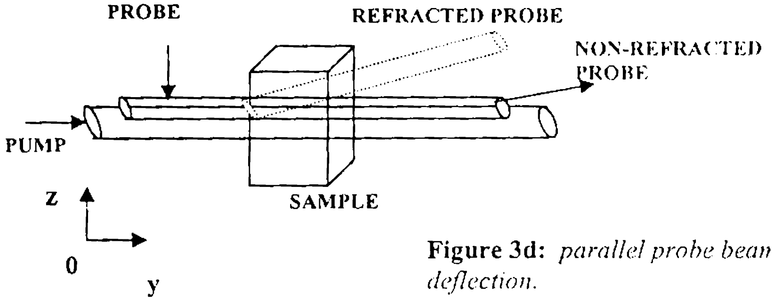

Figure 3d: *parallel probe beam deflection.*

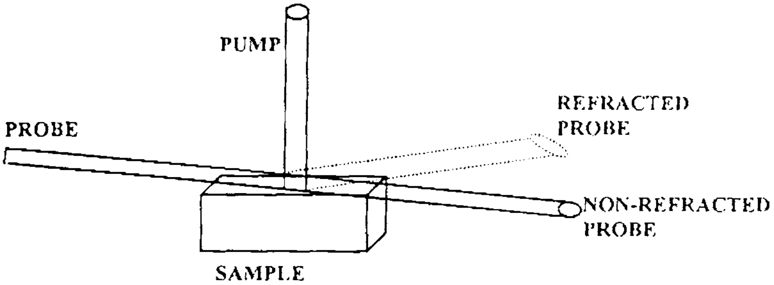

Figure 3e: Perpendicular probe beam deflection outside the sample surface (mirage effect)

Surface deformation: Under steady state isobaric conditions, the density is related to temperature through the volume expansion coefficient. Though temperature dependent density changes are difficult to measure directly, these changes can affect the samples in several different ways. In solid samples, the density change alters the physical dimensions at sample surface. Sample dimension changes give rise to two optical methods for monitoring temperature changes based on surface deformation. A homogeneous deformation displaces the surface of the sample. Interferometry can be used on reflective samples. Since small displacements of the order of few parts per million of the wavelength of the probe beam light can be measured using interferometry, this method may be used for sensitive measurements. Spatially heterogeneous expansion (contraction) can also cause the surface angle to change. A probe beam reflected from the surface will change angle when heterogeneous expansion occurs. Measurement of probe beam angle gives rise to the method of PT surface displacement technique [22,23,24].

Infrared emission changes: Temperature changes can also be indirectly measured using methods, which monitor infrared emission since the thermal infrared emission is related to sample temperature. The method of photothermal radiometry [25] can be used to measure the infrared emission changes. Although not very sensitive, this method has great potential application in non-destructive material analysis and testing. Using infrared sensitive cameras, it can be used for imaging the thermal properties of large samples.

Other PT changes: Modulated PT heating of many types of metal or semiconductor samples causes modulated reflectivity changes [26] or transmission and scattering changes [27] that can be due to density change or the photoacoustic carrier generation at the surface. Transient thermal reflectance can be used to monitor thermal properties. PT heating can cause changes in absorptivity of the sample. Zapka and Tam have used probe beam absorption measurements to detect the change in the Boltzmann molecular population distribution due to PT heating of a gaseous sample [28].

Photothermal signals depend on the thermodynamic and energy transfer properties of the sample. Temperature changes resulting from optical absorption are directly related to heat capacity and thermal conductivity. Since the thermal and optical properties are to be known to a high accuracy, absolute sample absorption measurements are difficult. Hence, the dependence on thermodynamic and energy transfer properties allows for the analysis of thermal structure of materials. Photothermal methods have been efficiently used for the measurement of acoustic velocities, thermal diffusion coefficients, sample temperature, bulk flow rates, phase transition, volume expansion coefficients and heterogeneous thermal conductivities in the solids [29-36].

Photothermal measurements are usually performed using laser light sources. There are two main reasons for this. One is the high spectral purity and power of the laser beam. For an excitation of a sample with a given absorption coefficient, the temperature change will be proportional to the optical power, in the case of continuous excitation or pulsed excitation. The photothermal signal is generally proportional to the temperature change. Thus, the greater the power or energy, the greater is the photothermal signal. Lasers can deliver high power or pulsed energies over very narrow optical bandwidths thereby enhancing the photothermal signals. The second reason is the spatial coherence. The temperature change is proportional to the optical power or energy, but at the same time is inversely proportional to the volume over which light is absorbed since the heat capacity scales with the amount of substance. The spatial coherence properties of the laser light also allow the light to be focussed to small, diffraction-limited volumes. The small volumes enhance the signal magnitude and allow the photothermal spectroscopy to be used in small volume sample analysis and allow for microscopic analysis of heterogeneous samples.

In the present thesis, major emphasis is on photothermal beam deflection (Mirage) and photoacoustic studies. As the photothermal techniques are based on the heating effects, the temperature distribution in the sample as well as in the surrounding media are to be discussed, which can be related to the signal amplitude and phase in both the above techniques. This is done in the next two sections.

1.2 PHOTOACOUSTIC EFFECT: ROSENCWAIG-GERSHO THEORY [37].

In the case of Photoacoustic technique the excitation beam is not focussed in order to minimize the lateral heat flow. Hence, the heat diffusion can be analysed by one-dimensional calculation of the periodic temperature field [38].

Consider a simple cylindrical cell of length L and diameter D as shown in figure 4. Assume that the length L is small compared to the wavelength of the acoustic signal. The sample is considered to be in the form of a disk having diameter D and thickness l. The sample is mounted so that its front surface is exposed to the

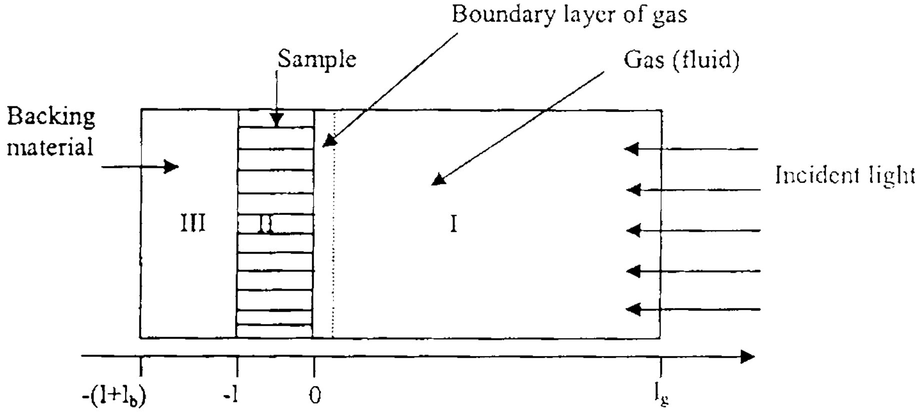

Figure 4: Geometry of 1-D Rosenwaig-Gersho model

gas (air) within the cell and its back surface is a poor thermal conductor of thickness l_b. The length l_g of the gas column in the cell is then given by l_g= L-l- l_b. Further assumption is that the gas and backing materials are not light absorbing.

Let k_i, ρ_i, C_i, α_i represent the thermal conductivity, density, specific heat and thermal diffusivity respectively of the material i. Then $a_i = (\omega/2\alpha_i)^{1/2}$ is the thermal diffusion co-efficient and $\mu_i = 1/a_i$, is the thermal diffusion length of the material. i can take subscripts s, g and b for solid, gas and backing material respectively. ω denotes the chopping frequency of the incident light beam in radians per second.

Assume that the sinusoidally chopped monochromatic light source with wavelength λ is incident on the solid with intensity $I = (1/2)\, I_0\, (1+ \cos \omega t)$

The thermal diffusion equation in the three regions can be written as

$$\frac{\partial^2 \varphi}{\partial t^2} = \frac{1}{\alpha_b} \frac{\partial \varphi}{\partial t} \quad , -l-l_b \le x \le -l \qquad \text{Region III} \qquad (1)$$

$$\frac{\partial^2 \varphi}{\partial t^2} = \frac{1}{\alpha_g} \frac{\partial \varphi}{\partial t} , 0 \le x \le -l_g \qquad \text{Region I} \qquad (2)$$

$$\frac{\partial^2 \varphi}{\partial t^2} = \frac{1}{\alpha_s}\frac{\partial \varphi}{\partial t} - A\exp(\beta x)\left[1 + \exp(j\omega t\right] \,, -l \leq \; x \leq 0 \qquad \text{Region II} \tag{3}$$

with $A = \dfrac{\beta I_0 \eta}{2k_s}$

where φ is the temperature and η is the light conversion efficiency. The real part of the complex-valued solution $\varphi(x, t)$ of the above equations is the solution of physical interest and represents the temperature in the cell relative to the ambient temperature as a function of position and time. Thus, the actual temperature field in the cell is given by

$$T\,(x,t) = \text{Re}[\varphi(x, t)] + \phi$$

where Re stands for "the real part of " and ϕ is the ambient (room) temperature.

The complex amplitude of the periodic temperature distribution, θ at the solid-gas boundary (x=0) is given by

$$\theta = \frac{\beta I_0}{2k_s\left(\beta^2 - \sigma_s{}^2\right)}\left(\frac{(r-1)(b+1)\exp(\sigma_s l) - (r+1)(b-1)\exp(-\sigma_s l) + 2(b-r)\exp(-\beta l)}{(g+1)(b+1)\exp(\sigma_s l) - (g-1)(b-1)\exp(-\sigma_s l)}\right) \tag{4}$$

where $b = \dfrac{k_b a_b}{k_s a_s}$, $g = \dfrac{k_g a_g}{k_s a_s}$, $r = (1-j)\dfrac{\beta}{2a_s}$ and $\sigma_s = (1+j)a_s$.

The main source of acoustic signal arises from the periodic heat flow from the solid to the surrounding gas. The periodic heating causes the boundary layer of gas to expand and contract periodically. This can be thought of as the action of an acoustic piston on the rest of the gas column, producing an acoustic pressure signal that travels through the entire gas column. The displacement of the gas piston due to the periodic heating can be estimated using the ideal gas law,

$$\delta x(t) = 2\pi\mu_g \frac{\bar{\phi}(t)}{T_o} = \frac{\theta\mu_g}{\sqrt{2}T_o}\exp\left[j\left(\omega t - \frac{\pi}{4}\right)\right] \tag{5}$$

where the average dc temperature of the gas boundary layer is set as dc temperature at the solid surface, $T_0=\phi+\theta_0$, ϕ being the ambient temperature at the cell walls. Assuming that the rest of the gas responds to the action of the piston adiabatically, the acoustic pressure in the cell due to the displacement of the gas piston can be obtained from the adiabatic gas law PV^{γ} = constant, where P is the pressure, V is the gas volume in the cell, and γ ratio of the specific heats. Thus the incremental pressure is

$$\delta P(t) = \frac{\gamma P_0}{V_0}\delta V = \frac{\gamma P_0}{l_g}\delta x(t) \tag{6}$$

where P_0 and V_0 are the ambient pressure and volume respectively and $-\delta V$ is the incremental volume. Then from equations (5) & (6)

$$\delta P(t) = Q\exp\left[j\left(\omega t - \frac{\pi}{4}\right)\right] \tag{7}$$

where $Q = \dfrac{\gamma P_0\theta}{\sqrt{2}l_g a_g T_0}$

The actual physical pressure variation is given by the real part of $\delta P(t)$ and Q specifies the complex envelop of the sinusoidal pressure variation.

Substituting for θ

$$Q = \frac{\beta I_0 \gamma P_0}{2\sqrt{2} k_s l_g a_g T_0 \left(\beta^2 - \sigma_s^2\right)} X$$

$$\left(\frac{(r-1)(b+1)\exp(\sigma_s l) - (r+1)(b-1)\exp(-\sigma_s l) + 2(b-r)\exp(-\beta l)}{(g+1)(b+1)\exp(\sigma_s l) - (g-1)(b-1)\exp(-\sigma_s l)} \right) \qquad \text{...............} (8)$$

Thus, equation (8) can be evaluated for obtaining the amplitude and phase of the acoustic pressure wave produced in the cell by photoacoustic effect. It can be observed that interpretation of the full expression for $\delta P(t)$ is difficult because of the complex expression of Q. Physical insight can be gained easily if certain special cases according to the optical opaqueness of solids are examined. For each category of optical opaqueness, three cases according to the relative magnitude of the thermal diffusion length μ_s, as compared to the physical length l and the optical absorption length μ_β.

Defining $Y = \frac{\gamma P_0 I_0}{2\sqrt{2} l_g T_0}$, ... (9)

CASE I: Optically Transparent solids ($\mu_\beta > l$)

1. Case Ia : Thermally Thin Solids ($\mu_s >> l$; $\mu_s >> \mu_\beta$)

We can set $e^{-\beta l} \cong 1 - \beta l$, $e^{\pm\sigma l} \cong 1$ and $|r| > 1$ in equation (8) and hence we obtain

$$Q = \frac{(1-i)\beta l}{2 a_g} \left(\frac{\mu_b}{k_b} \right) Y \qquad \text{...............} (10)$$

Thus the acoustic signal is proportional to βl and varies as f^{-1}. In addition, the thermal properties of the backing material come into play in the expression for Q.

2. *Case Ib: Thermally Thin Solids* ($\mu_s > l$; $\mu_s < \mu_\beta$)

Here we can set $\exp(-\beta l) \cong 1-\beta l$, $e^{\pm\sigma l} \cong 1 \pm \sigma_s l$ and $|r| < 1$ in equation (8).

Then. $$Q = \frac{(1-j)\beta l}{2a_g}\left(\frac{\mu_b}{k_b}\right)Y \qquad (11)$$

This equation is identical with equation (10) and hence the acoustic signal behaves in the same fashion.

3. *Case Ic: Thermally Thick Solids* ($\mu_s > l$; $\mu_s << \mu_\beta$)

In this case we set $\exp(-\beta l) \cong 1-\beta l$, $e^{\pm\sigma l} \cong 0$ and $|r| << 1$ in equation (8)

Now $$Q = -j\frac{\beta l}{2a_g}\left(\frac{\mu_s}{k_s}\right)Y \qquad \ldots\ldots\ldots\ldots (12)$$

The acoustic signal is now proportional to $\beta\mu_s$ rather than βl. This means that light absorbed within the first thermal diffusion length contributes to the signal, although light is being absorbed throughout the length of the solid. Moreover, μ_s being less than the thickness l, thermal properties of the backing material will not influence the signal. Here the signal varies as $f^{3/2}$.

CASE II: Optically Opaque Solids

1. *Case II a: Thermally Thin Solids* ($\mu_s >> l$; $\mu_s >> \mu_\beta$)

In equation (8), we set $\exp(-\beta l) \cong 0$, $e^{\pm\sigma l} \cong 1$ and $|r| >> 1$

Then we obtain $$Q = \frac{(1-j)}{2a_g}\left(\frac{\mu_b}{k_b}\right)Y . \qquad \ldots\ldots\ldots\ldots (13)$$

Here the photoacoustic signal is independent of β. The signal depends on the thermal properties of the backing material and varies as $1/f$.

2. *Case II b : Thermally Thick Solids* $(\mu_s < l\,;\ \mu_s > \mu_\beta)$

We set $\exp(-\beta l) \cong 0$, $e^{-\sigma l} \cong 0$ and $|r| > 1$ in equation (8)

We obtain $$Q = \frac{(1-j)}{2a_g}\left(\frac{\mu_s}{k_s}\right)Y\,. \qquad \ldots\ldots\ldots\ldots\ (14)$$

Though equations (13)& (14) are similar, in the present case there is no contribution from the thermal properties of the backing material.

3. *Case II c: Thermally Thick Solids* $(\mu_s << l\,;\ \mu_s < \mu_\beta)$

We set $\exp(-\beta l) \cong 0$, $e^{-\sigma l} \cong 0$ and $|r| < 1$ in equation (8). Then we obtain

$$Q = \frac{-j\beta\mu_s}{2a_g}\left(\frac{\mu_s}{k_s}\right)Y \qquad \ldots\ldots\ldots\ldots\ (15)$$

The photoacoustic signal will be proportional to $\beta\mu_s$. The signal is independent of the thermal properties of the backing material and varies as $f^{-3/2}$.

The theoretical analysis of the photoacoustic effect applied to different cases discussed above can be suitably applied to the study of any kind of sample.

1.3 PHOTOTHERMAL PROBE BEAM DEFLECTION (PBD) OR MIRAGE EFFECT [1,15,16,17,39,40,41]

In the case of photothermal beam deflection technique, the pump beam or the excitation beam is focussed. Hence, instead of the above 1-D calculation of periodic distribution of temperature, we have to resort to 3D calculations.

The heat diffusion equation in cylindrical geometry [38] is given by

$$\frac{\partial T}{\partial t} = D\left(\frac{\partial^2 T}{\partial r^2} + \frac{1}{r}\frac{\partial T}{\partial r} + \frac{1}{r^2}\frac{\partial^2 T}{\partial \theta^2} + \frac{\partial^2 T}{\partial z^2}\right) \qquad \text{............. (16)}$$

When heat flow takes place in planes through z-axis then the heat diffusion equation becomes

$$\frac{\partial T}{\partial t} = D\left(\frac{\partial^2 T}{\partial r^2} + \frac{1}{r}\frac{\partial T}{\partial r} + \frac{\partial^2 T}{\partial z^2}\right) \qquad \text{.............. (17)}$$

The assumption that the homogeneous sample is the absorbing medium and the fluid and the backing are transparent still holds. The heat diffusion equation in three regions can be written as

$$\frac{\partial^2 T_g}{\partial r^2} + \frac{1}{r}\frac{\partial T_g}{\partial r} + \frac{\partial^2 T_g}{\partial z^2} = \frac{1}{D_g}\frac{\partial T_g}{\partial t} \qquad 0 \le z \le l_g \qquad \text{............ (18)}$$

$$\frac{\partial^2 T_s}{\partial r^2} + \frac{1}{r}\frac{\partial T_s}{\partial r} + \frac{\partial^2 T_s}{\partial z^2} = \frac{1}{D_s}\frac{\partial T_s}{\partial t} - A(r,t)\exp(\alpha z)(1 + \exp(j\omega t)) \quad -l \le z \le 0 \quad \text{.... (19)}$$

$$\frac{\partial^2 T_b}{\partial r^2} + \frac{1}{r}\frac{\partial T_b}{\partial r} + \frac{\partial^2 T_b}{\partial z^2} = \frac{1}{D_b}\frac{\partial T_b}{\partial t} \qquad -(l + l_b) \le z \le -l \qquad \text{.......... (20)}$$

$A(r,t)=\dfrac{\eta P\alpha}{k_s\pi a^2}e^{\left(\frac{-2r^2}{a^2}\right)}(1+\cos(\omega t))$ is the heat deposited per unit volume where P is the exciting beam power, α is the optical absorption coefficient, η is the light conversion efficiency, 'a' is the beam radius defined at $1/e^2$ intensity.

The boundary conditions are

$$k_s\frac{\partial T_s}{\partial z}(z=0)=k_g\frac{\partial T_g}{\partial z}(z=0) \quad \text{........(21)}$$

$$k_s\frac{\partial T_s}{\partial z}(z=-l)=k_b\frac{\partial T_b}{\partial z}(z=-l) \quad \text{.......(22)}$$

$$\left.\begin{array}{l} T_s(z=-l,t)=T_b(z=-l,t) \\ T_s(z=0,t)=T_g(z=0,t) \\ T_g(z=\infty,t)=T_b(-\infty,t)=0 \quad \text{with } l_g\sim\infty,\ l_b\sim\infty \end{array}\right\} \quad \text{.......(23)}$$

Assume that l_g and l_b are very large compared to the heated area and neglect the backward heat propagation in these two regions.

In order to obtain the periodic steady state temperature, the above differential equations are reduced to simpler partial differential equation by Hankel transformation and Laplace transformation is used to obtain ordinary differential equation from the partial differential equation. Furthermore, the modulated source is replaced by the unit source $A(r)\delta(t)$

$$-\lambda^2T_0(\lambda,z,p)+\frac{\partial^2T_0(\lambda,z,p)}{\partial z^2}=\frac{p}{D_g}T_0(\lambda,z,p) \quad \text{..........(24)}$$

$$-\lambda^2 T_0(\lambda,z,p)+\frac{\partial^2 T_0(\lambda,z,p)}{\partial z^2}=\frac{p}{D_s}T_0(\lambda,z,p)-A_0(\lambda)\exp(\alpha z) \quad \text{...........(25)}$$

$$-\lambda^2 T_0(\lambda,z,p)+\frac{\partial^2 T_0(\lambda,z,p)}{\partial z^2}=\frac{p}{D_b}T_0(\lambda,z,p) \quad \text{...........(26)}$$

where

$$A_0(\lambda)=\int_0^\infty A(r)J_0(\lambda r)rdr \quad = \quad \frac{\alpha P\eta}{k_s\pi a^2}\int_0^\infty e^{\frac{-2r^2}{a^2}} J_0(\lambda r)rdr$$

$$=\frac{\alpha P\eta}{4k_s\pi}e^{\frac{-\lambda^2 a^2}{8}}$$

1) Assuming solution of the form to eq (24)

$$T_0(\lambda,z,p)=e^{\sqrt{\lambda^2+\frac{p}{D}}z}$$

The general solution is

$$T_0(\lambda,z,p)=T_s(\lambda,p)e^{-\sqrt{\lambda^2+\frac{p}{D}}z}+B(\lambda,p)e^{\sqrt{\lambda^2+\frac{p}{D}}z}$$

B (λ,p) =0, since the fluid is supposed to be very thick.

Equations (25) and (26) can be solved similarly.

Thus solution to equations (24), (25) and (26) are

$$T_0(\lambda,z,p)=T_s(\lambda,p)e^{-\sqrt{\lambda^2+\frac{p}{D}}z} \qquad \text{.............(27)}$$

$$T_0(\lambda,z,p)=U(\lambda,p)e^{\sqrt{\lambda^2+\frac{p}{D}}z}+V(\lambda,p)e^{-\sqrt{\lambda^2+\frac{p}{D}}z}-\frac{A_0(\lambda)e^{\alpha z}}{\alpha^2-\left(\lambda^2+\frac{p}{D}\right)} \qquad \text{..........(28)}$$

$$T_0(\lambda,z,p)=W(\lambda,p)e^{\sqrt{\lambda^2+\frac{p}{D}}z} \qquad \text{.............(29)}$$

After applying the Hankel inversion, to the above three equations the steady periodic state solution obtained is of the form

$$T(r,z,t)=T_0(r,z,p)\Big|_{p=j\omega}\exp(j\omega t) \qquad \text{.............(30)}$$

Thus the expressions for the modulated temperature field in the three regions are

$$T_g(r,z,t)=\int_0^\infty T_s(\lambda)\exp\left(-\beta_g z\right)\exp(j\omega t)J_0(\lambda r)\lambda d\lambda \qquad \text{.............(31)}$$

$$T_b(r,z,t)=\int_0^\infty W(\lambda)\exp\left(\beta_b(z+l)\right)\exp(j\omega t)J_0(\lambda r)\lambda d\lambda \qquad \text{.............(32)}$$

$$T_s(r,z,t)=\int_0^\infty \left[U(\lambda)\exp\left(\beta_s z\right)+V(\lambda)\exp\left(-\beta_s z\right)-E(\lambda)\exp(\alpha z)\right] \mathrm{x}\ \exp(j\omega t)J_0(\lambda r)\lambda d\lambda \quad \text{... (33)}$$

where

$$E(\lambda)=\frac{P\eta}{\pi k_s}\frac{\exp\left(\frac{-\lambda^2a^2}{8}\right)}{\left(-\lambda^2-j\frac{\omega}{D_s}+\alpha^2\right)} \qquad \text{.................(34)}$$

The final temperature distribution is obtained by substituting the following expressions in the above equations.

$$T_s(\lambda)=-E(\lambda)+U(\lambda)+V(\lambda) \qquad \text{................(35)}$$

$$W(\lambda)=-E(\lambda)\exp(-\alpha l)+U(\lambda)\exp(-\beta_s l)+V(\lambda)\exp(\beta_s l) \qquad \text{................(36)}$$

$$U(\lambda)=\left[(1-g)(b-r)\exp(-\alpha l)+(g+r)(1+b)\exp(\beta_s l)\right]\frac{E(\lambda)}{H(\lambda)} \qquad \text{................(37)}$$

$$V(\lambda)=\left[(1+g)(b-r)\exp(-\alpha l)+(g+r)(1-b)\exp(-\beta_s l)\right]\frac{E(\lambda)}{H(\lambda)} \qquad \text{..................(38)}$$

and

$$H(\lambda)=(1+g)(1+b)\exp(\beta_s l)-(1-g)(1-b)\exp(-\beta_s l) \qquad \text{... ....(39)}$$

with $g=\frac{k_g\beta_g}{k_s\beta_s}$ $b=\frac{k_b\beta_b}{k_s\beta_s}$ $r=\frac{\alpha}{\beta_s}$

$$\overline{T_s(\lambda)} = \frac{P\eta}{4k_s\pi}\frac{r}{\beta_s}\frac{e^{-\lambda^2a^2/8}}{r^2-1}\left[\frac{2(b-r)e^{-\alpha l}+(1+b)(r-1)e^{\beta_s l}+(1-b)(r+1)e^{-\beta_s l}}{(1+g)(1+b)e^{\beta_s l}-(1-g)(1-b)e^{-\beta_s l}}\right] \quad \text{......(40)}$$

The surface temperature can be written as

$$T_s(0,t) = \int_0^\infty \overline{T_s(\lambda)} J_0(\lambda r)\lambda d\lambda \exp(j\omega t) \quad \text{............... (41)}$$

The geometry for the mirage deflection is as shown in figure 5. The propagation of the beam through the spatially varying index of refraction is given by

$$\frac{d}{ds}\left(n\ \frac{dr_0}{ds}\right) = \nabla_\perp n(r,t) \quad \text{..............(42)}$$

where r_0 is the perpendicular displacement of the beam from its original direction, n is the uniform index of refraction and $\nabla_\perp n(r,t)$ is the gradient of the index of refraction perpendicular to S(the ray path). This relation can be integrated over the ray path S

$$\frac{dr_0}{ds} = \frac{1}{n}\int_{path} \nabla_\perp n(r,t) ds \quad \text{...............(43)}$$

Since the deviation is small, one can get the expression of the deflection θ(t)

$$\theta = \frac{dr_0}{ds} = \frac{1}{n}\frac{\partial n}{\partial T}\int \nabla_\perp T(r,t) ds \quad \text{..............(44)}$$

$$= \frac{1}{n}\frac{\partial n}{\partial T}\int_{-\infty}^{+\infty} \nabla T_g \times ds$$

In our case, the probe beam is propagating through the fluid along the x-direction. Hence, the probe deflects with components in x-y plane and z-x plane so that after calculating the vector product in the integrand of the above expression, we get the transverse (θ_t) and the normal (θ_n) components of the deflection, respectively.

$$\theta_n = -\frac{1}{n}\frac{dn}{dT}\int_{-\infty}^{+}\frac{\partial T_g}{\partial z}dx\,\hat{j} \qquad \text{................(45)}$$

$$\theta\theta_t = \frac{1}{n}\frac{dn}{dT}\int_{-\infty}^{+\infty}\sin\alpha\alpha\frac{\partial T_g}{\partial r}dx\,\hat{k} \qquad \text{................(46)}$$

θ_n and θ_t are the deflections normal and parallel to the sample surface.

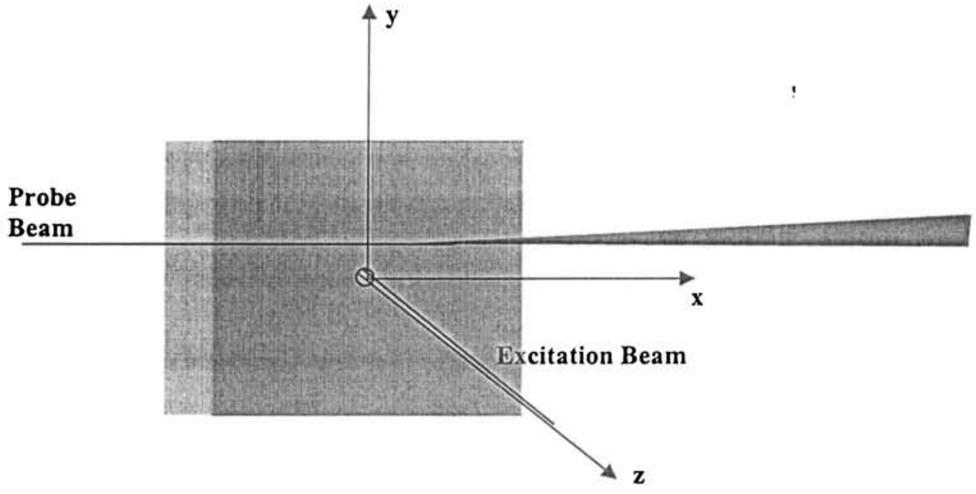

***Figure 5:* Geometry for 'mirage' deflection. The probe beam is along x direction and excitation beam or pump beam is along z direction.**

Using the standard result

$$\int_{-\infty}^{\infty}T_s(x)dx = 2\int_{0}^{\infty}\overline{T_s}(\lambda)\cos(\lambda y)d\lambda \qquad \text{.............(47)}$$

Hence substituting for the integral in eq (34)

$$\theta_n = \frac{2}{n}\frac{dn}{dT}\exp(j\omega t)\int_0^{\infty}\overline{T_s(\lambda)}\beta_g \exp(-\beta_g z)\cos(\lambda y)d\lambda\hat{j} \quad \ldots\ldots\ldots\ldots(48)$$

Similar treatment of the integral in eq (35) results in

$$\theta_t = \frac{2}{n}\frac{dn}{dT}e^{jwt}\int_0^{\infty}\overline{T_s(\lambda)}\lambda \exp(-\beta_g z)\sin(\lambda y)d\lambda\hat{k} \quad \ldots\ldots\ldots\ldots(49)$$

Substituting the value of T_s (λ) from eq. (30) in the above equation the general expression for θ_t and θ_n can be obtained. θ_n is related to the heat diffusion process perpendicular to the surface whereas θ_t represents the heat diffusion process parallel to the sample surface.

Depending upon the optical absorption co-efficient, sample can be divided into optically opaque and optically transparent. According to the thermal properties, each are subdivided into thermally thick and thermally thin. Equation (30) will be modified accordingly for each of these special cases [42]. The basic assumption is that the thermal diffusivity of the sample is greater than that of fluid as well as backing *i.e.* b $= g \sim 0$

Case I: Optically Opaque (αl >>1)

In these materials, the optical absorption length is much smaller than the sample thickness.

$$\frac{r}{1+r} = \frac{\alpha}{\beta_s + \alpha} \approx 1$$

$$\frac{r}{1-r}=\frac{\alpha}{\beta_s-\alpha}\approx -1$$

Then the expression for the tangential component of deflection

$$\theta_t=-\frac{1}{n}\frac{dn}{dT}\frac{P}{2k_s\pi}e^{j\omega t}\int_0^{\infty}\lambda\sin(\lambda y)e^{-\beta_g z}e^{-\lambda^2a^2/4}\frac{1}{\beta_s}\frac{\left[1+e^{-2\beta_s l}\right]}{\left[1-e^{-2\beta_s l}\right]}d\lambda\hat{k}$$

.................(50)

and that of normal component is given by

$$\theta_n=\frac{1}{n}\frac{dn}{dT}\frac{P}{2\pi k_s}\exp(j\omega t)\int_0^{\infty}\beta_g\cos(\lambda y)\exp\left(\frac{-\lambda^2a^2}{4}\right)\frac{1}{\beta_s}\left(\frac{1+\exp(-2\beta_s l)}{1-\exp(-2\beta_s l)}\right)\exp(-\beta_g z)d\lambda\hat{j}$$

.......(51)

For thermally thick solids, $l>\mu$. Hence $\exp(-\beta_s l)\sim 0$ and the integrands are further reduced. For thermally thin solids, $l<\mu$. And the equations are suitably modified.

Case II Optically Transparent solids ($\alpha l<<1$)

$$\frac{r}{1+r}\approx\frac{r}{1-r}\approx\frac{\alpha}{\beta_s}$$

Now the tangential component and normal components are given by

$$\theta_t = -\frac{1}{n}\frac{dn}{dT}\frac{P}{2\pi k_s}\exp(j\omega t)\int_0^\infty \lambda \mathrm{Sin}(\lambda y) e^{\frac{-\lambda^2 a^2}{4}} \frac{\alpha}{\beta_s{}^2} e^{-\beta_g z} \, d\lambda \hat{k} \qquad \ldots\ldots\ldots(52)$$

$$\theta_n = -\frac{1}{n}\frac{dn}{dT}\frac{P}{2\pi k_s}\exp(j\omega t)\int_0^\infty \beta_g \cos(\lambda y)\exp\left(\frac{-\lambda^2 a^2}{4}\right)\frac{\alpha}{\beta_s^2}\exp\left(-\beta_g z\right) d\lambda \hat{j} \quad \ldots.(53)$$

Both the above-mentioned cases are again classified into two according to the thermal properties. For thermally thick solids, $l > \mu$. Hence $\exp(-\beta_s l) \sim 0$ and the integrands are further reduced. For thermally thin solids, $l < \mu$, and the equations are suitably modified.

The two techniques detailed in this chapter can be suitably applied to various materials for the optical as well as thermal characterisation non-destructively. The analysis of the PTD signal and PA signal are discussed in the subsequent chapters, along with their successful applications to measure various thermal and transport parameters.

References:

1. Jeffrey A.Sell, *Photothermal Investigations of Solids and Liquids*, Academic Press Inc, New York (1988)
2. Stephen E.Bialkowski, *Photothermal Spectroscopy Methods for Chemical Analysis*, John Wiley &Sons, Inc.
3. G.H. Brilmyer, A.Fujishima, K.S.V. Santhanam, A. J.Bard, *Anal.Chem.*49, (1977) 2057
4. M.Bass, L.Liou, *J.appl.Phys.*56 (1984)184
5. H.Coufal, P.Hefferle, *Appl.Phys A,* **38** (1985)213
6. H.Coufal, P.Hefferle, Can.J.Phys.**64**, (1986)1200
7. A.Mandelis, Martin M Zver, *J.Appl.Phys* 57(9), (1985) 4421
8. A.Rosencwaig, *Photoacoustics and Photoacoustic spectroscopy,* Wiley, NewYork (1980).
9. A.Rosencwaig, J.B.Willis, *J.Appl.Phys.* **51(8)**, (1980) 4361
10. David A.Hutchins, Andrew C.Tam, *IEEE Transactions on Ultrasonics, Ferroelectrics and Frequency Control*, **Vol.UFFC-33 (5)** (1986) 429
11. R.C.Leite, R.S.Moore, J.R.Whinnery, *Appl.Phys.Lett,* **5**, (1964) 141
12. R.L.Swofford, M.E.Long, A.C.Albrecht, *J.Chem.Phys*, **65** (1976)179
13. Howard L.Fang, Robert L.Swofford, *J.Appl.Phys.*50(11) (1979) 6609
14. A.C.Boccara, D.Fournier, J.Badoz, *Appl.Phys.Lett*. **36**, (1979)130.
15. J.C.Murphy, L.C.Aamodt, *J.Appl.Phys* **51(9)** (1980) 4580
16. L.C.Aamodt, J.C.Murphy, *J.Appl.Phys.* **52(8)** (1981)4903
17. J.C.Murphy, L.C.Aamodt, *Appl.Phys.Lett* 39(7) (1981) 519
18. A.C.Boccara, D.Fournier, W.Jackson, D.Fournier, *Opt. Lett* 5(9) (1980) 377
19. N.J.Dovichi, T.G.Nolan, W.A.Weimer, *Anal.Chem.* 56 (1984) 1700
20. J.F.Power, M.A.Schweitzer, *Opt.Eng.*36(2), (1997) 521
21. S.E.Bialkowski, A. Chartier, Appl.Opt.36(27), (1997) 6711
22. M.A.Olmstead, N.M.Amer, *Phy.Rev.Lett*, **52**, (1984) 1148

23. J.-C. Cheng and S.-Y. Zhang, J. Appl. Phys. 70, (1991) 7007

24. G.L.Bennis, R.Vyas, R.Gupta, S.Ang, W.D.Brown, *J.Appl.Phys.*84 (1998) 3602

25. P.E.Nordal, S.O.Kanstad, *Phy.Scr.*20, (1979) 659

26. A.Rosencwaig, J.Opsal, W.L.Smith, D.L.Willenborg, *Appl.Phys.Lett.* 46, (1985) 1013

27. A.Rosencwaig, J.Opsal, W.L.Smith, D.L.Willenborg,, *J.Appl.Phys.* 59 (1986)1392

28. W.Zapka, A.C.Tam, *Opt.Lett.* 7, (1982) 86

29. C.J.Dasch, J.A.Sell, *Opt.Lett.* 11, (1986) 603

30. W.A.Weimer, N.J.Dovichi, *Appl.Opt.* 24, (1985) 2981

31. P.Hess, Photoacoustic, *Photothermal and Photochemical processes in gases*, Springer-Verlag, New York (1989)

32. P.Hess, *Photoacoustic, Photothermal and Photochemical processes at surfaces and Thin films*, Springer-Verlag, New York (1989)

33. H.B.Lin, A.J.Campillo, *Appl.Opt.*24, (1985) 222,

34. D.Fournier, A.C.Boccara, A.Skumanich, N.Amer, *J.Appl.Phys.*59, (1986) 787

35. Nibu A.George, C.P.G.Vallabhan, V.P.N Nampoori, A.K.George, P.Radhakrishnan, *J.Phys.D:Appl.Phys.*33 (2000) 3228

36. N.Mikoshiba, H.Nakamura, K.Tsubouchi, *Proceedings of the IEEE ultrasonic symposium San Diego*, San Diego, CA (1982).

37. A.Rosencwaig, A.Gersho, *J.Appl.Phys.*47, (1976) 64

38. H.S. Carslaw and J.C. Jaeger, *Conduction of heat in solids*, Oxford, Clarendon (1959)

39. A.Figari, *J.Appl.Phys.* 71(7) (1992) 3138

40. F.Lepoutre, B.K.Bein, L.J.Inglehart, *Can.J.Phys.* 64 (1986) 1037

41. A.Hadj-Sahraoui, G.Louis, B.Mangeot, P.Peretti, J.Billard, *Phy.Rev.A* 44(8) (1991)5080

42. A.Salazar, A.Sanchez-Lavega, J.Fernandes, *J.Appl.Phys* 65(11) (1989) 4150

CHAPTER II

ANALYSIS OF PHOTOTHERMAL DEFELECTION SIGNAL FOR DETERMINATION OF THERMAL DIFFUSIVITY: THEORETICAL EXTENSION TO AMPLITUDE METHOD

2.1 EXPERIMENTAL CONFIGURATIONS

Photothermal deflection technique is in the class of laser heating methods that creates a temperature distribution within a material by impingement of a laser on to its free surface. As discussed in the last chapter, this technique uses two laser beams, one for heating the sample (pump) and the other to detect the produced refractive index gradient (probe). The pump and probe beams can be aligned with respect to each other in two configurations [1]. *Transverse PBD:* In this case, the pump and probe beams are perpendicular to each other. *Collinear PBD:* Here the pump and probe beams are parallel to each other. Moreover, the probe beam can be directed to the sample surface in two ways [2,3,4] 1*) Skimming configuration*: In this configuration, the probe beam just grazes the sample surface. This implies that the probe beam travels at a certain height above the sample surface, which is determined by the size of the probe beam. The main problem connected with the skimming configuration is thus related to the size of the probe beam. Though the probe beam is focussed to a small spot size, it increases at the edge and in order to avoid probe beam scattering the beam has to travel a distance 'z' far from the surface which is at least $z = \sqrt{\lambda L / \pi}$, where λ is the probe optical wavelength and 'L' is the sample size along the probe beam path. 2) *Bouncing configuration or surface reflection scheme:* The probe beam impinges on the sample surface at a certain angle and the deflection of the reflected beam is noted. Hence, the height of the probe beam above the sample surface is zero. In the bouncing configuration, the probe beam deflection is obtained as a result of two different mechanisms, the thermal gradient in the areas near to the heated sample (mirage) and the sample deformation due to thermal expansion. The bouncing scheme however cannot be applied to samples with no relevant probe reflection i.e. absorbing, rough or non-reflecting samples. This problem can be overcome by covering the surface with a thin reflecting layer. However, use of this layer can cause the pump beam reflection too. It is suggested that this problem can also be overcome by covering only a small region of surface in order to guarantee probe beam reflection only. But the small dimension of the covered area limits the use of bouncing to large angles only.

The effects introduced in both the configurations by the finite size of the heating beam, finite height of the probe beam above the sample surface, the secondary effects like finite size of the probe beam, sample temperature, optical misalignment, diffusivity of the deflecting medium are discussed in detail by Salazar *et a l* [2]
There are two methods for making the optical beam deflection measurements [5].

Method 1: The Standard Method:

In this method the separation between the pump and probe beams (transverse offset, 'y') is fixed (usually y=0 when the two beams intersect). The signal amplitude and phase are measured as some physical or operational parameter of the system is changed. Thus when an infinitesimal probe beam skims the sample surface and when there is no heat diffusion in the gas, this method measures the normalized surface temperature τ along a line passing through the excitation beam axis. Although theoretically, this temperature is integrated along a line infinite in extent, it is effectively determined only by the temperature in the region of the sample significantly heated by the absorbed light. Thus as the pump and probe beams are moved across the sample surface, the localized area contributes effectively to the OBD signal changes, whereby the optical and thermal properties of the sample can be measured as a function of the beam position.

Method 2: The Transverse Scan Method:

In this method, the pump beam is fixed to a particular position on to the sample surface. The probe beam is then scanned across the sample surface perpendicular to the pump beam. Hence, the separation between the pump and the probe beams (transverse offset 'y') is a variable. Thus, the normal and tangential beam deflection profiles are measured about the center position of the exciting laser beam.

In all the above-mentioned methods and configurations of the probe beam deflection, one condition is strict which is regarding the size of the probe beam. This is so because the basic equations dealing with the normal and tangential component of the deflection requires that the size of the probe beam must be small compared to the gas thermal diffusion length. Large probe beams can be treated as a bundle of infinitesimal light filament each satisfying these basic equations and hence each of them will be deflected differently and the finite probe beam will have no well-defined deflection. In addition, the beam spreads and its cross sectional shape will be distorted. Thus in short if the ratio of the probe beam radius R_p to the thermal diffusion length (μ_g) of the deflecting medium 'g', R_p/μ_g is small enough, then the different parts or rays of the probe beam are submitted to approximately the same thermal gradients and they undergo almost the same deflection. On the contrary when this ratio is large enough, then each individual ray of the beam is deflected in a particular direction with given amplitude and phase. Under high excitation power, it was proved that there was deformation in the probe beam shape due to constant heat gradient [6]. In the collinear configuration, the effect of absorption of the probe beam must be taken into account. An absorption change is always present when there is an increase in thermal refractive index induced by the pump beam, which is of the same order as that of magnitude of the refractive index change. It has been theoretically analyzed by Bertolotti *et al* [7] to extract the expression for the deflection signal eliminating the probe beam absorption effects from the experimental data.

2.2 ANALYSIS OF EXPERIMENTAL DATA

As already explained above, the PTD experiment consists of a pump source for excitation of the sample, which is modulated using a chopper and a probe source to probe the refractive index gradient. The deflection of the probe beam is detected using a position sensitive detector. The vectorial nature of the deflection implies that the magnitude has two spatial components. The components are referred to as the normal component φ_n and tangential component φ_t [1,8]. Different methods are developed by many workers to analyze the amplitude and phase data for determination of thermal diffusivity. Some of the important methods of analysis are given below.

a) Zero crossing technique:

The theory of the technique has been developed by *Kuo et al*[9,10]. In this technique, the transverse scan method is used and amplitude of the tangential component of the deflection signal (A_t) is measured using the lock-in-amplifier. A graph is plotted between A_t and the transverse offset 'y' as shown in figure. The antisymmetric plot is explained on the fact that the probe beam deflection switches from left to right as one passes from one side of the heated region to the other. The two points at which the plot of real part of A_t just goes to zero on either side of the central zero corresponds to points that are shifted in phase by ± π/2 relative to the central position. It is to be noted that these points do not correspond to quarter wavelength distance on each side of the center. However, this is not so for two reasons.

1) The effect of finite heating beam size is such as to effectively add a constant to this distance.
2) Cylindrical waves are not exactly periodic and first zero do not occur precisely at ±π/2 radians from the origin. It was later proved that the distance x_0 between two ninety degree phase points on either side of the origin is given by

$x_0 = d + \sqrt{\gamma}\,\lambda/_2 = d + \sqrt{\gamma\pi\,\frac{\alpha}{f}}$, where γ is a parameter which depends on the kind of material, 'd' is the distance on the order of the heating beam diameter and 'f' is the modulation frequency.

$\gamma=1.4$ when the sample is optically opaque and thermally thick.

$\gamma=1$, for optically opaque thermally thin solids and optically transparent ones.

Thus, a plot of x_0 vs $1/f^{1/2}$ gives a straight line with a slope $\sqrt{1.4\pi\alpha}$, where α is the thermal diffusivity of the sample.

Though this method of determination is direct and simple, it cannot be applied to materials whose thermal diffusivity is lower than that of the surrounding fluid medium. If the thermal diffusivity of the fluid is higher than that of the sample, then the mirage signal will be dominated by the thermal properties of the fluid. Thus, when the thermal diffusivity of the specimen is much lower than that of the surrounding fluid, the applicability of the zero crossing method becomes complicated as either no zero-crossing exists or the signal level at the zero-crossing point is so small that noise makes its accurate determination impossible.

b) Multiparameter fitting [11,12]:

This method has been suggested as a new method to determine the anisotropic thermal diffusivities parallel to the surface of a solid sample. Moreover, this method can be employed for the determination of low thermal diffusivity. The thermal diffusivity of specimen has to be calculated from entire mirage measurement data, which contains information on the thermal properties of both the specimen and gas, the size of both heating beam and probe beams and their alignment as well as the modulation frequency of heating. Initially a possible data analysis method for this kind of problem is the multiparameter least square regression fitting developed by Anthony *et al* [13]. It was applied for the determination of thermal diffusivity of diamonds. Later this method was extended by Rantala *et al* [12] for determination of low thermal diffusivity of materials like polymers, ceramics etc. The severe thermal expansion of polymer samples, which causes difficulties in the case of optical measurement, has been taken into account. The sensitivity of the multiparameter to the sample diffusivity is studied by calculating the variance of the fitting when the sample thermal diffusivity is held as fixed. Other variables whose values are unknown are fitted. For example the height of the probe beam, thermal diffusivity of the coating and the phase shift and the amplitude of the signal. However, the thickness of the sample affects the accuracy of measurement. The method is reliable only for samples with thickness exceeding 100 μm. When applied to a polyvinyl film of thickness 50 μm, the thermal diffusivity obtained was double that of expected value.

c) Thermal wave coupling method [14,15]:

Photothermal measurements on thin films are not easy. While dealing with thin films, it is to be noted that they are always coated on to a substrate. If the film is very thin then a significant portion of the pump power will be absorbed by the substrate. Thus the true sample is a film-substrate composite. Wong *et al* derived explicit expressions for the thermal diffusivity for film substrate composites by including contributions from the thin film as well as the substrate to the temperature field at the probe beam position. This method requires the measurement of the phase of deflection at two positions (y_0) over a range of pumping frequency from which the thermal diffusivity of the film can be found out. From the regression line of the phase - $f^{1/2}$ plot, the thermal diffusivity of the substrate can be determined. The measurements are made with probe beam well beyond the pump spot so that the influence of the pump beam profile is negligible and also the frequency range used is very high. Hence, measurable signal results only if the sample is a highly absorbing one.

d) Phase Method [16,17]:

This method utilizes the phase of the tangential component of deflection signal (φ_t).

Theoretically,

$$\varphi_t = \varphi_0 \exp\left[-j\left(y/l_t + \phi\right) - j\omega t\right] \tag{1}$$

This implies that the phase varies linearly with the pump-probe offset 'y'. l_t is the characteristic length , which is the distance corresponding to one radian phase shift.
From the slope of plot of phase vs. 'y', s, thermal diffusivity of the sample can be determined using the relation

$$D = \frac{\pi f}{s^2} \tag{2}$$

This direct determination is possible only if the thermal diffusivity of the sample is greater than that of the coupling medium. On the contrary, if the thermal diffusivity of the sample is lower than that of the coupling medium, modified phase method must be applied. In such a case, slope 's' is determined for various modulation frequencies 'f' and a graph is plotted between $1/s$ and $1/\sqrt{f}$. The slope of this straight line graph, s', gives the thermal diffusivity using the relation

$$D = \pi s'^2 \tag{3}$$

e) Amplitude Method:

The method developed by Quelin *et al* took into account the linear variation of logarithm of amplitude of the tangential component of the deflection signal with the pump-probe offset. The three-dimensional thermal conductivity tensor of a polymer crystal is determined in the front configuration where the pump and probe runs on the same side of the sample [18] This is similar to the Phase method and the thermal diffusivity is obtained from the relation $D = \pi f / s'^2$ where s' is the slope of graph between *ln* [A_t] and 'y'. Further they observed that only a numerical simulation led to the thermal conductivity co-efficient perpendicular to the sample surface. Hence in order to determine the thermal conductivity coefficient in the normal direction, they used amplitude of normal component of deflection in the rear configuration, which means that the pump and probe are running on either side of the sample [19].

2.3 THE PROPOSED MODIFIED AMPLITUDE METHOD

We propose a modification to the Amplitude Method to analyze the photothermal probe beam defection signal for the determination of low thermal diffusivity values of materials. This simple theoretical model, takes into account the dependence of the photothermal signal on the height of the probe beam above the sample surface, which affects mirage measurements when the thermal diffusivity of the coupling medium is greater than that of the sample. The present work is similar to the modification to the phase method proposed by Bertolotti *et al* for determination of low thermal diffusivity. The method can be applied irrespective of whether the sample is optically transparent or optically opaque and is independent of thickness.

In the amplitude method as discussed earlier, the slope (S_{high}) of the plot of *ln* [A_t] vs. pump-probe separation 'y' is evaluated. Since $S_{high} = \frac{1}{l_t}$, the determination of high thermal diffusivity is simple as it can be directly obtained from the relation,

$$D_t = \frac{\pi f}{S_{high}^2} \tag{4}$$

The result of numerical simulation of ln [A_t] vs. y for various modulation frequencies for optically opaque and optically transparent cases is shown in Fig (1-2).

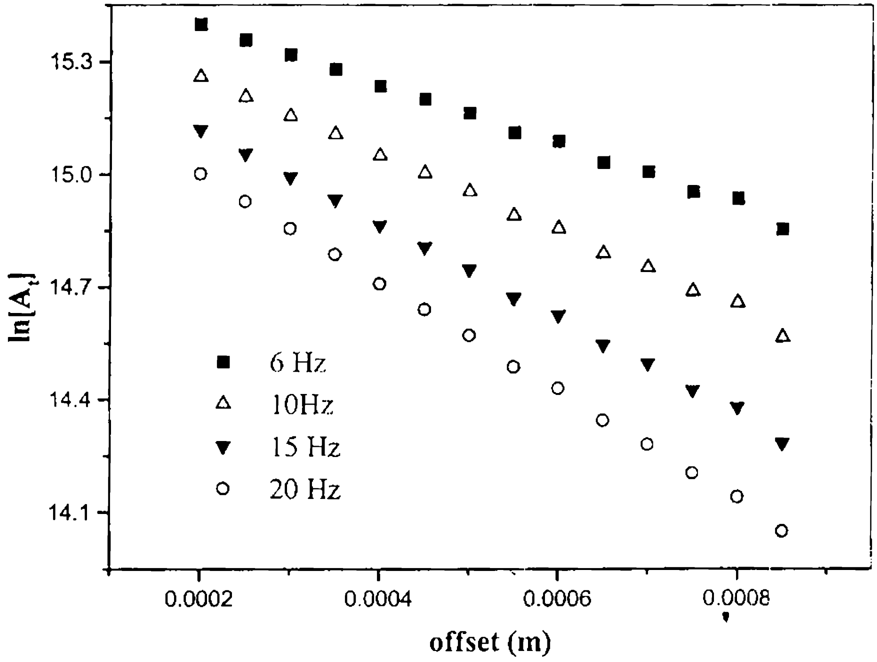

Figure 1 Plot of ln[A_t] vs pump-probe offset for four different modulation frequencies (■)ν=6 Hz, (Δ)ν=10 Hz, (•)ν=15 Hz, (o) ν=20 Hz for optically opaque samples with high thermal **diffusivity.**

The plots are linear with their slopes increasing with the modulation frequency. This implies that the characteristic length decreases as modulation frequency increases. Table I shows the thermal diffusivity values obtained using equation (4) for four different modulation frequencies. It is observed that the diffusivity values obtained for each frequency, is in perfect agreement with the value used in computer simulation ($0.3\times10^{-4}\ m^2s^{-1}$) irrespective of whether the sample is optically transparent or optically opaque.

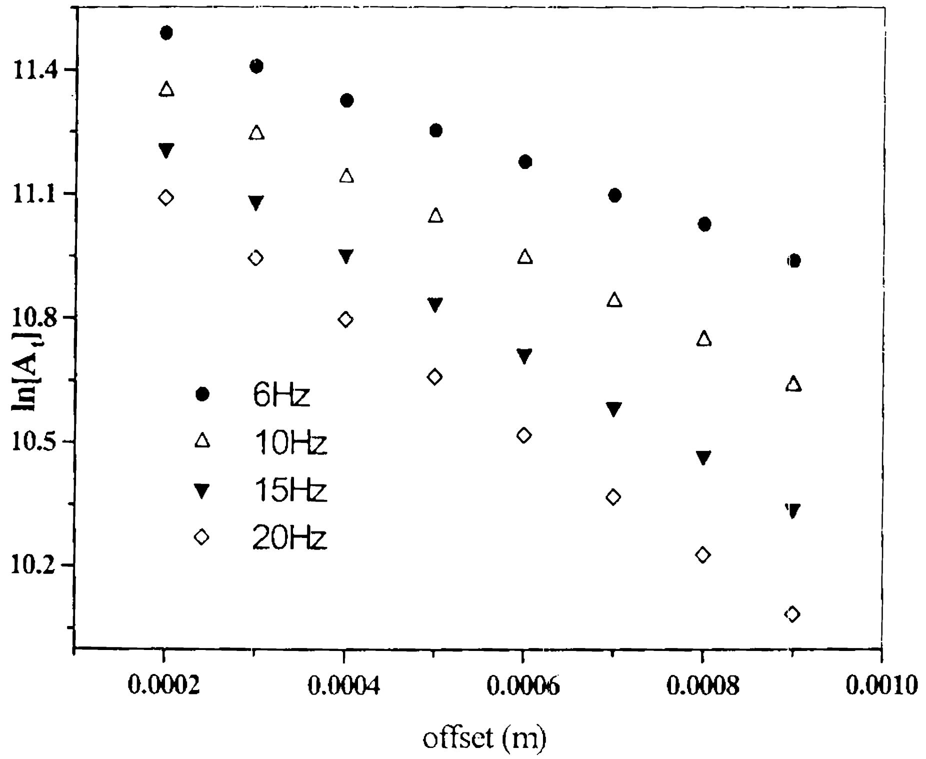

Figure 2: Plot of $\ln[A_t]$ vs pump-probe offset for four different modulation frequencies (•)$\nu=6$ Hz, (Δ)$\nu=10$ Hz, (•)$\nu=15$ Hz, (◊) $\nu=20$ Hz for optically transparent samples with high thermal diffusivity.

Frequency (Hz)		**6**	**10**	**15**	**20**
$D_1(10^{-4}\ m^2s^{-1})$ Eq(4)	**Optically opaque**	**0.293**	**0.294**	**0.296**	**0.298**
	Optically transparent	**0.309**	**0.310**	**0.309**	**0.306**

TableI: Thermal diffusivity value calculated using Eq. 4 for optically opaque as well as optically transparent samples possessing high thermal diffusivity.

However, for samples with low thermal diffusivity, the characteristic length is different from the thermal diffusion length and has a strong dependence on the vertical offset 'z' given by [4]

$$l_t = \mu + k.z \tag{5}$$

where 'k' is a coefficient depending on the ratio of diffusivities of the surrounding medium and the sample. Hence, the vertical offset dependence has to be taken into account while characterizing samples possessing low thermal diffusivity. It is to be noted that the criteria for classification of materials possessing high or low thermal diffusivity depends on whether the thermal diffusivity of the sample is higher or lower than that of the coupling medium used. In our theoretical calculations, the thermal diffusivity of the coupling medium is taken to be that of carbontetrachloride (D~0.731 x 10^{-2} cm^2 s^{-1}).

The difficulty in measurement of low thermal diffusivity arises due to the contribution of the thermal properties of the coupling fluid to the photothermal signal. When the thermal diffusivity value of the sample is low, the thermal diffusion length is also low and becomes comparable with the second term of equation (5). Therefore, the height of the probe beam above the sample surface has to be taken into account. Hence, in skimming configuration, one can no longer take the slope of ln $[A_t]$ vs. 'y' to be equal to $1/l_t$. The problem can be easily overcome by using the bouncing configuration (z = 0) whereby the dependence of the characteristic length on 'z' can be eliminated. The bouncing configuration can be applied in the case of ceramics and rare earths provided the surfaces are clean and polished. For materials like polymers, this configuration can result in thermal expansion, due to their low thermal conductivity and high thermal expansion coefficient, which will adversely affect the mirage measurement. Thus, the skimming configuration is more suitable for thermal diffusivity determination in the case of polymers, which possess very low thermal diffusivity.

Hence, while applying the skimming configuration to low thermal diffusivity measurements, the amplitude method is slightly modified considering the vertical offset dependence of the characteristic length. We can eliminate this dependence by determining the slope

$\left[S_{low} = \dfrac{l_t(f_1) - l_t(f_2)}{{}^{1}\!/_{f_1} - {}^{1}\!/_{f_2}}\right]$, of the plot of characteristic length l_t vs. $\frac{1}{\sqrt{f}}$, as suggested by equation (5). The thermal diffusivity can be obtained using the relation,

$$D = \pi S_{low}^{2} \tag{6}$$

Figure (3a & 4a) shows the numerically simulated plots of logarithm of signal amplitude $\ln[A_t]$ against the pump-probe separation, for optically opaque and optically transparent cases respectively for four distinct modulation frequencies 6Hz, 10Hz, 15Hz, 20Hz. The thermal diffusivity value used for the simulation is 0.3 x 10^{-8} m^2s^{-1} so that the D_{sample}/D_{fluid} =0.4. Table II shows the thermal diffusivity values calculated using equations (4) & (6) for optically opaque and optically transparent cases. Though the plots show a linear dependence, the thermal diffusivity values calculated for each modulation frequency using equation (4) is found to be different. Unlike the case of high

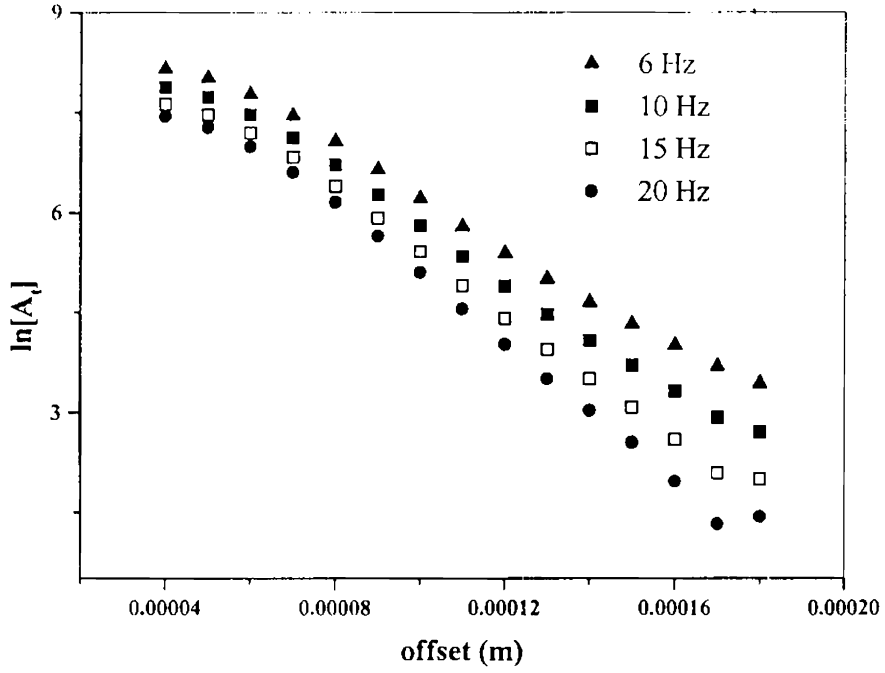

Figure 3a: Plot of ln[A_t] vs pump-probe offset for four different modulation frequencies (•)v=6 Hz, (■)v=10 Hz, (•)v=15 Hz, (•) v=20 Hz for optically opaque samples with

thermal diffusivity, these values differ from the value used for computer simulation too, implying a non-negligible dependence of the characteristic length (l_t) on vertical offset (z). Applying the modification suggested eliminates this dependence. Figures (3b) & (4b) shows the plots of l_t vs. $1/\sqrt{f}$ for the optically opaque and optically transparent cases. It is seen from Table II that the thermal diffusivity value calculated with equation (6) using the slopes of plots (fig (3b) & (4b)) yield the value used in computer simulation for optically opaque as well as transparent cases.

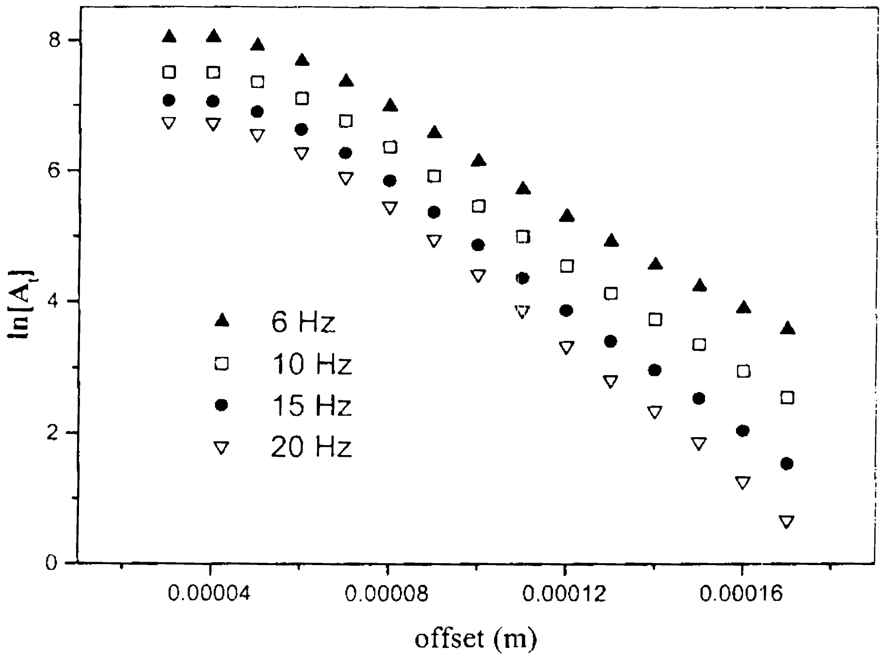

Figure 4a: ***Plot of*** $\boldsymbol{ln[A_t]}$ ***vs pump-probe offsetfor four different modulation frequencies(•)v=6 Hz, (•)v=10 Hz, (•)v=15 Hz, (∇) v=20 Hz for optically transparent samples with low thermal diffusivity***

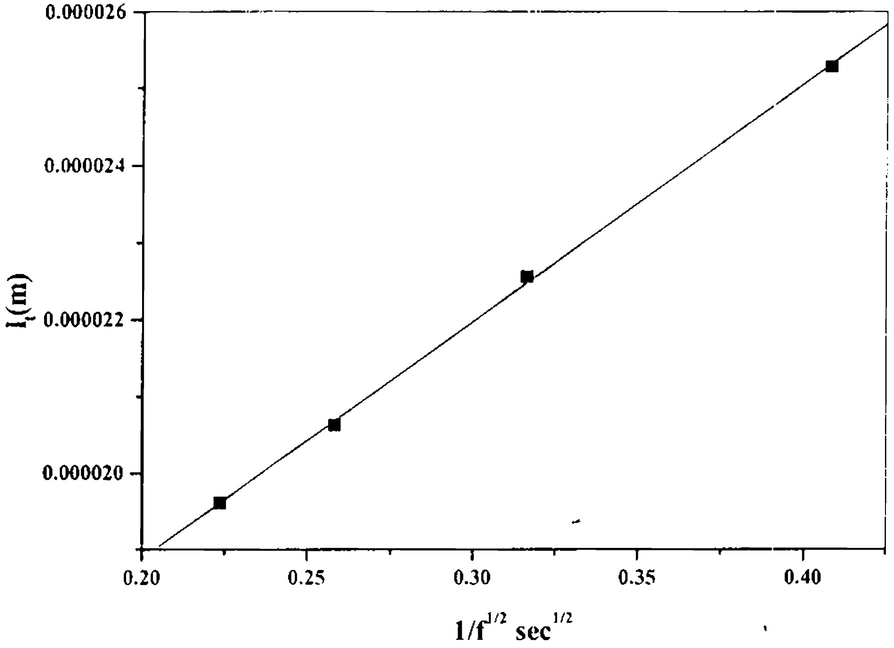

Figure 3 b: Characteristic length l_t (μm) against $1/f^{1/2}$ from the data of Figure 3a

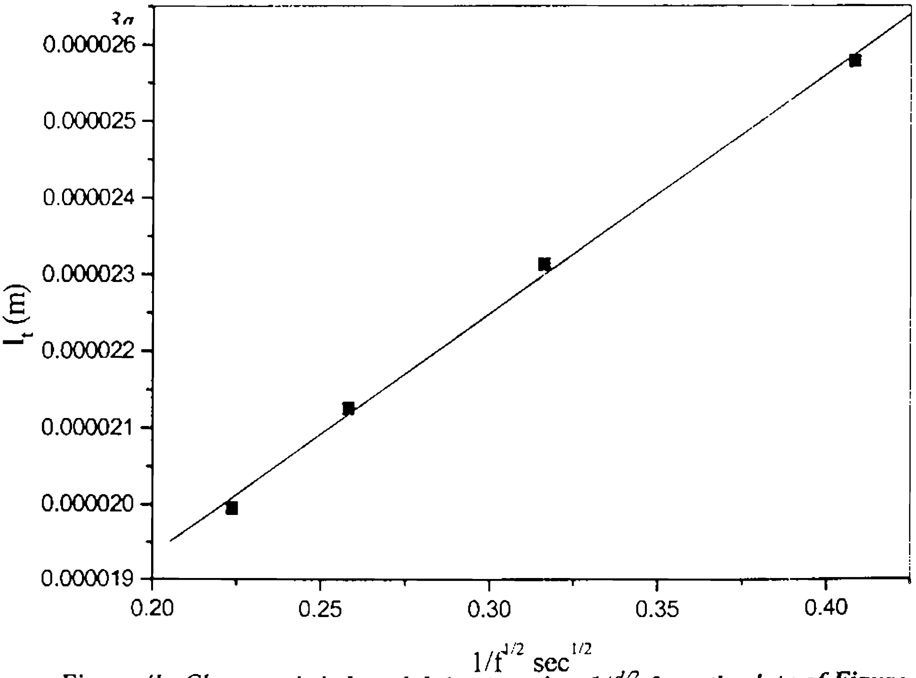

Figure 4b: Characteristic length l_t (μm) against $1/f^{1/2}$ from the data of Figure 4a.

Frequency (Hz)		**6**	**10**	**15**	**20**
Optically opaque	**D_l(10^{-8} m^2s^{-1}) Eq(4)**	**1.204**	**1.590**	**2.00**	**2.410**
	D (10^{-8} m^2s^{-1}) Eq(6)	**0.300**			
Optically transparent	**D_l(10^{-8} m^2s^{-1}) Eq(4)**	**1.252**	**1.679**	**2.126**	**2.498**
	D(10^{-8} m^2s^{-1}) Eq(6)	**0.308**			

***Table 2**: Thermal diffusivity calculated using Eq. 4 and Eq. 6 for optically opaque as well as optically transparent samples possessing low thermal diffusivity.*

The method is applicable only if the height of the probe beam above the sample surface is less than half the thermal diffusion length. Hence, the accuracy of the method depends on the spot size of the beam and the chopping frequency [16]. If the height of the probe beam above the sample surface is very large then the linearity between the characteristic length l_l and $1/f^{1/2}$ will not be exhibited.

However, if the geometrical configuration is the 'bouncing' one then the vertical offset is zero. Thus in this scheme, the characteristic length is the same as the thermal diffusion length even for low diffusivity samples. So equation (4) can be used for the determination of their thermal diffusivity and is found to be equal for all modulation frequencies. For very low modulation frequencies (~0. 1Hz), the dependence of the characteristic length on the vertical offset is negligible. Hence, equation (4) is valid even in the case of low diffusivity samples. However, this frequency range is not practical due to the 1/f noise appearing in the measurements.

To conclude, a new method is proposed for the analysis of the photothermal deflection signal for the determination of thermal diffusivity when the measurements are taken on samples, which possess low thermal diffusivity compared to that of the adjacent coupling media. This method can be applied to both optically transparent and optically opaque materials and no knowledge of the thickness of the sample is required for the successful evaluation of thermal diffusivity.

REFERENCES:

1. Jeffrey A.Sell, *Photothermal Investigations of Solids and Liquids*, Academic Press Inc, New York (1988)
2. A.Salazar, A.Sanchez-Lavega, J.Fernandez, *J.Appl.Phys*. 69(3), (1991)1216
3. M.Bertolotti, G.L.Liakhou,R.Li Voti, S.Paoloni, C.Sibilia, *J.Appl.Phys*. **83** (2) (1998) 966.
4. M.Bertolotti, G.L.Liakhou, R.Li Voti, S.Paoloni, C.Sibilia, *Appl.Phys B* **67** (1998) 641
5. L.C.Aamodt, J.C.Murphy, *J.Appl.Phys*. **52**(8) (1981) 4903
6. E.Legal Lasalle, F.Lepoutre, J.P.Roger, J.Appl.Phys. **64** (1) (1988)1
7. M.Bertolotti, L.Fabbri, E.Fazio, R.Li Voti, C.Sibilia, G.Leakhou, A.Ferrari, **69**(6) (1991) 3421
8. J.C.Murphy, L.C.Aamodt, *Appl.Phys.Lett*, **39**(7) (1981) 519
9. P.K.Kuo, M.J.Lin, C.B.Reyes, L.D.Favro, R.L.Thomas, D.S.Kim, Shu-yi Zhang, L.J.Inglehart, D.Fournier, A.C.Boccara, N.Yacoubi, *Can.J.Phys*. **64** (1986)1165
10. P.K.Kuo, E.D.Sendler, L.D.Favro, R.L.Thomas, *Can.J.Phys*. **64** (1986)1168
11. J.Rantala, J.Jaarinen, P.K.Kuo, *Appl.Phys*. A. **55**(1992) 586
12. J.Ranatala, Lanhua Wei, P.K.Kuo, J.Jaarinen, M.Luukkala, R.L.Thomas, *J.Appl.Phys*. **73** (6) (1993) 2714
13. T.R.Anthony,W.F. Benholzer, J.F.Fleischer, lanhua Wei, P.K.Kuo, R.L.Thomas,R.W.Pryor *Phy.Rev.B*. **42,** (1990) 1104
14. P.K.Wong, P.C.W.Fung, H.L.Tam, J.Gao, *Phys.Rev.B* **51**(1) (1995) 523
15. P.K.Wong, P.C.W.Fung, H.L.Tam, *J.Appl.Phys* **84**(12) (1998) 6623
16. M.Bertolotti, R.Li Voti, G.Liakhou, C.Sibilia, *Rev.Sci.Instrum* **64**(6) (1993)1576
17. M.Bertolotti, R.Li Voti, G.Liakhou, C.Sibilia, *Rev.Sci.instrum* **66** (1) (1995) 277

18. X.Quelin,B.Perrin, G.Louis, P.Peretti, *Phys.revB* **48** (6) (1993) 3677
19. X.Quelin, B.Perrin, G.Louis, *J.Appl.Phys* 77(6) (1995) 2292

CHAPTER III

PREPARATION AND OPTICAL CHARACTERIZATION OF CERTAIN R.F. PLASMA POLYMERIZED THIN FILMS

3.1 INTRODUCTION

The term *Plasma* is derived from the ancient Greek language, which meant, 'that what is built' or 'that what is formed'. In modern language *Plasma* describes the state of ionized gas. An ionized gas mainly consists of positively charged (ionized) molecules or atoms (ions) and negatively charged electrons. Crookes (1879) was the first to give a description of this ionized gas. Finally, fifty years later in 1928, the fourth state of matter was given its own name by Irving Langmuir, when he introduced the term *plasma* in his studies of electrified gases in vacuum tubes. Each and every person has his/her own encounter with plasma. Lightning for instance is an electric discharge in air and can be considered as plasma. In general when a molecule is subjected to a severe condition such as intense heat, ionization of the molecule occurs. The classical definition of Plasma limits the term to an appreciably ionized gas or vapour that conducts electricity and is at the same time electrically neutral fluid, hot and viscous. However, modern definition of plasma is less restrictive; the term simply denotes a more or less ionized gas. A gaseous complex that may be composed of electrons, ions of either polarity, gas atoms and molecules in the ground or any higher state of any form of excitation as well as light quanta is referred to as plasma. Plasma in this sense may be called cold and can be generated using different techniques [1,2,3,4,5]. Plasma created from an electric glow discharge is often called low temperature plasma to distinguish it from hot plasma.

In laboratory, combustion, flames, electric discharge, controlled nuclear reactions, shocks and other means generate plasma. Since plasma loses energy to its surroundings mainly by radiation and conduction to the walls in order to maintain plasma state continuously in a laboratory apparatus, energy must be supplied as fast as it is lost. In order to maintain plasma state for a relatively long period of time, the most obvious and most common method is the use of electric discharge. Most experimental work in the study of polymerization is carried out using some kind of electric discharge. There are many types of electric discharges, all characterized by the presence of free electrons and or an electric field. Among the many types of electric discharge, all are characterized by the presence of free electrons and or an electric field. Among these, glow discharge is by far the most frequently used in plasma polymerization.

Hence, Plasma polymerization refers to formation of polymeric materials under the influence of plasma (partially ionized gas), which is generated by some kind of electric discharge. However, little attention was paid either to the properties of these materials or to the process as a means of forming useful materials as these materials were initially regarded undesirable. At the earlier stages of the discovery, the plasma polymerization technique was not treated as standard method for preparation of polymers [1,3]. These methods gained importance when they were used to make special coatings on metals and began to be recognized as techniques for synthesizing polymers.

Although a great number of research studies have been published and numerous potential application and uniqueness of polymer formation process have been demonstrated, the subject has not drawn much academic interest as a new subject area of polymer science. This is largely due to the fact that the very unique and advantageous feature of forming insoluble, infusible polymers has hampered the basic study of the process at the molecular level. The well recognized concept of conventional polymerization is based on molecular processes by which the size of the molecule increases. The arrangement of atoms that constitute the molecules of a monomer is accomplished during the organic synthesis of the monomer. During the polymerization of a monomer rearrangement of atoms within a molecule seldom occurs. However, polymer formation in plasma is recognized as an atomic process in contrast to the above molecular process.

In short, plasma polymerization was dealt with in the 1960's and 1970's as a new and exotic method of polymerization. But the materials formed by plasma polymerization are significantly different from conventional polymers and also differ from most inorganic materials. Plasma polymers have no repeating monomer units unlike the conventional polymers processed through ionic or radical mechanisms. They are composed of a mixture of molecules cross-linked or fragmented and rearranged from monomer molecules. Thus, the technique can be considered as a method for forming new types of materials rather than a method of preparation of conventional polymers. Certain molecules, which cannot be polymerized conventionally because of the absence of active species to propagate the polymer chain can be plasma polymerized.

Initially polymers formed under the plasma conditions were recognized as an insoluble deposit that provided only difficulty in cleaning and nothing else. The two most important characteristics of this undesirable deposit, which are the most sought later, in modern technology of coatings, are excellent adhesion to substrate materials and strong resistance to most chemicals. There are various steps involved in obtaining a good coating by conventional methods while with the plasma polymerization technique, a single step can produce a good polymer coating. Thus, simplicity also favours plasma polymerization technique.

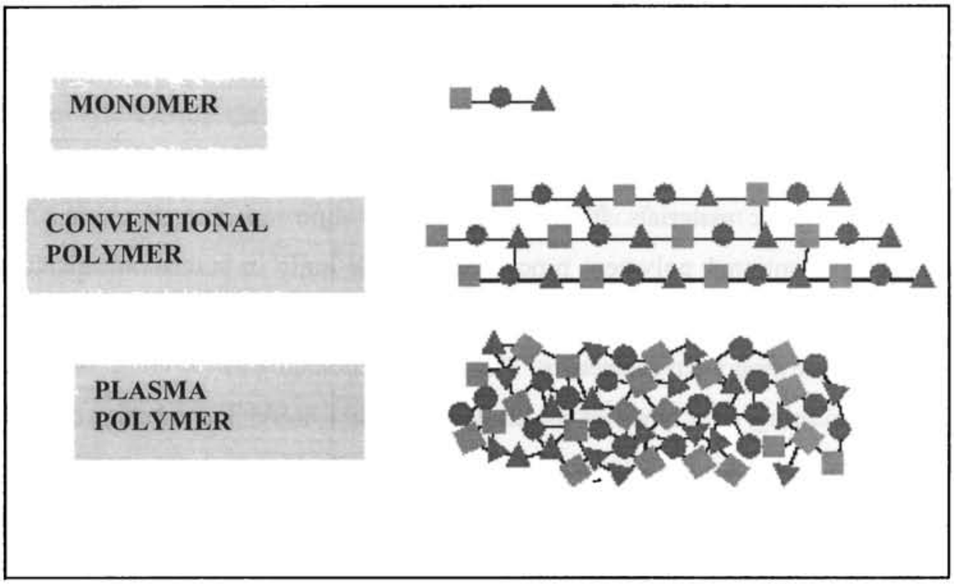

Figure 1: differentiates the plasma polymer from a conventional polymer of the same monomer

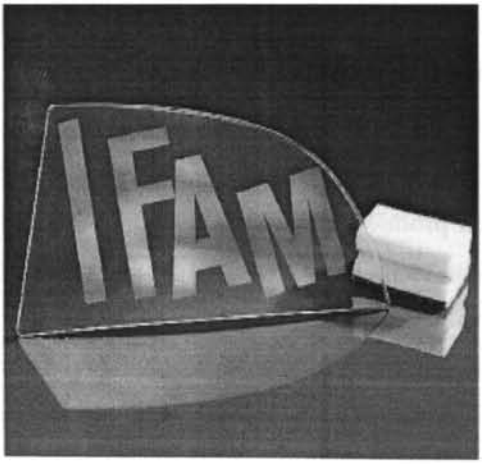

Figure 2

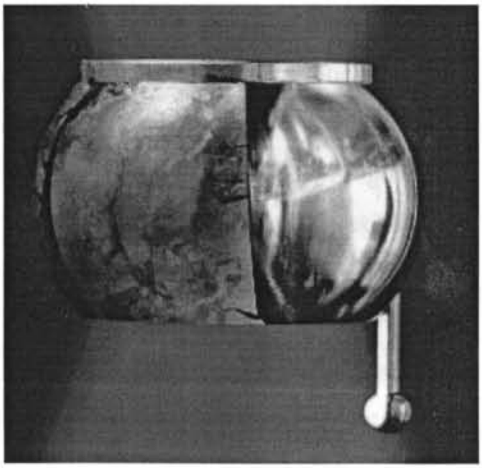

Figure 3

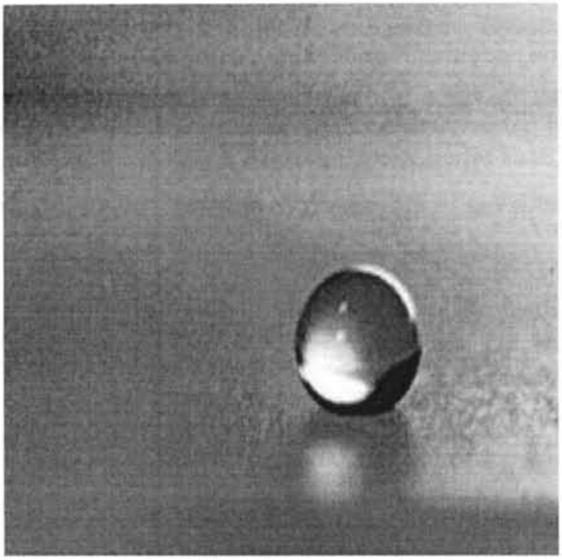

Figure 4

Figure 2:Scratch resistant layer on a polycarbonate pane. The fields that are recognized as letters are uncoated. After treatment with a sponge it becomes obvious that these fields are more severely attacked than the coated fields.

Figure 3: Ship lamp of Aluminium, left side uncoated, right side coated with a plasma-polymeric anticorrosive layer, after salt-spray-test..

Figure 4: Water drop on a surface being coated by plasma-polymerization

Figure 1 gives a general idea of conventional polymerization and plasma polymerization. The plasma polymerized thin films are highly adhesive, pinhole free, dielectric, hydrophobic, cross-linked, highly branched and highly resistant to physical and chemical treatment [1, 6-12]. Some of the aspects of these films are exhibited in figures 2-4.

Chemical reactions occurring under the plasma conditions are generally very complex and consequently are non-specific in nature. These polymerization techniques are advantageous when special excited states are required as intermediate states. This cannot be achieved using other conventional polymerization techniques. Thus, plasma polymerization is recognized as special means of preparing unique polymers that cannot be made by other methods.

Generally, many bulk properties of polymer films such as permeability, electric volume, resistivity and dielectric constant can be considered as characteristic material constants. The parameters do not change as the thickness of the film varies. This is true for a film as its thickness is above a certain critical value i.e. 0.05 - 0.1μm depending upon the parameters under consideration. As the thickness of the film is below a critical value, the constancy of the parameters is no longer observed. This might be probably due to the increased contribution of flaws to the total film. As the thickness of the film decreases the contribution from the flaws to the film increases. It is difficult to prepare flawless films with thickness below a critical value. However, with plasma polymerization, we can obtain ultra thin film containing minimum amount of flaws, which is a valuable asset in material characterization [1].

Before discussing in detail the mechanisms of formation of polymeric materials in plasma, it is necessary to review some of the fundamental aspects of polymerization.

According to the growth mechanisms, polymerization is classified into two. a) **step-growth polymerization** and b) **chain-growth polymerization** [1, 13].

3.1.1 STEP GROWTH POLYMERIZATION

In **step-growth polymerization**, a polymer is formed by the step-wise repetition of the same reaction. If the monomer is represented by M, and the growing molecules by M_l, step growth polymerization can be represented by

$$M_1+M=M_2+H_2O$$

$$M_2+M=M_3+H_2O$$

$$M_m+M_n=M_{n+m}+H_2O$$

It is seen that the reaction at each step is identical to the first reaction. Since the overall polymerization is the multiplication of the same reaction, the enthalpy change ΔH, entropy change ΔS and the Gibb's free energy change ΔG for overall polymerization are nearly identical to those in each step as long as the condition that the reactivities of the functional groups are independent of the size of the reacting molecules.

3.1.2 CHAIN GROWTH POLYMERIZATION

In **chain-growth polymerization**, a long chain molecule is formed by a series of consecutive steps that is completed in a very short time. In this case, products are only final polymers. Unlike the case of step growth polymerization, intermediate size molecules cannot be isolated. Consequently, entire polymer formation can be essentially considered a one step process, as long as the concept of chemical reaction that relies on the identification of reactants and products is concerned.

If the chain carrying species is indicated by M* and the monomer by M, the chain growth mechanism can be shown by

$$M^* + M = M_2^*$$

$$M_2^* + M = M_3^*$$

$$M_n^* + M = M_{n+1}^*$$

&

$$\mathbf{M_m^* \rightarrow M_m}\ \textbf{(Polymer)}$$

The first three reactions represent the propagation reaction and the last reaction in which the chain carrying species is lost is the termination reaction. In short, in the step growth polymerization, each growth step is a chemical reaction between two molecules whereas in chain growth polymerization, each individual growth step is a chemical reaction between a chain carrying species and a molecule.

A typical example of the chain growth polymerization is the **addition polymerization**. Depending on the nature of the reactive species, the addition polymerization can be classified as *free radical polymerization, cationic polymerization, anionic polymerization* and so on.

Free radical polymerization:

Since most of the studies of plasma polymerization suggests that free radicals are the most likely reactive species in the formation of polymers under plasma conditions, it is necessary to review the fundamental aspects of free radical polymerization. The reactions of the free radical polymerization can be looked upon in four steps.

Step 1: Initiation

$$I \xrightarrow{K_d} 2R$$

$$R\bullet + M \xrightarrow{K_f} M\bullet$$

Step 2: Propagation

$$M\bullet + M \xrightarrow{K_p} MM\bullet$$

$$M_n\bullet + M \xrightarrow{K_p} M_{n+1}$$

Step 3: Termination

Recombination $$M_m\bullet + M_n \xrightarrow{K_{t,c}} P_{m+n}$$

Disproportionation $$M_m\bullet + M_n\bullet \xrightarrow{K_{t,d}} P_m + P_n$$

Step 4: Chain Transfer

$$M_n\bullet + A \xrightarrow{K_{tr}} P_n + A$$

$$A\bullet + M \xrightarrow{K_{tr}} M\bullet + A$$

The important aspects of free radical polymerization are 1) The rate of polymerization is proportional to the square root of the initiator concentration or the square root of the rate of initiation. 2) The degree of polymerization is inversely proportional to the square root of the square root of the initiator concentration or the square root of the rate of initiation.

Hence, faster polymerization leads to shorter chain length of the resulting polymer.

Ionic polymerization

Depending on whether the chain carrying reactive species is electrophilic initiator or nucleophilic initiator they are classified into *cationic polymerization* or *anionic polymerization* respectively. In the following schematic representations, electron used in the A-B bond are represented by 'dot' and the electron in monomer double bond is expressed by 'colon'.

Electrophilic Initiator:

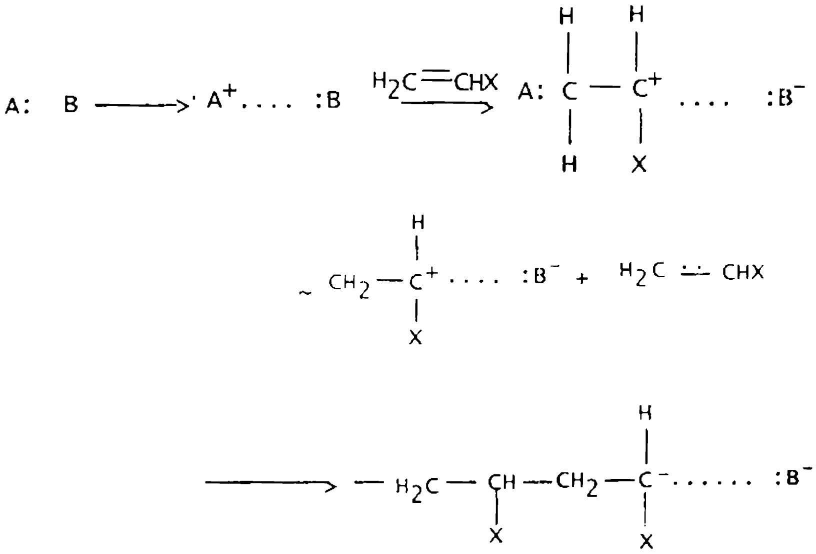

This is also referred to as cationic polymerization.

Nucleophilic Initiator:

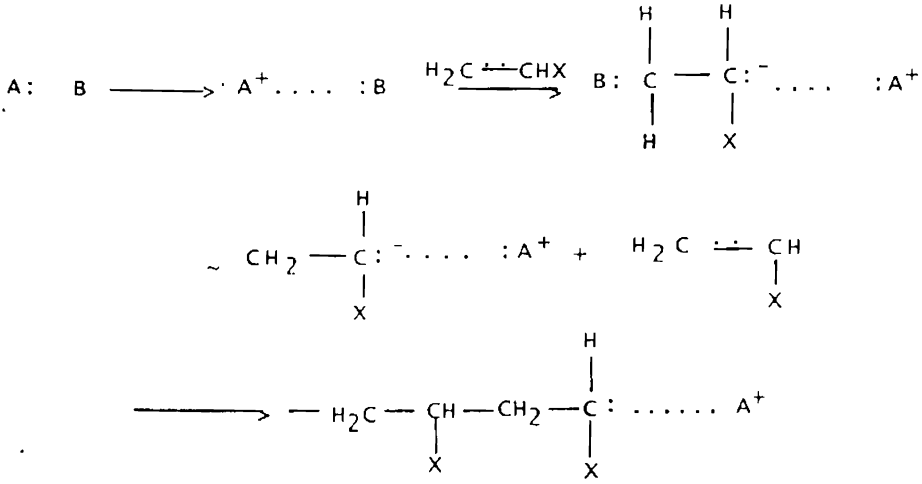

This is referred to as anionic polymerization.

The difference between ionic polymerization and free radical polymerization is the fact that the growing chains in ionic polymerization are accompanied by corresponding counter ions. Therefore in ionic polymerization, chain propagation is highly dependent on the type of initiation (which determines the counter ion) and the nature (particularly the dielectric constant) of the solvent used in the polymerization. In the case of free radical polymerization, the reactivity of growing chain is nearly independent of the nature of R or of the type of solvent. The initiator moiety R remains at the non- reactive end of the growing chain. Another notable difference is in the mode of chain termination. In ionic polymerization, the growing chain possesses the electric charge and two growing chains cannot react due to the coulombic repulsion of two similarly charged species. Hence, the termination by a molecular reaction of the growing chain is absent in the cationic and anionic polymerizations. Therefore, the termination occurs by other reactions such as chain transfer and reactions with impurities. On the contrary in free radical polymerization, the chain termination occurs by reaction between two free radicals (growing chains). Consequently, the termination is an apparent monomolecular reaction (first-order reaction).

3.1.3 RADIATION POLYMERIZATION:

Polymerization initiated by ionizing radiation such as γ rays from ^{60}Co or high-energy beams is somewhat similar to Plasma polymerization. For elucidating the mechanism of plasma polymerization, an understanding of radiation polymerization is helpful.

The significant difference between radiation polymerization and the polymerizations discussed so far is that no initiator is employed in radiation polymerization. The chain carrying species are created by ionization of a monomer molecule. It is this aspect of radiation-induced polymerization, which is similar to plasma polymerization.

Under irradiation, the monomer is ionized ejecting an electron forming a cation radical $M^{+\cdot}$

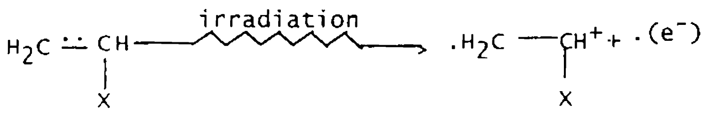

$$H_2C = \underset{X}{\underset{|}{CH}} \xrightarrow{\text{irradiation}} \cdot H_2C - \underset{X}{\underset{|}{CH^{+}}} + \cdot (e^{-})$$

The cation radical and the ejected electron may either recombine or separate depending upon the distance of the initial separation. A cation radical that is sufficiently separated from electron will then proceed with the polymerization procedures.

The cation radical first adds to another monomer forming a dimer structure that has a free radical at one end (expressed by.) and a cation site at the other end.

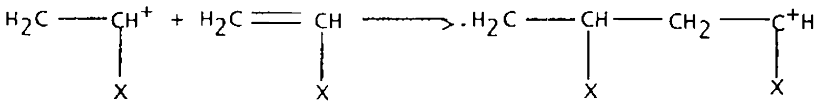

$$H_2C-\underset{X}{\underset{|}{C}}H^{+} + H_2C=\underset{X}{\underset{|}{C}}H \longrightarrow \cdot H_2C-\underset{X}{\underset{|}{C}}H-CH_2-\underset{X}{\underset{|}{C}}{}^{+}H$$

Propagation then proceeds independently at each site according to the respective characteristic rate constant of the particular active site.

At the same time, some of the ejected electrons from the initial ionization are captured by monomers to form anionic radicals $\underline{\mathbf{M}^{-\cdot}}$. The anionic radicals also then add to another monomer to form dimeric structure with free radical at one end and an anionic site at the other. Propagation again proceeds independently at each active site according to the respective rate constants of the anionic and free radical polymerization.

Radiation induced polymerization differs from the polymerization by an initiator in that (i) free radical and ionic polymerization co-exist, (ii) ion radicals contribute to the initiator reaction and (iii) ionic sites have no counter ions.

3.1.4 PARYLENE POLYMERIZATION:

This kind of polymerization can be described as a rapid step- growth polymerization by polycombination of difunctional active species. The reactive species, hence do not add onto the monomer but they react with each other to form polymer. In this sense, this kind of polymerization differs from the classes of polymerization discussed in the preceding sections.

Parylene polymerization utilizes a dimer of p-xylylene or p-xyleylene derivatives. Unsubstituted p-Xylene dimer is designated as Parylene N where as monochloro substituted dimer is designated as Parylene C. Various other kinds of substitution are also possible.

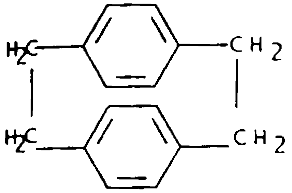

Parylene N

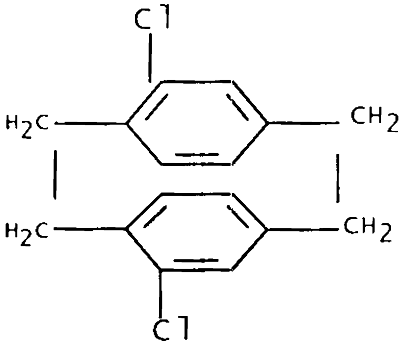

Parylene C

Parylene C is used industrially and in research applications whereas Parylene N is used in the study of Parylene polymerization and characterization of polymer properties. In Parylene polymerization process, the system is first evacuated to the level of 10^{-3} to 10^{-2} Torr with a known amount of dimer charged in the sublimation chamber. Then the sublimation chamber is heated to 120-160 ^{0} C and the cracking chamber is heated to 600-650 ^{0} C respectively. The sublimated dimer molecules dissociate into p-Xylene at the cracking temperature.

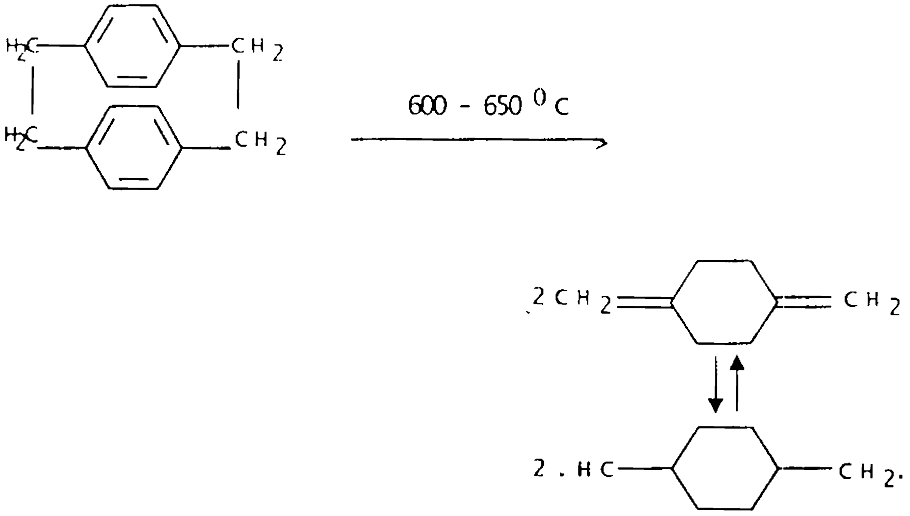

The cracked species reach the deposition chamber, which is at room temperature and the polymer is deposited on the surface, including the wall of the reaction chamber. The polymer formed is often highly crystalline and insoluble in organic solvents.

Hence among the polymerizations described, plasma polymerization is close to radiation polymerization and parylene polymerization. The radiation polymerization is similar to plasma polymerization in that the primary step is the ionization of monomers. However, radiation polymerization does not yield polymers in vacuum. The similarity between plasma polymerization and parylene polymerization is in the formation of polymer deposits in vacuum and differ in that parylene polymerization does not involve the ionization process. In short, plasma polymerization can be viewed as a hybrid of these two polymerization mechanisms.

3.2 PLASMA SOURCES

In the plasma polymerization, plasma of the monomer vapour is generated by different sources like

a) ***Direct current (DC) Glow Discharge:*** This can be established by passing a D.C. electric current through gas under low pressure. The cathode is bombarded with positive ions, which results in the generation of secondary electrons. These electrons are accelerated away from cathode until they gain sufficient energy to ionize the gas molecules or atoms that collide with the electrons.

b) ***Alternating Current Glow Discharges:*** The polymerization mechanism depends upon the frequency of alternation. Some of the AC discharges are given below.

Silent Discharge: In the typical arrangement, the discharge tube consists of a co-axial section and the linear and outer surfaces of the co-axial sections are connected to high ac voltage of 1000V and a frequency of 50 to 60 Hz. The polymerization takes place near the electrodes.

Low Frequency Discharge: Two metal electrodes are placed inside a reactor and is connected to a variable high voltage source. The required voltage depends upon the pressure, the nature of the substance and the distance between the electrodes.

Microwave discharge: Plasma can be produced using microwave generators of few kW powers and is found to be successful with inorganic compounds.

R.F. Discharge: At frequencies above 1MHz., no direct contact between electrodes and plasma is necessary. Hence in r.f plasma polymerization, the energy can be fed to plasma by inductive or capacitative coupling. Hence r.f plasma can be initiated and sustained by external electrodes at a much lower voltage than it is required for maintaining DC glow discharges.

This chapter describes the method of preparation of plasma polymerized thin films and investigations on their structural and optical characteristics, which include the analysis of FTIR spectra, absorption spectra and transmission spectra. The IR spectra give information about possible bond linkages, whereas the optical parameters like direct and indirect band gaps and refractive indices are evaluated from the absorption and transmission spectra.

3.3 PREPARATION OF PLASMA POLYMERIZED THIN FILMS

Three different polymers namely poly o-toluidine, poly m-toluidine and poly diethyl aniline are prepared in a plasma deposition system comprising of an r.f. generator source that uses four 807 RCA tetrode valves. The tuned plate, tuned grid r.f. source oscillates in the frequency range 4.5 to 13 MHz and has an output power of 35 Watts. Poly-o toluidine and poly m-toluidine are prepared at a frequency of 6MHz and poly diethyl aniline at a frequency of 7 MHz. The deposition chamber is a long tube of length 35cms and diameter of 3.5 cms. The energy is fed to the deposition chamber by capacitative coupling using aluminum foils for maintaining plasma. The tube is connected to a rotary pump and is evacuated to a pressure of 10^{-2} Torr. The monomer flow into the tube is regulated using a manually operated needle valve.

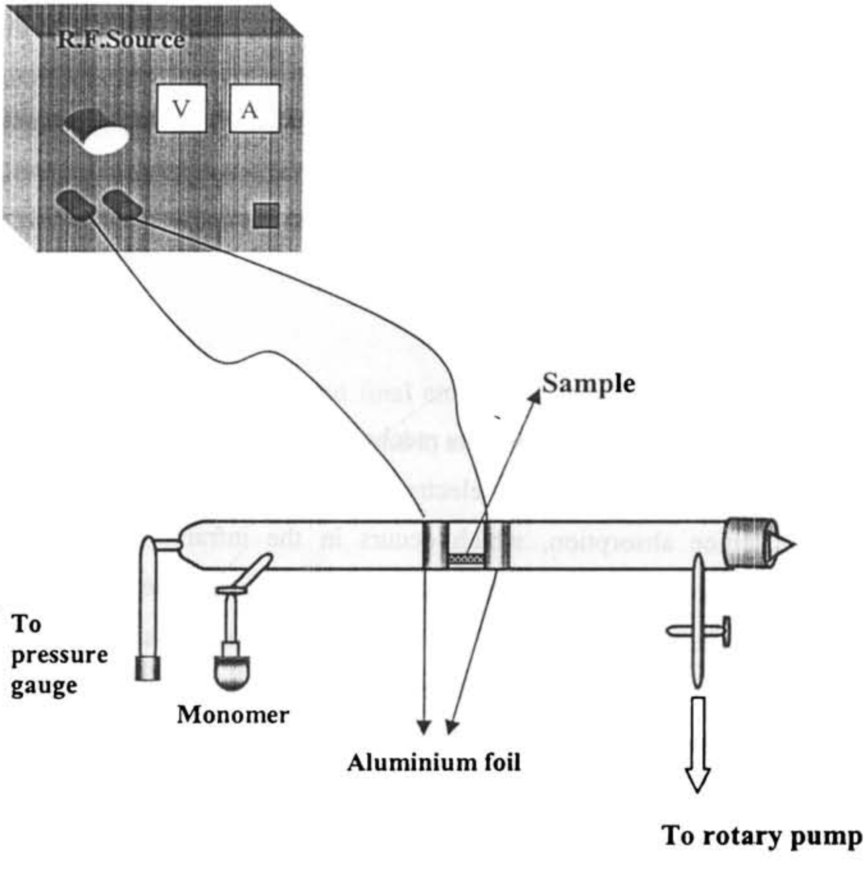

Figure (5): Schematic of the plasma polymerization unit.

The polymer thin films are prepared on optically flat glass slides of dimensions 75 x 25 x 1.4 mm. The glass plates are first cleaned in running water and are immersed in chromic acid for about 1-2 hours in order to remove alkaline impurities. The slides are then washed in distilled water and are cleaned ultrasonically. The microscopic impurities are stripped off by ultrasonic agitation in water. The glass slides are then dried and placed in the deposition chamber. The chamber is evacuated to a pressure of approximately 10^{-2} Torr keeping the monomer needle valve closed. The r.f. power is switched on and a bluish glow appears in between the electrodes. The monomer needle valve is opened gradually. After a deposition time of about 25-30 minutes, a thin film of the corresponding polymer is coated on to the glass plate.

3.4 OPTICAL CHARACTERISATION

3.4.1 BANDGAP MEASUREMENTS:

Optical absorption in solids occurs by various mechanisms. In all cases photon energy will be absorbed by the lattice or by electrons and transferred energy will be conserved. The lattice absorption, which occurs in the infrared region of the spectrum, gives information about the atomic vibrations involved. The higher energy parts of the spectrum associated with the inter-band electronic transition, provides information about the electron states. In such process, the electrons are excited from a filled band to empty band by the absorption of photons. This results in a sharp increase in the absorption coefficient and the onset of this rapid change in absorption coefficient is called the *fundamental absorption edge*. The corresponding energy is referred to as the *optical energy-gap* or the *band gap energy*. There are two kinds of optical transitions at the fundamental absorption edge of crystalline and amorphous solids- *direct absorption* (or *transition) and Indirect absorption* (or *transition).*

a) DIRECT ABSORPTION

For a direct transition from the valence band to the conduction band, the wave vector of the electron must be conserved. This can be explained as follows: In any optical transition process, the total energy and momentum of the electron-photon system must be conserved. i.e.

$$E_f = E_i + h\nu; \quad k_f = k_i + q;$$

where E_i and E_f are the initial and final energies of the electron in the valence and conduction bands respectively and k_i and k_f are the corresponding electron momenta.

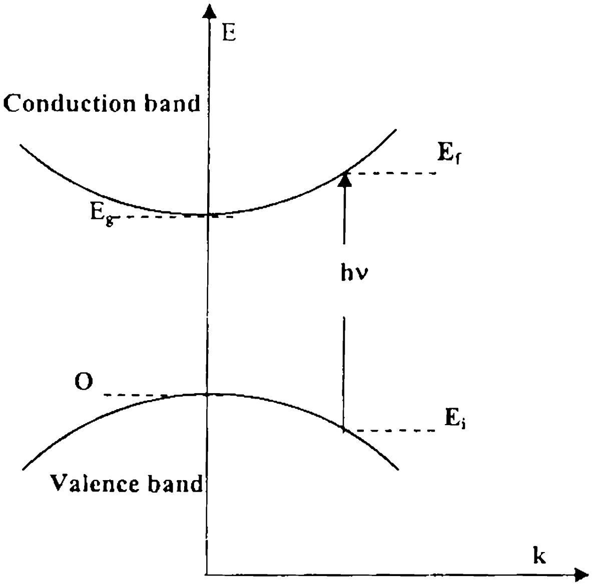

Figure 6: Direct Absorption

'q' is the wave vector of the absorbed photon. The wave vector of the photon in the optical region is usually small. The momentum condition therefore reduces to

$$\mathbf{k}_f = \mathbf{k}_i$$

Hence the momentum of electron alone is conserved. This selection rule indicates that only vertical transitions are allowed between the valence and conduction band. The bottom of conduction band and top of valence band lies at k=0 as shown in figure (6) so that electrons near the top of valence band can make direct transition to the states near the bottom of conduction band.

The density of states for a direct transition is given by [14]

$$N(E) = \frac{(2m_r)^{3/2}}{2\pi^2\hbar^3}(h\nu - E_g)^{1/2}$$

Theoretically by this equation, at $h\nu = E_g$, N (E) =0; In reality this is wrong. This means that the density of states is not nil in the band gap of the material and their presence is attributed to the *band tails*. Band tails are nothing but perturbation of the conduction and valence bands by the formation of tails of states extending the bands into the energy gap (figure (7)). These are referred to as localized states and are characteristic of amorphous solids or when defects, impurities etc are present.

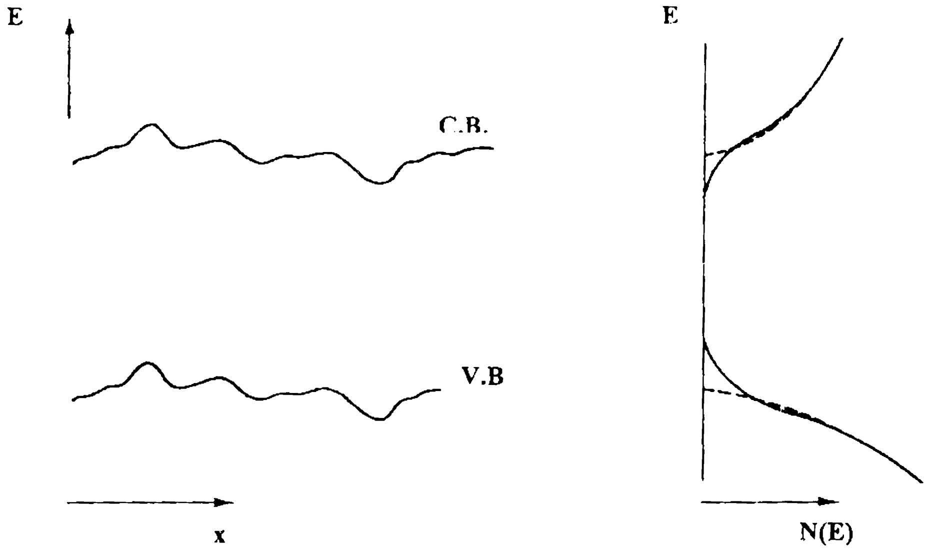

Figure (7): The left diagram shows the perturbation of the band edges by Coulomb interaction with inhomogeneously distributed impurities. This leads to the formation of tails of states shown on the right side. The dashed lines show the distribution of states in the unperturbed case.

The transition between the band tails causes an exponentially increasing absorption coefficient α , $(d(\ln\alpha)/d(E)=1/kT)$ and is known as **Urbach's rule.**

Hence in amorphous materials, three different types of optical transitions are to be dealt with as shown in figure (8). They are

1) ***Extended to extended transitions***:

The transitions from extended to extended states are very similar to the ones known from crystalline materials. The absorption coefficient in this case has the form [15,16]

$$\alpha h\nu = A\left(h\nu - E_g\right)^{1/2}$$

where 'α' is the absorption coefficient, '$h\nu$' is the energy of absorbed light A is a constant for different transitions indicated by the different values of 'm'. $(\alpha h\nu)^2$ is to be plotted against $h\nu$ in eV to determine the allowed direct transition energy band gap from the intercept of the extrapolation of $(\alpha h\nu)^2$ to zero on the photon energy axis.

2) ***Localized to extended and extended to localized transitions***:

In ideal crystalline materials, no transition takes place in the gap. However, in amorphous materials, there can be transitions from occupied extended states of valence band to empty tail states of conduction band and also from occupied tail states of valence band to empty extended states of conduction band. Both these transitions will have similar matrix elements. The density of states of localized states decays exponentially into the gap. Hence for transitions from localized to extended states and for extended to localized states, there is an exponential relation between absorption coefficient and frequency [17].

$$\alpha(\omega) \sim \exp\left(\frac{\hbar\omega}{E_u}\right)$$

where E_u is called the Urbach energy.

Since

$$\ln\alpha(\omega) = C + \frac{\hbar\omega}{E_u}$$

$$E_u = \frac{\hbar}{\frac{d}{d\omega}(\ln\alpha(\omega))}$$

Hence Urbach energy can be obtained from the inverse of the slope of plot between *ln* $\alpha(\omega)$ and frequency (ω).

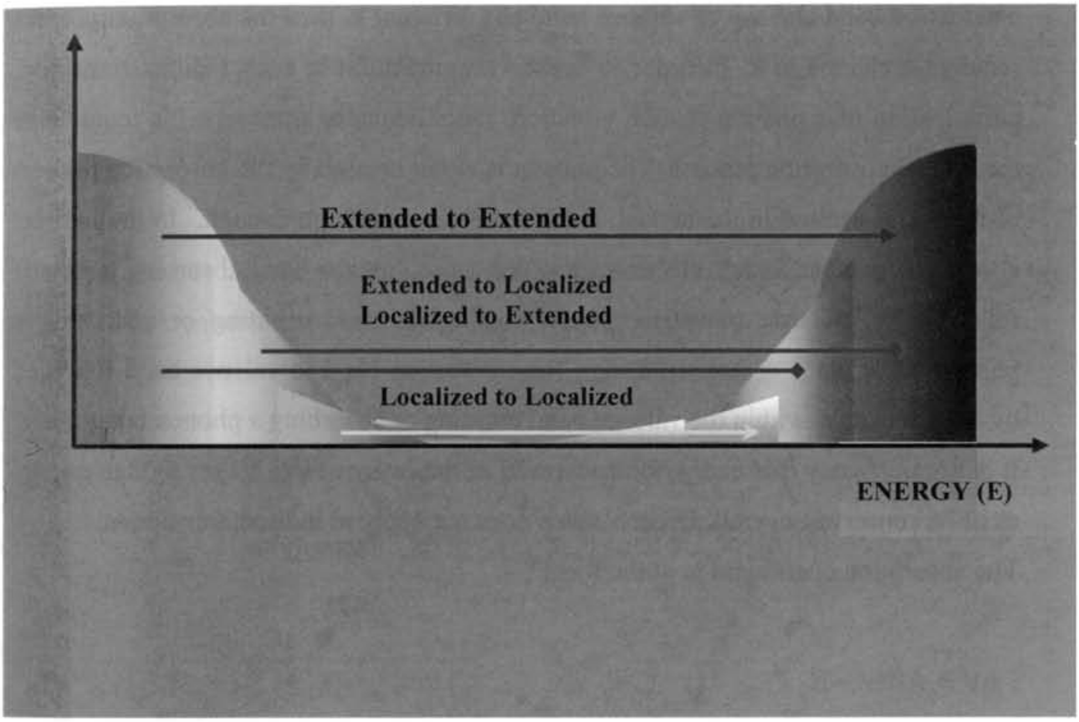

Figure (8): Different optical transitions involved in the direct absorption.

3) ***Localized to localized transitions*:** These transitions usually are not very important since the number of states involved is low and the transition matrix elements are significantly smaller compared to those of the above-mentioned transitions. This is due to the fact that the matrix elements are integrals over all space over the product of two functions (the initial and the derivative of the final state) which are separated in space and hence do exhibit almost no overlap. Transitions from localized to localized states would lead to absorption in the low energy regions of the spectrum which in most cases is the near to mid infrared region.

b) INDIRECT ABSORPTION:

As seen in direct absorption, if the bottom of conduction band and top of valence band lies at the same k (momentum) value then absorption process do not require change in k and hence direct transition is possible. However, if the bottom of conduction band and top of valence band has different k, then the absorption process requires a change in k. In order to conserve momentum in such indirect transition, participation of a phonon (lattice vibration, longitudinal or transverse) is required in the optical absorption process. The phonon is either created by the absorption process or thermally excited in the crystal, if the temperature is high enough. In the indirect absorption process, either electron transition from valence band absorbing a photon followed by electron transition within conduction band emitting or absorbing a phonon takes place or hole transition for conduction band to valence band followed by hole transition within the valence band emitting or absorbing a phonon takes place. It is not necessary that energy be conserved in the intermediate stages though energy must be conserved overall. Urbach's rule does not apply to indirect transitions.

The absorption coefficient is of the form

$$.\ h\nu = A\left(h\nu - E_g\right)^2$$

Hence the intercept on x-axis of the plot of $(\alpha h\nu)$ vs. $h\nu$ in eV gives the indirect band gap energy in eV.

3.4.2 REFRACTIVE INDEX MEASUREMENTS

The refractive index of a dielectric film can be determined by the measurement of the transmission T of light through the film using a simple method suggested by J.C.Manifacier etal [18].

Consider a thin film with a complex refractive index $\eta = n - ik$, bounded by two transparent media with refractive indices n_0 and n_1. Considering unit amplitude for the incident light, in the case of normal incidence, the amplitude of the transmitted wave is given by

$$A = \frac{t_1 t_2 \exp\left(-2\pi i \eta t / \lambda\right)}{1 + r_1 r_2 \exp\left(-4\pi i \eta t / \lambda\right)} \qquad (1)$$

in which t_1, t_2, r_1, r_2 are the transmission and reflection coefficients at the front and rear faces. The transmission of the layer is given by

$$T = \frac{n_1}{n_0} |A|^2 \qquad (2).$$

In the case of weak absorption with $k^2 << (n - n_0)^2$ and $k^2 >> (n - n_0)^2$

$$T = \frac{16 n_0 n_1 n^2 \alpha}{C_1^2 + C_2^2 \alpha^2 + 2C_1 C_2 \alpha \cos\left(4\pi n t / \lambda\right)} \qquad (3)$$

where $C_1 = (n + n_0)(n_1 + n), C_2 = (n - n_0)(n_1 - n)$ and

$$\alpha = \exp\left(-4\pi k t / \lambda\right) = \exp(-Kt) \qquad (4)$$

K is the absorption coefficient of the thin film.

Generally outside the region of fundamental absorption ($h\nu > E_g$ thin film gap) or of the free carrier absorption (for higher wavelengths), the dispersion of n and k are not very large. The maxima and minima of T in equation (3) occurs for

$$4\pi nt/\lambda = m\pi \qquad (5)$$

where m is the order number. In the usual case ($n>n_1$, $C_2< 0$), the extreme values of transmission are given by the formulae

$$T_{max} = 16n_0n_1n^2\alpha / (C_1 + C_2\alpha)^2 \qquad (6)$$

$$T_{min} = 16n_0n_1n^2\alpha / (C_1 - C_2\alpha)^2 \qquad (7)$$

By combining equations (6) & (7), Lyashenko and Miloslavskii developed an iterative method allowing the determination of n and α. J.C.Macifer etal proposed a simplification of this method by considering T_{min} and T_{max} as continuous functions of λ through n (λ) and α (λ). The ratio of equations (6) and (7) gives

$$\alpha = \frac{C_1\left[1-\left(T_{max}/T_{min}\right)^{1/2}\right]}{C_2\left[1-\left(T_{max}/T_{min}\right)^{1/2}\right]}$$

Then from equation [illegible]

$$n = \left[N + \left(N^2 - n_0^2 n_1^2\right)^{1/2}\right]^{1/2}$$

where $N = \frac{n_0^2 + n_1^2}{2} + 2n_0n_1 \frac{T_{max} - T_{min}}{T_{max}T_{min}}$

The above equation shows that n is explicitly determined from T_{max}, T_{min}, n_1 and n_0 at the same wavelength.

A Hitachi model U-3410 UV-Vis-NIR spectrophotometer is used to record the absorption and transmission spectra of the plasma polymerized samples. The optical absorption and transmission of samples prepared on glass substrate is measured against a blank substrate as reference. Direct band gap, indirect band gap and Urbach energy of the three plasma polymerized samples are determined form the absorption spectra and refractive indices of the corresponding samples are determined from the transmission spectra.

Figure (9) shows the absorption spectrum of the poly o toluidine thin film. The direct and indirect band gaps are determined from the plots (10) and (11) respectively. From the graph (12), Urbach energy is calculated. The transmission spectrum of the thin film sample is as shown in figure (13).

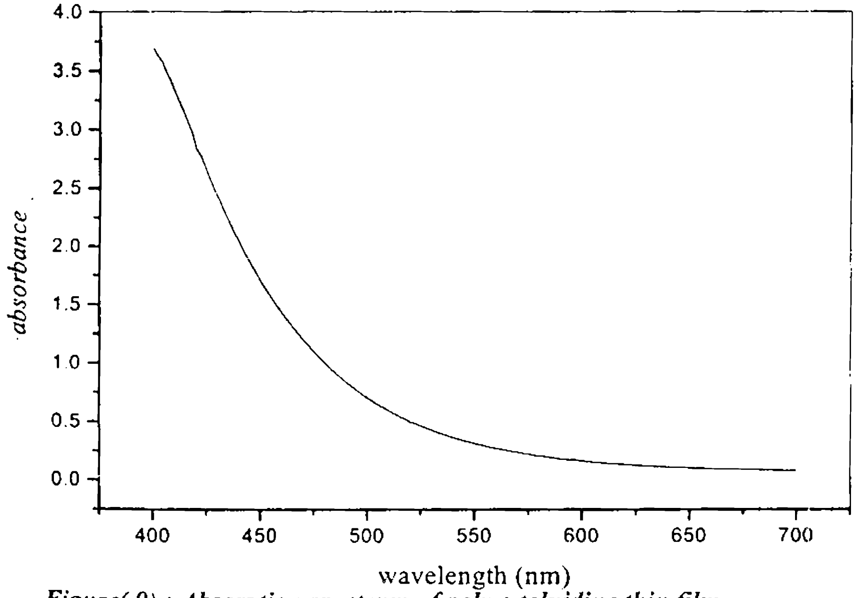

Figure(9) : Absorption spectrum of poly o toluidine thin film

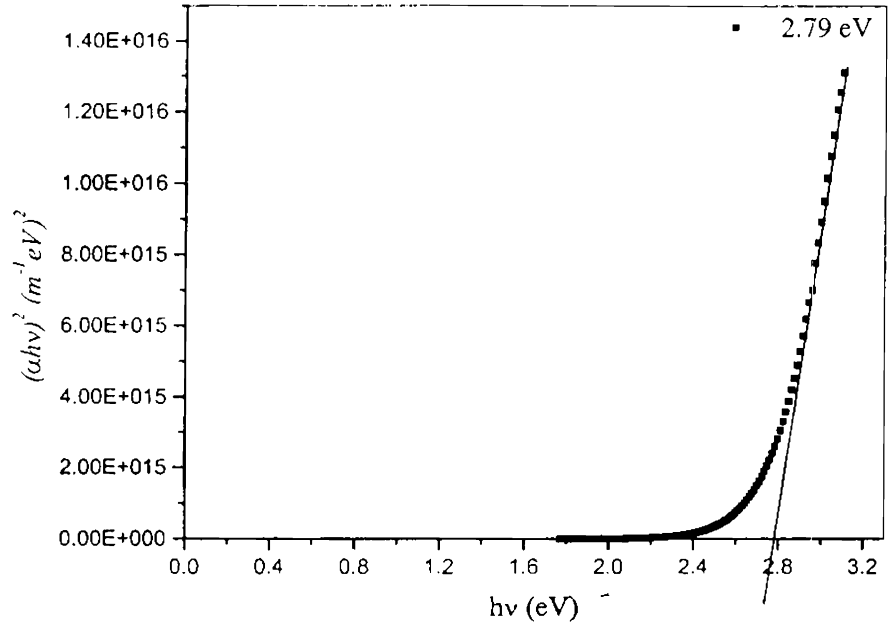

Figure (10): $(\alpha h\nu)^2$ vs. $h\nu$ plot for determining the direct band gap energy

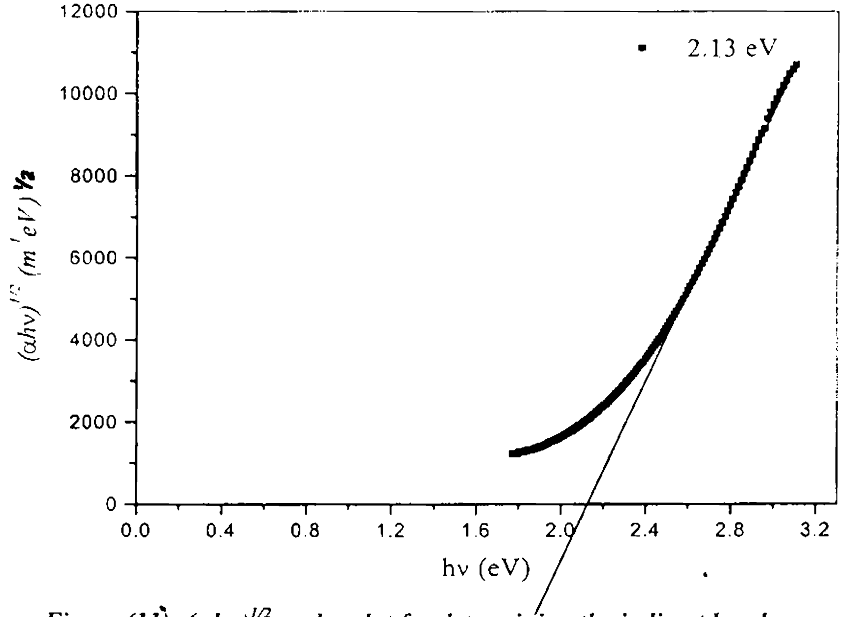

Figure (11): $(\alpha h\nu)^{1/2}$ vs. $h\nu$ plot for determining the indirect band gap energy

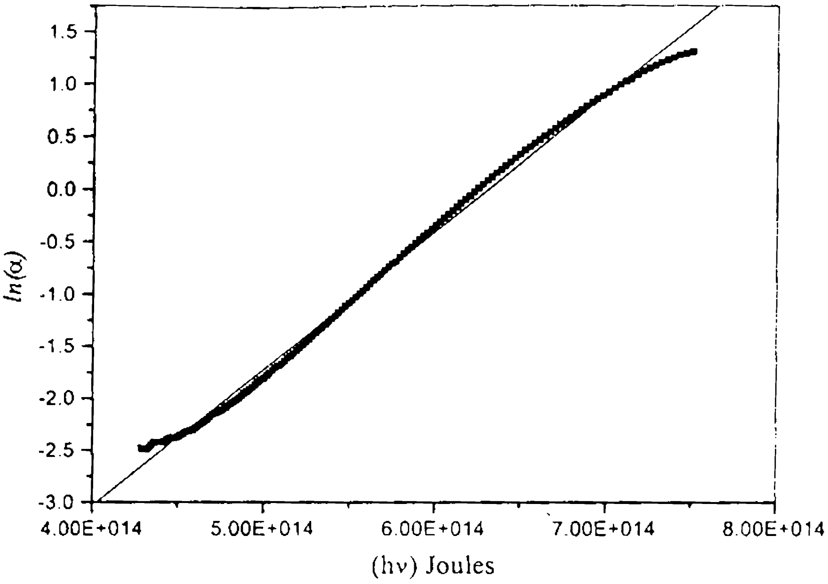

Figure (12): ln(α) vs hν (Joules) plot for determining the Urbach energy

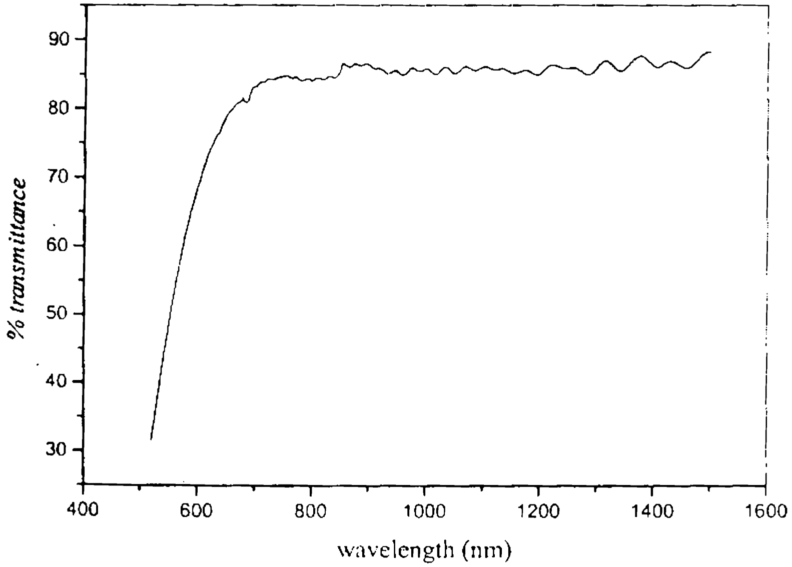

Figure (13): Transmission spectrum of poly o toluidine

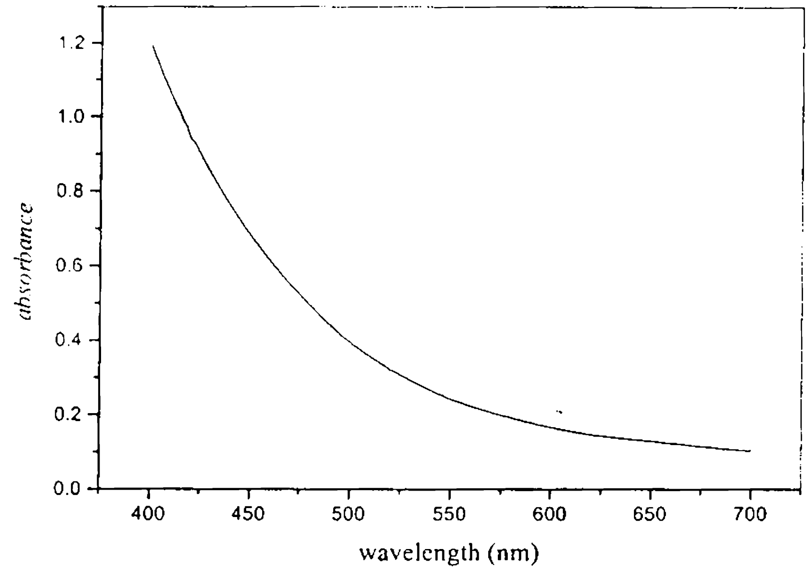

Figure (14): absorption spectrum of poly m toluidine

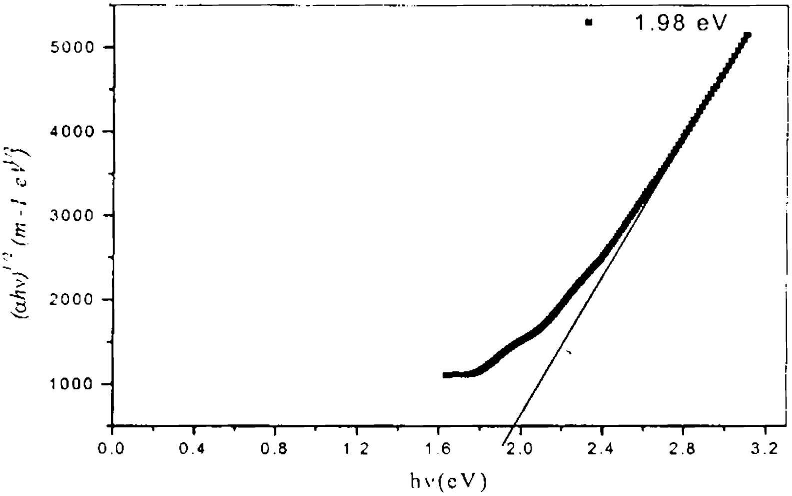

Figure (16):$(\alpha h\nu)^{1/2}$ vs. $h\nu$ in eV for determining the indirect bandgap energy

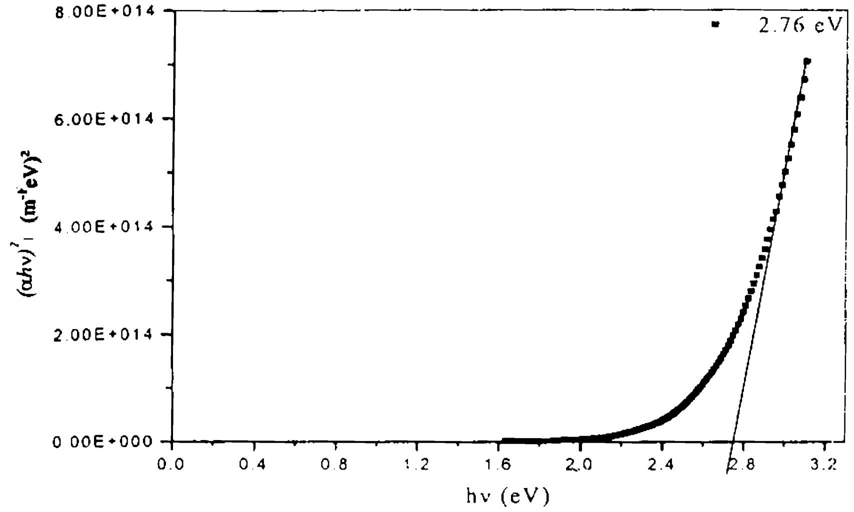

Figure (15): $(\alpha h\nu)^2$ vs. $h\nu$ in eV for determining direct band gap energy

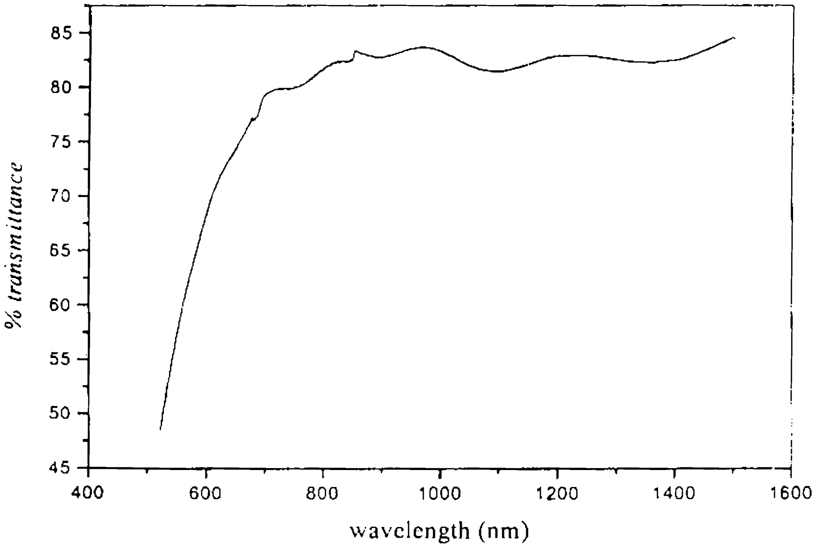

Figure (17): Transmission spectrum of poly m toluidine

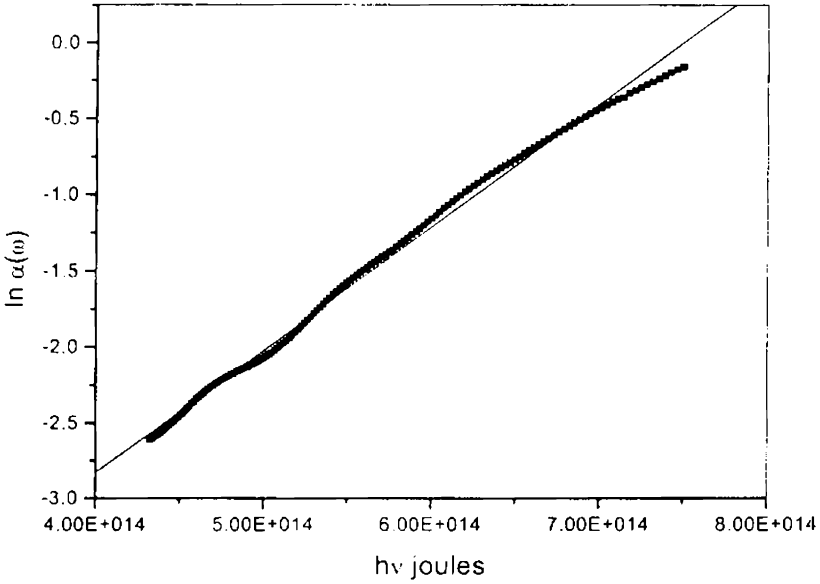

Figure (18) : ln(α) vs hν (Joules) plot for determining the Urbach energy

The absorption spectrum and transmission spectrum of poly m toluidine thin film is as shown in figures (14) & (17). The direct band gap, indirect band gap and Urbach energy are determined from the plots (15,16 &18).

Similarly, from the absorption spectrum of poly diethyl aniline (figure (19)), direct band gap (fig (20)), indirect band gap (fig (21)) and Urbach energy (fig (22)) are determined. Refractive index of the thin film sample is determined from the transmission spectrum (fig (23)).

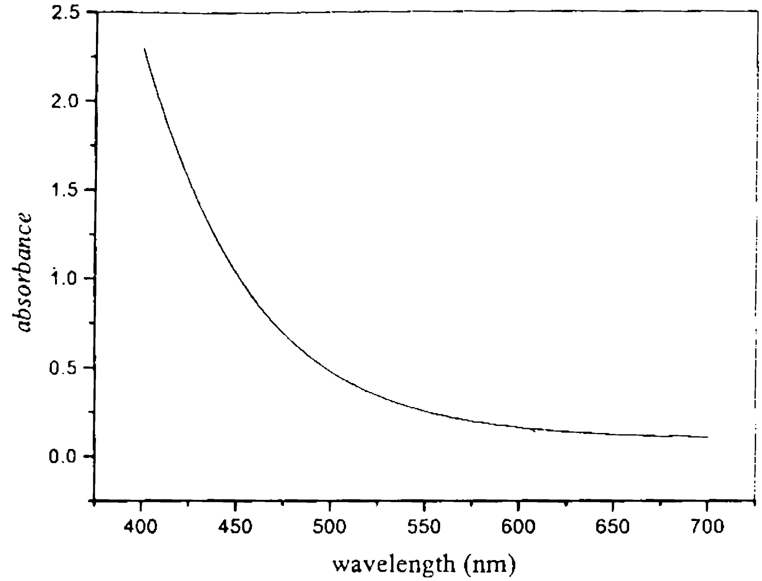

Figure (19): Absorption spectrum of poly diethylaniline

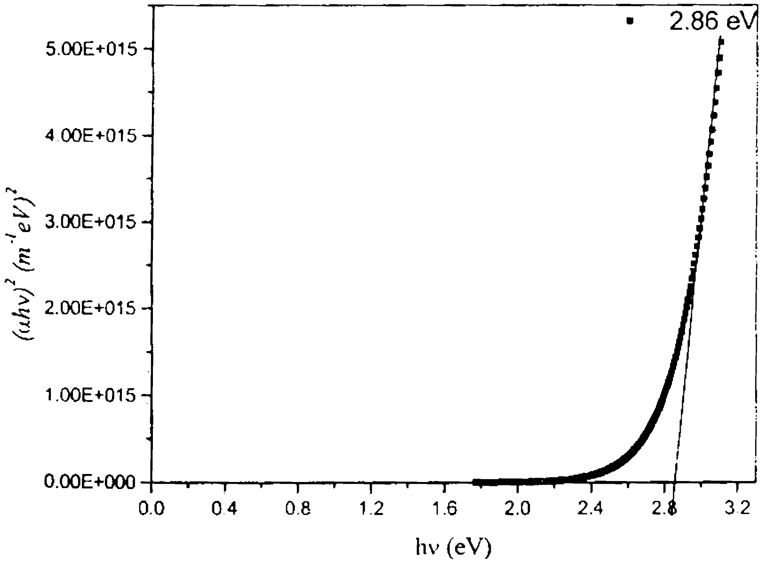

Figure (20): $(\alpha h\nu)^2$ vs hν plot for determining direct energy band gap

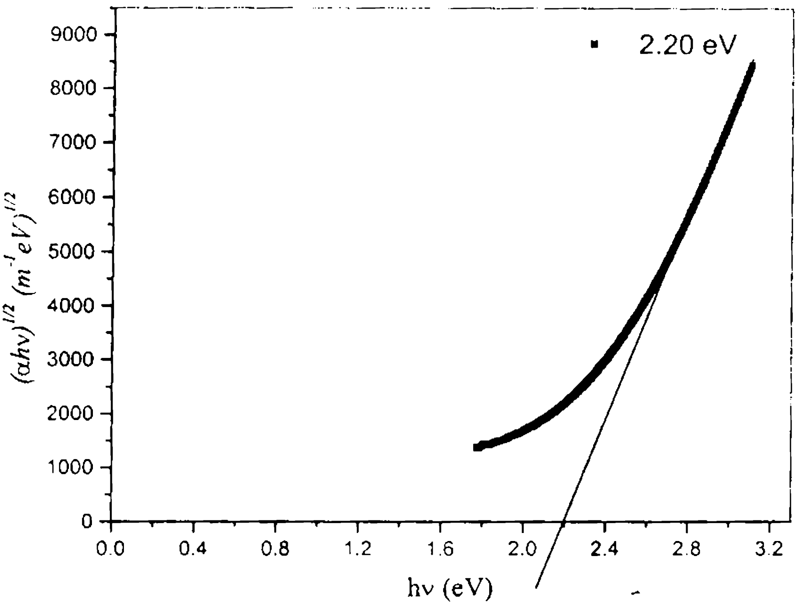

Figure (21): *$(\alpha h\nu)^{1/2}$ vs $h\nu$ plot for determining indirect energy band gap*

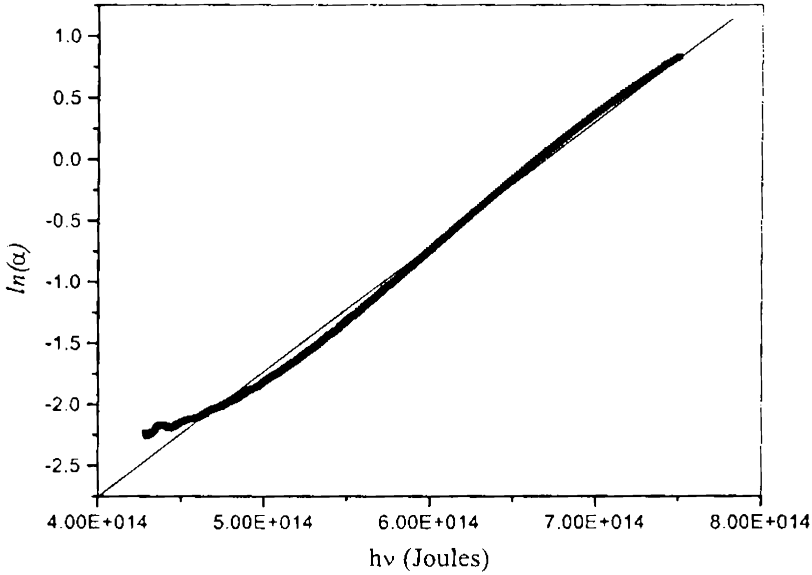

Figure (22): *$\ln(\alpha)$ vs $h\nu$ (in Joules) plot for determining Urbach energy*

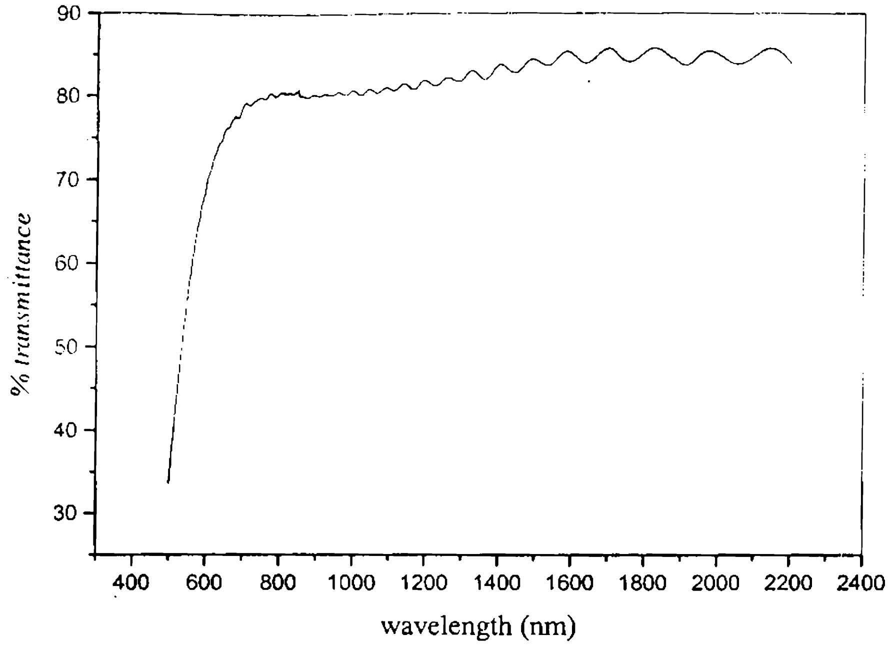

Figure (23): Transmission spectrum of poly diethylaniline

The direct bandgap energy, indirect bandgap energy, Urbach energy and the refractive index of the three samples are tabulated in Table I.

Sample	Direct energy bandgap (eV)	Indirect energy bandgap (eV)	Urbach energy (eV)	Refractive index
Poly o toluidine	2.79	2.13	0.316	1.522
Poly m toluidine	2.76	1.98	0.511	1.545
Poly diethylaniline	2.86	2.20	0.406	1.577

TABLE I showing the direct bandgap, indirect bandgap, Urbach energy and refractive index of the three plasma polymerized samples.

3.4.3 FTIR ANALYSIS [19,20,21]:

Michelson interferometer invented by Albert Abraham Michelson in 1880 forms the basis for the development of FTIR. Though originally, the Michelson interferometer was designed to test the existence of "luminiferous ether" a medium through which light waves were thought to propagate, Dr. Michelson was aware of the potential use of his interferometer in spectral analysis. He also manually measured many interferograms. Unfortunately the calculations required to convert an interferogram into a spectrum were time consuming and hence the use of an interferometer to obtain spectra was impractical. The invention of computers and advances in how computers perform mathematical operations made FTIR a reality. J.W. Cooley and J.W. Tukey, at Bell Labs, made the major advance in this area when they invented "Fast Fourier Transform" (FFT), or "Cooley-Tukey Algorithm". This algorithm quickly performs Fourier transforms on a computer, and is still the basis for the transformation routines used in commercial FTIRs. The marriage of the FFT algorithm and minicomputers was the breakthrough that made FTIR possible.

Infrared spectroscopy is the study of interaction of infrared light with matter. The infrared spectrum is generally regarded as one of the most characteristic properties of a compound. The range from 0.75 micron to 200 micron i.e. from just outside the visible region and extending up to the microwave region is called the infrared. The wavelength of infrared radiation is most frequently expressed in terms of wavenumbers, which are the reciprocal of wavelengths expressed in centimeter units. Two types of spectrophotometers are available, those linear in wavelengths and those linear in wavenumbers. The wavenumber unit is most widely used today. The majority of FTIRs operates in the mid infrared region of the spectrum, between 400-4000cm^{-1}. As the infrared radiation interacts with matter, it can be absorbed, causing chemical bonds in the material to vibrate. Since the vibrational energy levels of the molecules are quantized, only the infrared photon with a frequency exactly matching that required for a vibrational transition will be absorbed by the sample. When an infrared beam, whose frequency is changed continuously, irradiates the sample, the molecule will absorb certain frequencies as the energy is consumed in stretching or bending different bonds. The transmitted beam corresponding to the region of absorption will naturally be weakened and thus a recording of the intensity of the transmitted beam as a function of wavenumber gives the infrared spectrum. Hence, Fourier Transform Infrared Spectroscopy (FTIR) is a powerful tool for identifying types of chemical bonds in a molecule by producing an infrared transmission spectrum that is like a molecular "fingerprint".

Samples for FTIR can be prepared in a number of ways. In the case of liquid samples, the easiest way is to place one drop of sample between two plates of sodium chloride (salt) so that the drop forms a thin film between the plates. Salt is transparent to infrared light. In the case of solid samples there are two ways: 1) Solid samples can be milled with potassium bromide (KBr) to form a very fine powder. This powder is then compressed into a thin pellet, which can be analyzed. KBr is also transparent in the IR. 2) Solid samples can be dissolved in a solvent such as methylene chloride, and the solution placed onto a single salt plate. The solvent is then evaporated off, leaving a thin film of the original material on the plate. This is called a cast film, and is frequently used for polymer identification. Solutions can also be analyzed in a liquid cell. This is a small container made from NaCl (or other IR-transparent material), which can be filled with liquid, such as the extract for EPA 418.1 analysis. This creates a longer path length for the sample, which leads to increased sensitivity. Sampling methods include making a mull of a powder with a hydrocarbon oil (Nujol) or pyrolyzing insoluble polymers and using the distilled pyrolyzate to cast a film. Films can be placed in an Attenuated Total Reflectance cell and gases in gas cells.

All molecules are made up of atoms linked by chemical bonds. The movement of atoms and chemical bonds can be likened to that of a system comprised of springs and balls in constant motion. Their motion can be regarded as being composed of two components, the stretching and bending vibrations. The frequencies of vibrations are not only dependent on the nature of particular bonds themselves, such as the C-H or C-O bonds, but are also affected by the entire molecule and its environment.

An infrared spectrum is usually studied under two regions:

a) The functional group region, 4000-1300 cm^{-1} (2.5-7.7 μm)

b) The finger print region, 1300-909 cm^{-1} (7.7-11.0 μm)

The high frequency portion (4000-1300 cm^{-1}) is called the functional group region. The characteristic stretching frequencies for important functional groups such as OH, NH, C=O etc occur in this portion of the spectrum. The absence of absorption in the assigned ranges for the various functional groups in is an evidence for the absence of such groups in the molecule. Overtones and combination tones of the lower frequency bands frequently appear in the high frequency region of the spectrum. In general, the high frequency region shows absorption arising from stretching vibrations and is useful for the identification of functional groups.

The region from 1400 cm^{-1} – 650 cm^{-1} is called the finger print region since the pattern of absorptions in the region is unique to any particular compound. The intermediate portion of the spectrum 1300 cm^{-1} -909 cm^{-1} region is usually complex since both the stretching and bending modes give rise to absorption in the region. The absorption bands in the finger print region are also complex with the bands originating in interacting vibrational modes. Each organic compound has its own absorption in the region. This region contains many absorption bands due to bending vibrations and the region is particularly rich in number of bands and shoulders. Aromatic compounds display numerous bands in the finger print region than their aliphatic counterparts. The Patterns of the infrared spectrum in the finger print region are very sensitive and change even with minor chemical or stereo chemical alternations in a molecule. The finger print region of the spectrum is extremely valuable when examined in reference to the other regions.

The bands in an infrared spectrum are generally classified by the intensity of the bands: strong, weak and variable. The relative strengths of the absorption bands in spectrum is changed by the number of similar groups in a molecule.

In the present work, the FTIR spectra of the monomer samples and the corresponding polymers are recorded in the range 400cm^{-1}-4000cm^{-1}. The pellets of the polymer samples mixed with KBr are used for the IR measurements.

The FTIR spectra recorded in the range 400-4000cm^{-1} of the *o*-toluidine monomer and polymer are shown in figures (24) & (25). The *o*-toluidine molecule consists of a methyl group and an amino group on a benzene ring, with the methyl group attached to the *ortho* position of aniline. It is observed from the spectra of monomer and polymer that the group frequencies corresponding to the benzene ring are present in both the monomer and polymer implying that the benzene ring is retained in the polymer. The most important observation made by comparing the two spectra is that pertaining to NH stretching frequencies. In the monomer spectrum the group frequencies corresponding to the symmetric (3370 cm^{-1}) and asymmetric (3456 cm^{-1}) N-H stretching of the -NH_2 group are present whereas in the polymer spectrum only a single group frequency (3356) is present. The presence of the single frequency in the region 3350-3310cm^{-1} is characteristic of the secondary amines. Hence it can be inferred that -NH_2 group in the monomer is changed to -NH group in the polymer. Thus, the possible linkage is through the hydrogen abstraction of the -NH_2 group in the monomer. This is the linkage reported for polyaniline [22]. The presence of group frequencies 2925cm^{-1} and 2866 cm^{-1} indicates the presence of methylene group in the polymer. This implies that that the methyl group of the monomer is changed to the methylene group. Hence as evident from the FTIR spectra of the *o* toluidine monomer and polymer samples, there are two linkages one of which is from the amino group and the other from the methyl group. This substantiates the highly branched and cross-linked nature of the r.f plasma polymers.

Figure (26) and (27) shows the FTIR spectra of the *m* toluidine monomer and polymer sample. *m* toluidine also contains a methyl group and amino group on a benzene ring but the methyl group being attached to the *meta* position of the aniline molecule. The monomer exhibits two peaks 3423 cm^{-1} and 3350 cm^{-1} suggesting that it is a primary amine whereas the polymer spectrum exhibits only one peak in this region which is characteristic of secondary amine. Hence, here also the linkage is by hydrogen abstraction of the NH_2 group in the monomer.

The FTIR spectra of the monomer and polymer spectra of N, N Diethyl aniline are shown in figures (28) & (29). N, N Diethyl aniline is a tertiary amine with two ethyl groups replacing two hydrogen atoms of the amino group in the aniline molecule and hence no peak is observed in the amino region of the monomer spectrum. The observed peak in the polymer spectrum at ~3400 cm^{-1} region can be due to the –OH group of water molecule included while preparing the pellets. The asymmetric and symmetric stretching vibrations of methyl and methylene groups give rise to four absorption bands just below 3000 cm^{-1}. In monomer spectrum all the four bands are retained: 2960 cm^{-1} & 2866 cm^{-1} which corresponds to stretching of methyl group and 2925 cm^{-1} & 2853 cm^{-1}, which correspond to stretching of methylene group. In the polymer spectrum one of the frequencies, (2872 cm^{-1}) corresponding to the symmetrical stretching of methyl group is absent. In addition to this, another frequency 775cm^{-1} corresponding to the rocking of ethyl -CH_2 is absent in polymer. These two facts suggest that the possible linkage has taken place through the ethyl group of the N, N diethyl aniline molecule.

In all the above-mentioned cases we deal with the analysis of FTIR spectra of plasma polymerized compounds by comparing it with the corresponding monomer spectra. However, it is to be noted that the exact structure of the polymer molecules cannot be obtained only from such an analysis. This is so for various reasons, the most important being the highly branched and cross-linked nature of the r.f. plasma polymers. Due to the variable extent of fragmentation and/ or rearrangement of atoms and ligands during the process of plasma polymerization in plasma, the IR spectra also will vary with the conditions of the plasma polymerization [1]. Thus the complete information on branching and cross-linking is not readily obtained from the IR analysis alone.

To conclude, plasma polymerized thin films of three monomers, namely o-toluidine, m-toluidine and diethyl aniline are prepared using excitation by an r.f. source. The direct band gap, indirect band gap and Urbach energy are determined from optical absorption spectral studies. It is observed that the band gap values lie in the range of other plasma-polymerized samples [23]. Similarly the Urbach energies obtained for the three samples also lie in the expected range [24]. The approximate values of the refractive indices are estimated from the transmission spectra. The possible linkage in the formation of polymers is also suggested from the FTIR analysis, though it cannot accurately determine the exact structure, due to the highly cross-linked and highly branched nature of the plasma polymers [1].

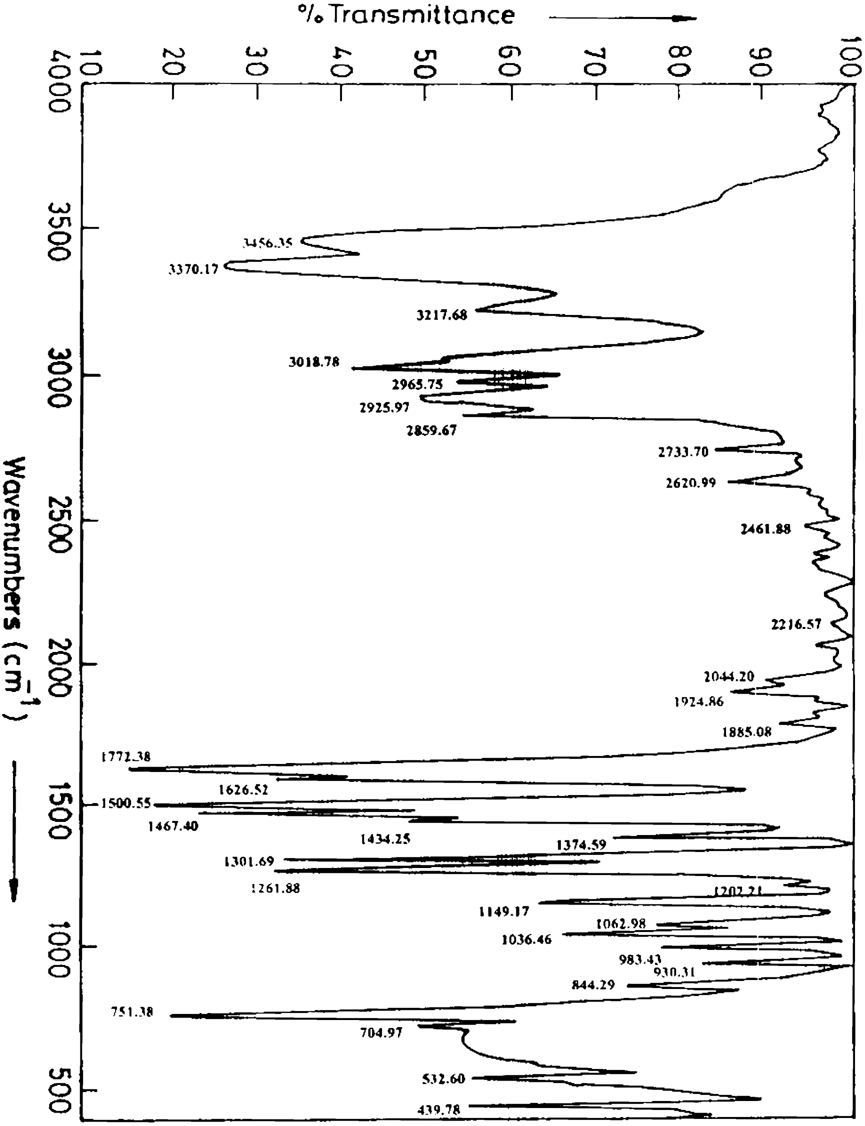

Figure 24 : FTIR spectrum of o-toluidine monomer

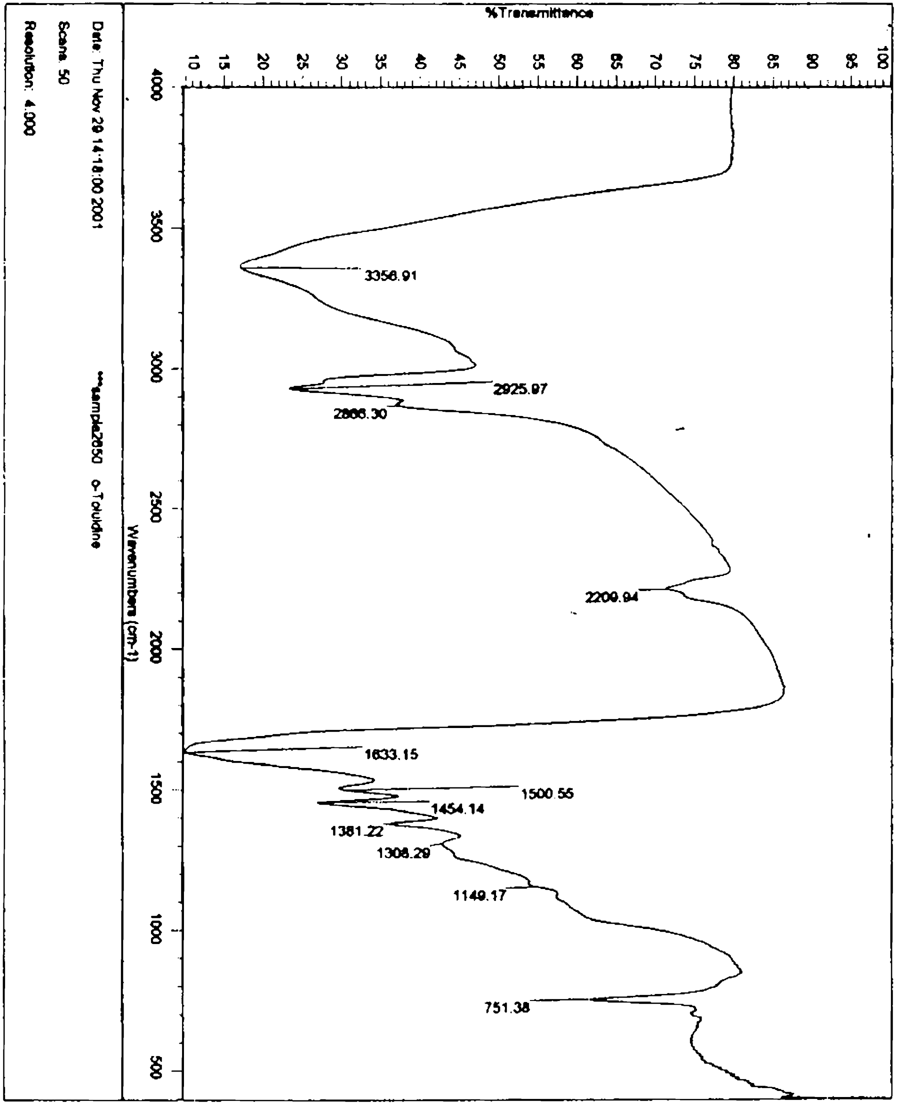

Figure 25 : FTIR spectrum of poly o-toluidine

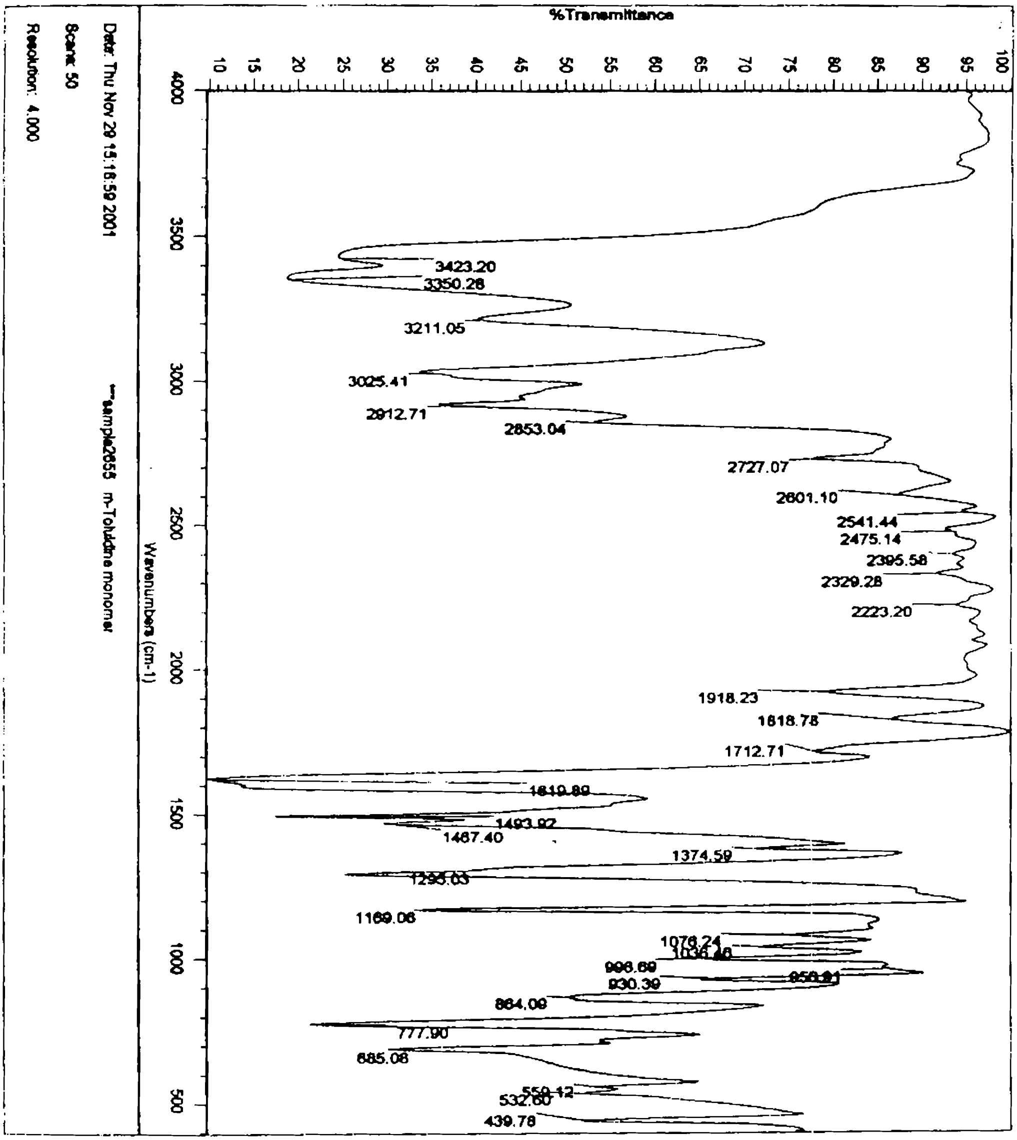

Figure 26 : FTIR spectrum of m-toluidine monomer

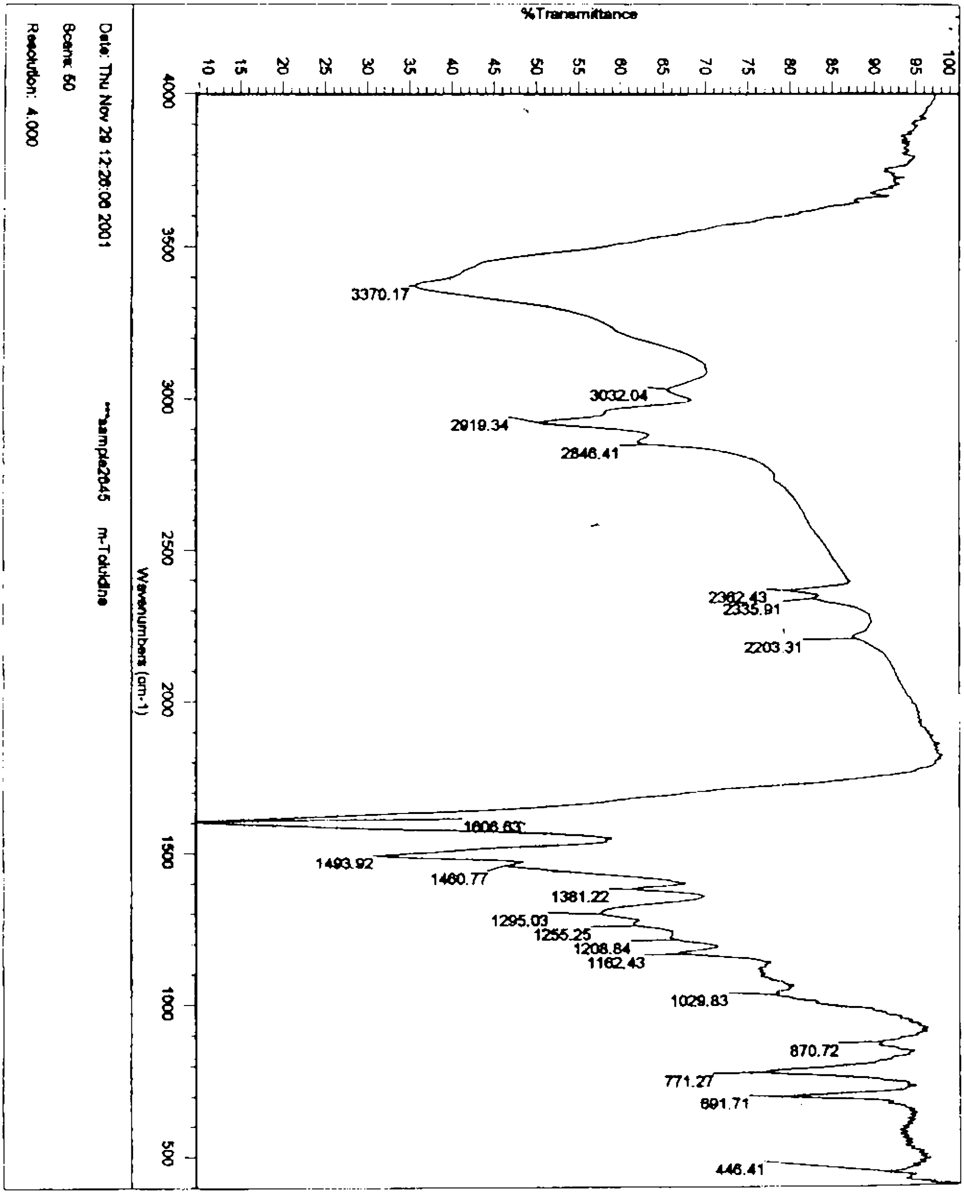

Figure 27 : FTIR spectrum of poly m-toluidine

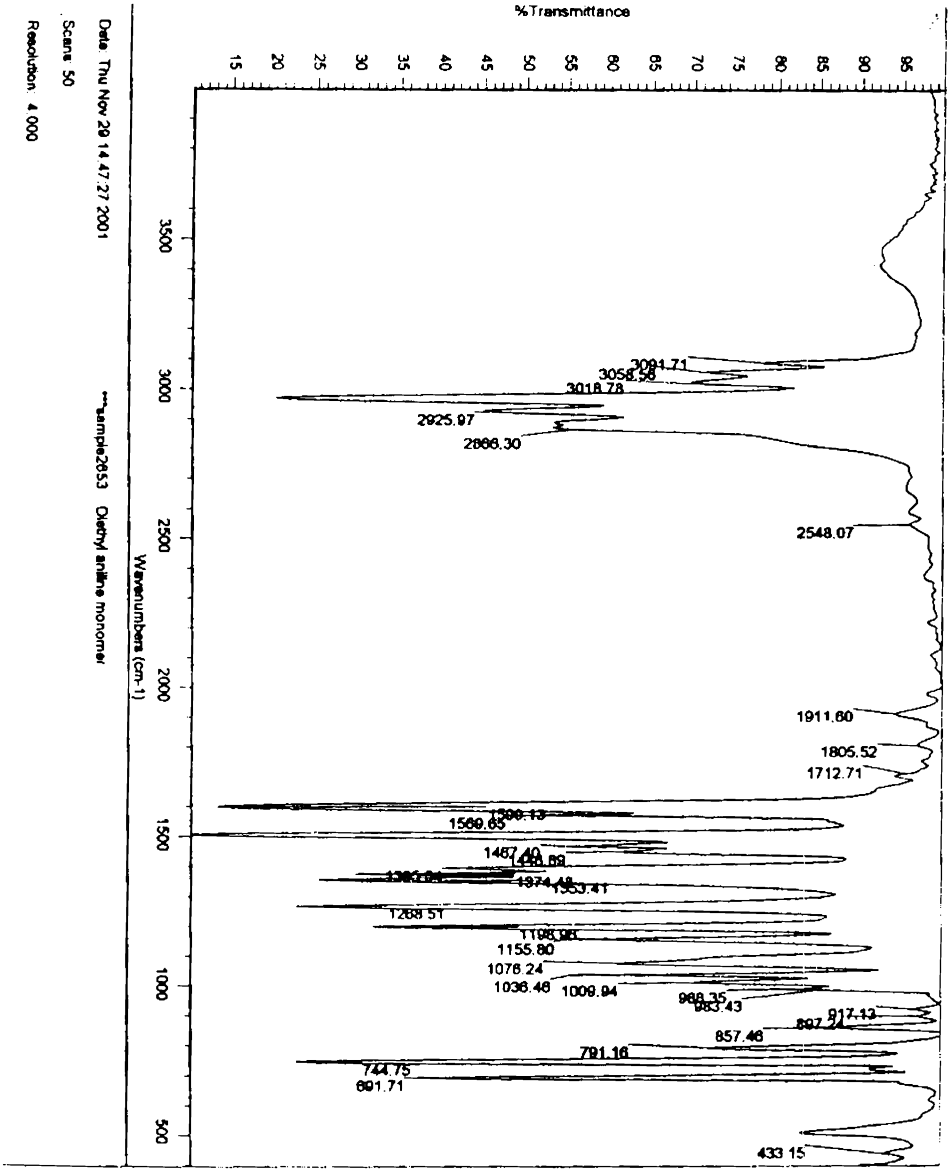

Figure 28: FTIR spectrum of diethyl aniline monomer

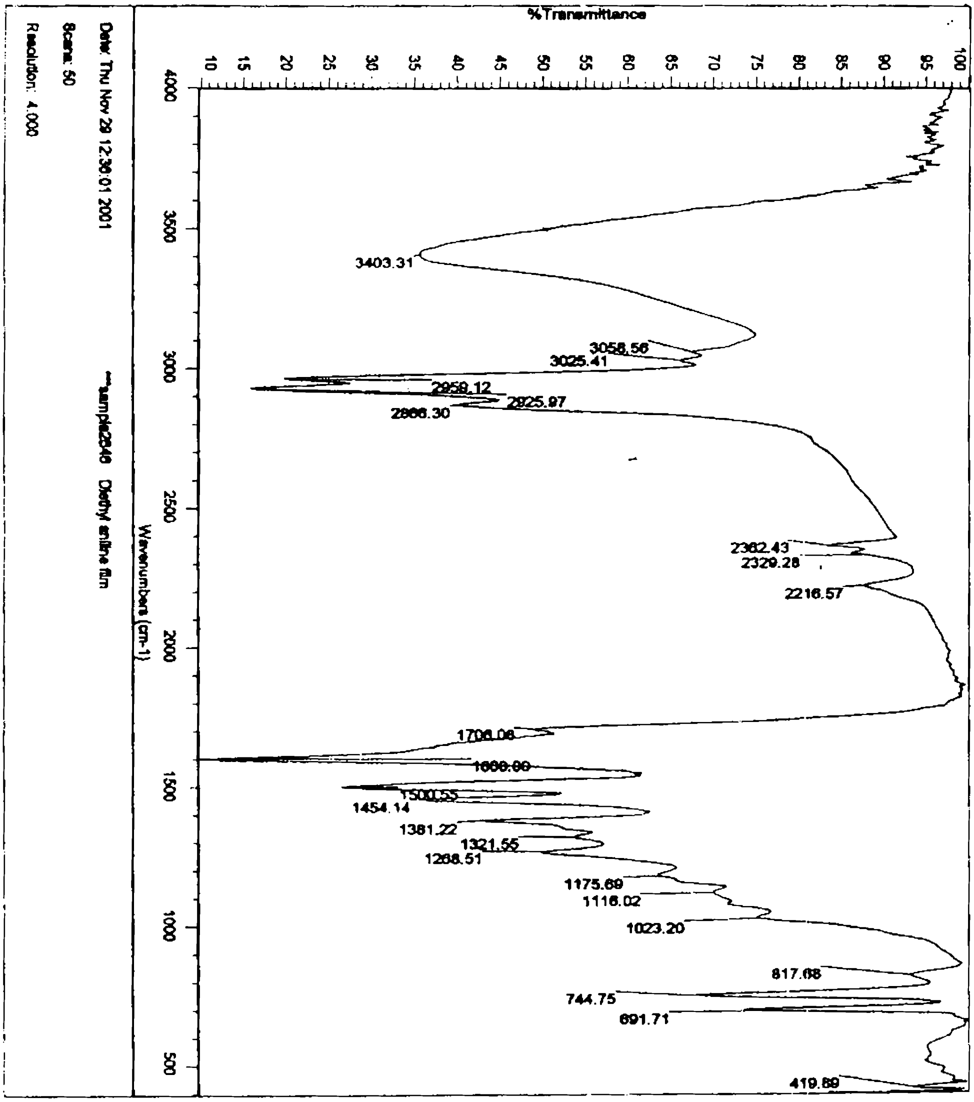

Figure 29: FTIR spectrum of poly diethyl aniline

References:

1. H.Yasuda, *Plasma Polymerization,* academic Press, New York, 1985
2. Alfred Gill, *Cold Plasma in Materials Fabrication*, IEEE press, New York, (1994)
3. H. Biederman and Y.Osada, *Plasma Polymerization Processes*, Elsevier, New York, (1970).
4. R.D. Agostino *Plasma Deposition, Treatment and Etching of Polymers*, Academic Press (1990).
5. J. Reecee Roth, *Industrial Plasma Engineering*, Volume 1 &2, IOP, Philadelphia, USA (2001).
6. R.H Turner, I.Segall, F.J.Boerio, G.D Davis, *J.Adhesion* **62**, (1997) 1
7. S.Kurosawa, N. Kamo, D. Matsui, Y.Kobtake, *Anal.Chem.* **62** (1990) 353
8. S. Kurosawa, *J. Jpn. Oil Chem. Soc.* **47** (1998) 1133.
9. L. O'Toole, R.D. Short, A.P. Ameen, F.R. Jones, *J.Chem.Soc., Faraday Trans* **91**(9) (1995)1363.
10. P.W. Kramer, Y-S Yeh, H.Yasuda. *J Membr Sci* **46**(1) (1989) 1.
11. H. Yasuda. *J Membr Sci* **18** (1984) 273.
12. Yoshinori Matsumoto, Makoto Ishida, *Sensors and Actuators A* **83** (2000) 179
13. F. W Billmayer Jr., *Text Book of Polymer science*, John Wiley and Sons, New York, (1970).
14. P.S.Kireev, *Semiconductor Physics*, Mir Publishers, Moscow,(1978)
15. J.Tauc, *Optical Propeties of solids*, North Holand, Amsterdam, (1972)
16. J.Tauc, *Amorphous and Liquid Semiconductors*, Plenum, London, (1974).
17. F.Urbach, *Phy.Rev.* **92** (1953) 1324.
18. J.C Manifacier, J.Gasiot and J.P Fillard, *J.Phys E: Sci.Instr.* **9**, (1976) 1002

19. B.K.Sharma, Spectroscopy, 11th and enlarged edition, Goel Publishing House, Meerut (1995-96).
20. Brian C. Smith, *Fundamentals of Fourier Transform Infrared Spectroscopy*, CRC Press, New York, 1996.
21. K.Nakanishi, P.H. Solomon, *Infrared Absorption Spectroscopy*, II edition, Holden- Day, Inc. Sanfrancisco (1977)
22. C.Joseph Mathai, S.Saravanan, M.R.Anantharaman, S.Venkitachalam, S.Jayalekshmi, *J.Phys.D: Appl.Phys.*35 (2002) 240.
23. F.U.Z.Chowdhury, A.H.Bhuiyan Thin Solid Films. 360 (2000) 69.
24. J.D.Dow, D. Redfield, Phy.Rev. B 5 (1972), 594.

CHAPTER IV

DESIGN AND FABRICATION OF A PROBE BEAM DEFLECTION EXPERIMENTAL SETUP AND DETERMINATION OF THERMAL DIFFUSIVITY OF R.F. PLASMA POLYMERIZED THIN FILMS

4.1 INTRODUCTION

Over the past two and a half decades, there has been a rapid increase in the development and application of new and improved materials for a broad range of applications in physics, chemistry, biology, medicine and in microelectronics. This has led to a corresponding increase in requirements for thermal performance data. The established thermal property measurement techniques include Differential Scanning Calorimetry, Contact Transient Methods etc. However, these techniques either require large samples or are too complex and time consuming. Above all, in these conventional measuring methods the sample must be kept in contact with the detector, which produces fluctuations in the thermal field to be measured. Meanwhile another set of non-destructive and non-contact techniques, commonly known as the Photothermal techniques [1] detailed in Chapter I, have been developed and applied to study matter. One of the most interesting applications of thermal wave physics is the measurement of thermal diffusivity of solids, liquids and gases. Different methods have been proposed for particular cases depending upon the thermo-optical properties and structure of samples: Photoacoustic [2-7], mirage or photothermal beam deflection [8-13], photopyroelectric [14-15]. All these techniques can be viewed, as alternatives to classical non-contact tools like Flash method [16]. The present chapter describes the design and fabrication of a compact photothermal probe beam deflection (PBD) experimental setup and its application to the determination of thermal diffusivity of certain plasma polymerized thin film samples.

4.2 THERMAL DIFFUSIVITY- SIGNIFICANCE

When different parts of a body are at different temperatures, heat flows from the hotter parts of the body to the cooler. Out of the three modes of heat transfer, convection is altogether absent in solids. In the present work, we study the conductive heat flow in certain solid samples, under conditions of negligible radiation losses. Thermal conduction is a process by which heat is transferred from one part of the sample to another as a result of the temperature gradient. Both electrons and phonons are instrumental in transferring energy from one place to another in a solid. Electrons are primary carriers in metals and these materials have fairly large thermal conductivities. For example at room temperature the thermal conductivity of aluminium is about 235 W/mK and that copper is about 400W/mK. Heat conduction in insulators can be considered as the diffusion of phonons from the hot to the cold end.

Jean Fourier derived a basic law defining the propagation of heat in one-dimensional solids as

$$\frac{\partial Q}{\partial t} = -kA\frac{\partial T}{\partial x}$$

This equation is known as the Fourier equation. The above equation implies that the quantity of heat conducted in the x-direction of a uniform solid in time dt is equal to the product of the conducting area A normal to the flow path, the temperature gradient (dT/dx) along the path and the thermal conductivity k of the conducting material.

The formal definition of thermal diffusivity arises from the expression for a transient temperature field in a conducting solid, which is given by

$$\nabla^2 T = \frac{1}{\alpha}\frac{\partial T}{\partial t}$$

where the thermal diffusivity α is given by $\alpha = \frac{k}{\rho c}$

where 'k' is the thermal conductivity, 'ρ' is the density and 'C' is the specific heat of the material. The thermal diffusivity (α) is expressed in m^2s^{-1}. It is evident from the units that, α represents the rate of heat flow. The reciprocal of thermal diffusivity ($1/\alpha$) expressed in sm^{-2} is a measure of the time required to heat-up a conducting material to a particular temperature level. Obviously, 'α' is a significant thermo physical parameter that determines heat diffusion in bulk as well as thin film samples.

4.3 DESIGN AND FABRICATION OF A TRASNVERSE PBD SETUP FOR THERMAL DIFFUSIVITY MEASUREMENTS

Though the photothermal deflection method has been a well established technique for the past two decades, efforts have been made by several workers [17] and are still going on to make the experimental setup compact, economic, sensitive and error free. For designing any experimental setup, thorough knowledge of the basic principle of the experiment and all the equipment including the cost (to make the setup economical) used in the measurement is a necessity. The essential components for the mirage (PBD) technique are: 1) Pump Source 2) Probe Source 3) Chopper 4) sample cell 5) Detection

& Data acquisition assembly consisting of the position sensitive detector (bi-cell, quadrant cell etc.), preamplifier and Lock-in amplifier.

1) **PUMP SOURCE:** Lasers with nearly monochromatic high spectral brightness enjoy significant advantageous over the lamp/monochromator combinations which account for their wide acceptance as light sources in Photothermal experiments. In addition, the laser output is highly collimated with cylindrical beam symmetry. The basic theory of the probe beam refraction treats the excitation beam as Gaussian. The strength or amplitude of the photothermal signal is directly proportional to the amount of laser light absorbed and to the laser power. However, the high excitation power is found to cause deformation of the probe beam [18]. In the present work, a He-Ne laser (λ=6328 A^0, power 20mW) with geometrical dimensions of length 50 cm and diameter 5 cm is used as the excitation source. The ($1/e^2$) beam diameter is 0.7 mm and the divergence is 1.2 milliradians. The beam is focused using a lens of focal length 10 cm and hence the beam is focused to a spot size of approximately 110μm. Compared to the traditional PT experimental setups where Argon ion laser is the commonly used excitation source, the present source is compact and economical. It also meets the requirements of the pump source to be used in mirage experiments, in terms of coherence and directional properties in addition to the important condition that the sample absorbs at least a small portion of the energy of the pump source.
2) **PROBE SOURCE:** Usually all the traditional setups use He-Ne laser as the probe source. However, the availability of cheap and compact semiconductor lasers operating in the visible region prompted us to use diode laser (λ=6500 A^0, 5mW, ($1/e^2$) beam diameter ~ 0.8mm) as the probe beam. Since the power

required for the probe source in mirage experiment is small, only a low power semiconductor laser is required. The size of the laser is about 7 cm long and 1.5 cm diameter and is focused using a lens of focal length 5cm to a spot size of ~ 52μm. The work by Charbonnier et al [17], specified that even though they used He-Ne laser as the probe beam, they obtained equally good results with a near infrared semiconductor laser (λ=7940A^0) and predicted that the availability of visible semiconductor lasers would be substitute for the He-Ne laser allowing reduction in setup dimensions and high frequency operation. The other advantages of using the semiconductor lasers include easy power stabilization and absence of high frequency pointing noise.

3) **CHOPPER:** Light from the excitation source should be modulated for observing the photothermal signal. The two main types of modulation are amplitude modulation and frequency modulation of which the former one is the most common technique. There are several ways for obtaining the amplitude modulation.

i) **Mechanical Chopper:** This is the most inexpensive, efficient and easy way to modulate with the depth of modulation being 100%. High quality, variable speed and low vibration noise chopper are available commercially. However, modulation up to a few kHz can be obtained with a mechanical chopper.

ii) **Electrical:** The output of electrically excited CW gas lasers such as CO_2 laser can be modulated by varying the discharge tube current. However, this method suffers a serious setback in that the depth of modulation is cannot approach 100%. Moreover, the electrical circuits in the commercial ion lasers are not designed for high frequency modulation (f>100 Hz). The only advantage of overcoming the vibrations associated with the mechanical chopper does not favor this kind of a modulation being used from practical point of view.

iii) **Electro optic:** This method is superior to electrical and mechanical modulation methods with a modulation frequency range 0-20 MHz. The modulation depth can be as high as 100% and produces three times lower noise than the mechanical choppers under identical conditions. However, these modulators are expensive and require wavelength specific half wave voltages.

iv) **Acousto optic:** Extra dense flint glass, lead molybdenate and tellurium oxide are some of the crystals used in acousto optic modulation. Power in the diffracted laser beam can be as high as 75% of the input laser beam.

In the present work, we have opted for mechanical chopper (Stanford Model SR 540) to meet our requirement. The unit can chop light beam at rates of 4Hz-4 kHz. Versatile, low jitter outputs provide the synchronizing signals required for several operating modes. The whole frequency range operation requires two blades: a 6-slot blade for operation in the frequency range 4Hz-400 Hz and 30-slot blade for 400 Hz 4 kHz.

The modulation frequency has a major role in determining whether the sample thermally thick or thermally thin. This is due to the fact that the thermal diffusion length follows an inverse relation with the square root of modulation frequency. As mentioned earlier in Chapter I, the sample is classified into thermally thick or thermally thin according to whether the thermal diffusion length is less than or greater than the thickness of the sample. Hence, by controlling the modulation frequency, the sample can be changed from thermally thick to thermally thin or vice versa. However, in the mirage measurements for thermal diffusivity, the technique can be applied irrespective of whether the sample is thermally thin or thermally thick. Only the analysis of the deflection signal must be made appropriately.

4) **SAMPLE CELL:** The sample cell used is a quartz cuvette of dimensions 10 mm x 10 mm x 5 mm. High purity carbon tetrachloride is used as the one of the coupling fluids surrounding the sample, mainly due to the high value of dn/dT compared to air. This implies that for each degree temperature rise there will be considerable change in the refractive index, which will lead to an appreciable beam deflection. The comparatively low values of thermal conductivity (k=0.099 $Wm^{-1}K^{-1}$)· specific heat capacity (C_p= 0.85 $Jg^{-1}K^{-1}$) and thermal diffusivity (0.731 x 10^{-3} cm^2s^{-1}) also make carbon tetrachloride an ideal coupling fluid for thermal diffusivity measurements. Another coupling fluid used is liquid paraffin which has a thermal diffusivity (0.3 x 10^{-3} cm^2s^{-1}, C_p=2.14 $Jg^{-1}K^{-1}$).

5) **DETECTOR &DATA ACQUISITION ASSEMBLY:** This assembly consists of a position sensitive detector, a preamplifier and Lock-in-amplifier.

Position Sensitive Detector

Silicon photodetectors are commonly used for light power measurements in wide range of applications such as spectroscopy, photography, optical remote control, optical switches, analytical instrumentation, medical imaging, laser printers, bar code readers and many more. However there is another application that utilizes the photodetectors as optical position sensors and hence are referred to as Position Sensitive detectors (PSD). Under this head they are widely used in ultra fast, accurate auto focusing schemes for a variety of optical systems, human eye movement monitoring etc. The position of beam with fractions of microns can be obtained using PSD's and hence are conveniently used in beam deflection or mirage experiments. The PSD's are broadly classified into *segmented PSD's* and *lateral effect PSD's*

Segmented PSD's are common substrate photodiodes divided into either two or four segments or photodiode elements separated by a gap or dead region and are referred to a s bi-cell and quadrant cell respectively. The photodiode elements are generally masked on to a common substrate so that their cathode is shared. A symmetrical optical beam generates equal photocurrents on all segments, if positioned at the centre. The relative position is obtained by measuring the output current of each segment. The bi-cell is used for one-dimensional measurement where as the quadrant cell is used for two dimensional measurements. The light spot diameter should be larger than the gap between the photodiode elements.

In the case of a quadrant cell, X and Y displacements of the light spot can be obtained using the simple relationships given below. If the segments of the quadrant cell are designated as A, B,C and D then

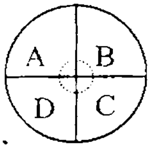

$$X= [(A+D)-(B+C)]/ [A+B+C+D]$$

$Y = [(A+B)-(C+D)]/[A+B+C+D]$

However, in the case of a bi-cell, there are only two segments say A & B and can measure only displacement in one direction, then

$X = (A-B)/(A+B)$.

Lateral effect PSD's are continuous single element planar diffused photodiodes with no gaps or dead areas. Though Schottky discovered lateral photo effect in 1930, devices using this principle became available only in the last decade or so. These detectors consist of only a single active element. Dividing photon-generated electrons within the substrate of the device rather than profiling the intensity distribution on the surface derives position. In fact the lateral effect detectors are not perfectly linear. Most devices exhibit ± 0.5% linearity over the central 25% of their area, ±3% out to 75 % and ±5% out to the periphery. The major contribution to this nonlinearity is the sheet resistance of the device. At the centre of the detector where the light spot is equidistant from all contacts these non-uniformities will tend to average out to a greater extent than at out lying areas on the detector.

In the present work we used a bi-cell (SPOT 2D from M/s UDT Sensors Inc) as the position sensitive detector for the probe beam deflection measurements. The important features of this bi-cell include high accuracy, excellent resolution, high-speed response, ultra low dark current and excellent response match. Spectral response range is from 350-1100nm and excellent stability over time and temperature. They have fast response times necessary for high speed or pulsed operation and position resolutions of better than 0.1 μm. Though the signal output can be directly read from each segment, electronic modules can be used in order to perform the task. We have constructed a preamplifier to obtain the amplified output since the deflection signal is usually small.

Preamplifier:

The block diagram of the preamplifier circuit used in the present setup is as shown in figure (1). Giving common signal from a function generator to the two different inputs initially, tests the preamplifier and it is ensured that the output is zero. Furthermore, two different inputs are fed to obtain the same result as expected theoretically.

Lock-in-Amplifier:

The *Lock-in Amplifier* is used to detect and measure very small a.c signals using a technique known as phase-sensitive detection in order to single out the component of the signal at a specific reference frequency and phase. The signals at other frequencies regarded as noise are rejected and do not affect the measurement. Lock-in-amplifiers use a phase locked loop (PLL) to generate the reference signal. The PLL locks the internal reference oscillator to the external reference signal provided to the lock-in-amplifier resulting in a reference sine wave of a particular frequency and a fixed phase shift. In the present work, SR830 (Stanford Research Model) is used. The SR 830 operates from 100V, 120V, 220V or 240V nominal a.c. power source having line frequency 50 Hz or 60Hz and can measure voltage from 2nV to 1 V.

The schematic of the experimental setup used for the measurement of thermal diffusivity is as shown in figure (2). In the present work, we employed the *transverse scan method* [9]. The measurements are performed by varying the distance between the pump and probe beams, and hence requires that either of these two beams be fixed. We chose to fix the pump beam and scan the probe beam across the sample surface, since our pump source is bulky compared to the probe source. In traditional mirage experimental

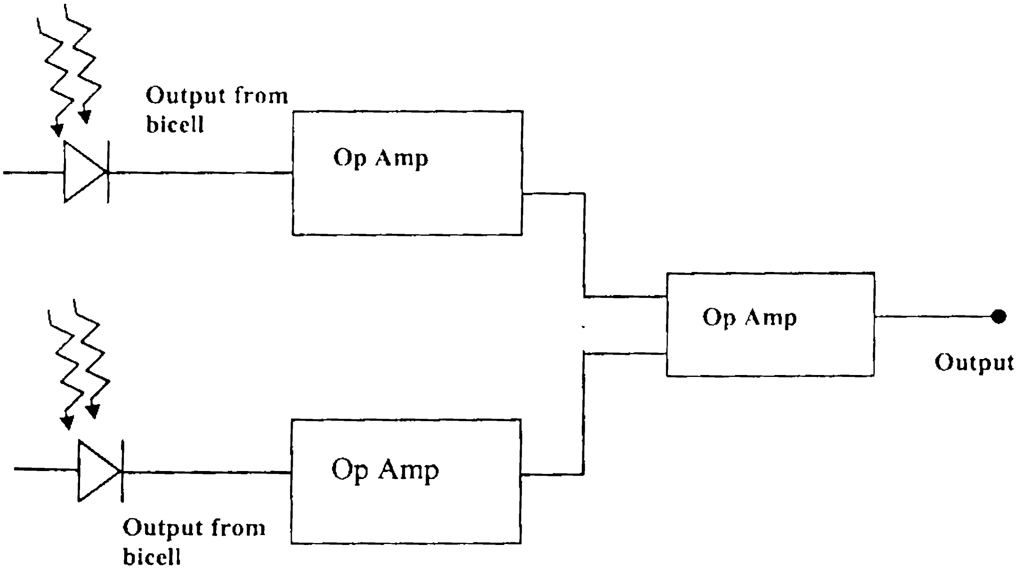

Figure (1): Block diagram of the pre-amplifier setups, usually the probe beam is fixed and the pump beam scans across the sample surface with the help of a mirror arrangement. This is because probe beam scanning requires a synchronous movement of the lens focusing the probe beam and the detector, which makes the system complex, especially when the probe source is bulky. In our experiment, the probe laser is of small size that, it together with the focusing lens and

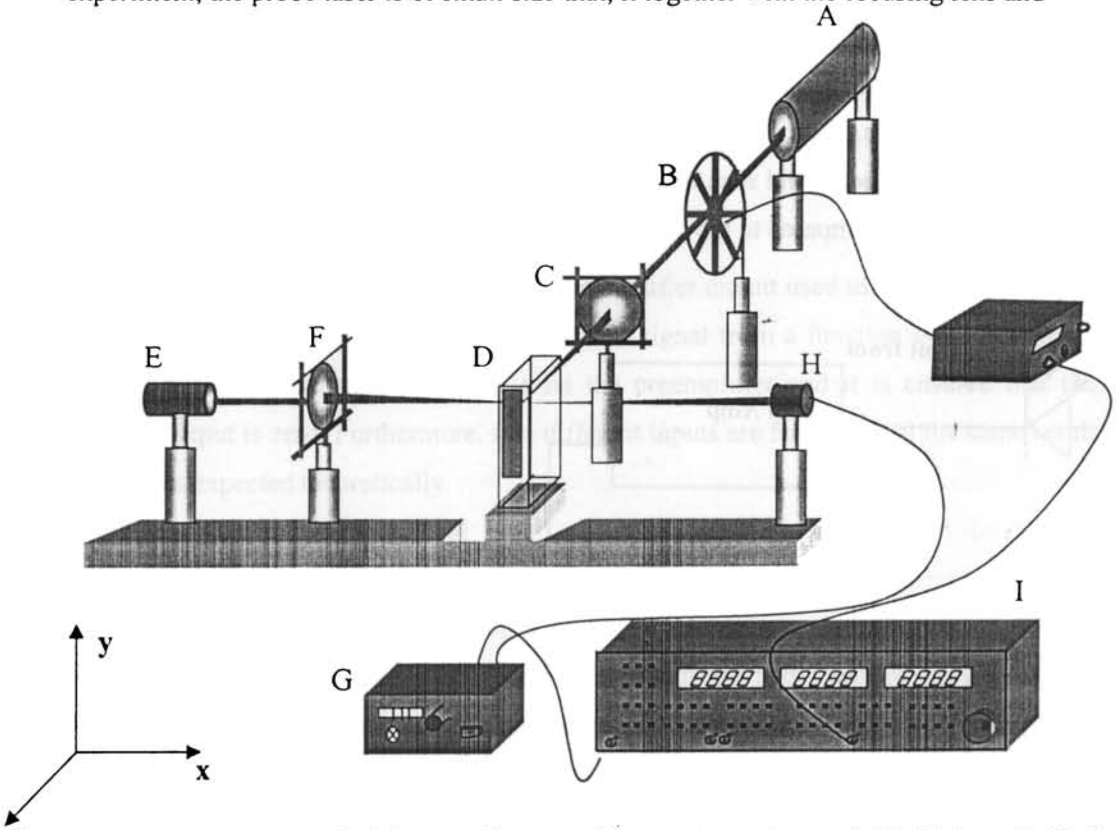

Figure 2: Schematic diagram of the experimental setup A: He-Ne laser. B: Mechanical ***Chopper. C: Lens. D: Sample cell. E: Diode laser. F: Lens. G: Amplifier. H: Bi-cell detector I: Lock-in-amplifier J: Aluminium Flat***

detector could be fixed on an aluminium flat of length 30 cm and width 1cm, which in turn is fixed onto an XYZ translation stage, so that all the three move in synchrony. The sample fixed in the cuvette is also fixed on a translation stage. The pump laser and these two translation stages are fixed on an optical breadboard with honeycomb structure, placed on a granite table so as to minimize the errors due to mechanical vibrations.

The experimental setup is standardized for thermal diffusivity using InP wafer of thickness 350μm using the Phase Method as described in Chapter II. Figure (3) shows the plot of phase vs. transverse offset at a modulation frequency 10 Hz. The thermal diffusivity value calculated from the slope of graph is 0.444 cm^2s^{-1} and is in good agreement with the literature value [19].

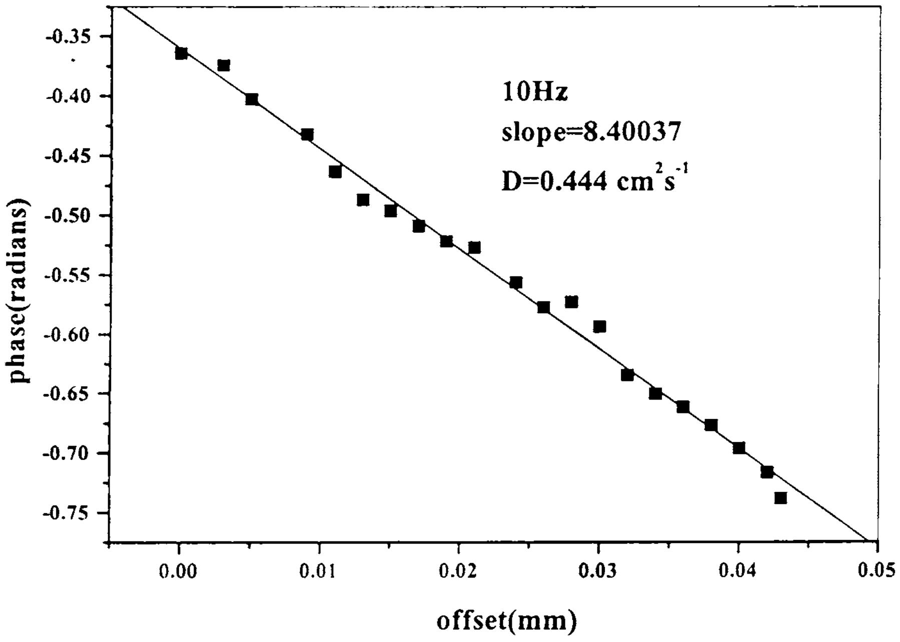

Figure (3): Plot of Phase vs. offset of InP

4.4 THERMAL DIFFUSIVITY OF PLASMA POLYMERIZED THIN FILMS

Plasma polymerized thin films find innumerable applications ranging from corrosion free adhesive coating materials to sensor technology and microelectronics [20-25]. The thermal diffusivity (and hence conductivity) is an equally important parameter like electrical conductivity, which is to be known for the effectively applying these materials for different purposes. The thermal conduction parameters of polymers are very low whose determination is really challenging and the sample being in thin film form adds to the difficulty. However, employing the Photothermal Beam deflection technique or mirage technique one can accurately determine the thermal diffusivity of thin film samples of low thermal diffusivity. To the best of our knowledge, the present work determined the thermal diffusivity values of R.F. plasma polymerized thin films poly o toluidine, poly m toluidine and poly diethyl aniline, for the first time. Hence we have used two different methods of analysis namely Phase method [26] and Amplitude method [27], which are described in detail in Chapter II. In the first set of experiments, carbon tetrachloride is used as the coupling medium. The experiment is repeated using liquid paraffin as the coupling medium. The measurements were performed at two different modulation frequencies in each case.

Figures (4,5) (8,9) and (12,13) show the phase vs. offset plot for poly – *o* toluidine, poly- *m* toluidine and poly diethyl aniline respectively for different modulation frequencies (which are indicated in the corresponding graphs). All the graphs are linear as expected in the phase method. The slopes evaluated from these graphs are the inverse of the characteristic length and thermal diffusivity values obtained from the slopes is tabulated in Table I. For confirmation, the analysis was done using the amplitude method for the same set of modulation frequencies as done in the case of Phase Method. The graphs between *ln* [amplitude] and offset are shown in figures (6,7), (10,11) and (14,15) which are also linear as expected. The thermal diffusivity values are calculated from the slope and are tabulated in Table II. These are in good agreement with the values obtained earlier in Table I by the Phase method.

Heat diffusion in solids can take place either through the lattice vibration, carrier diffusion and carrier recombination. The latter two mechanisms are mainly characteristic of the semiconductors [28]. However, the thin film samples prepared by the r.f plasma polymerization techniques are highly crosslinked, exhibit exceptional dielectric

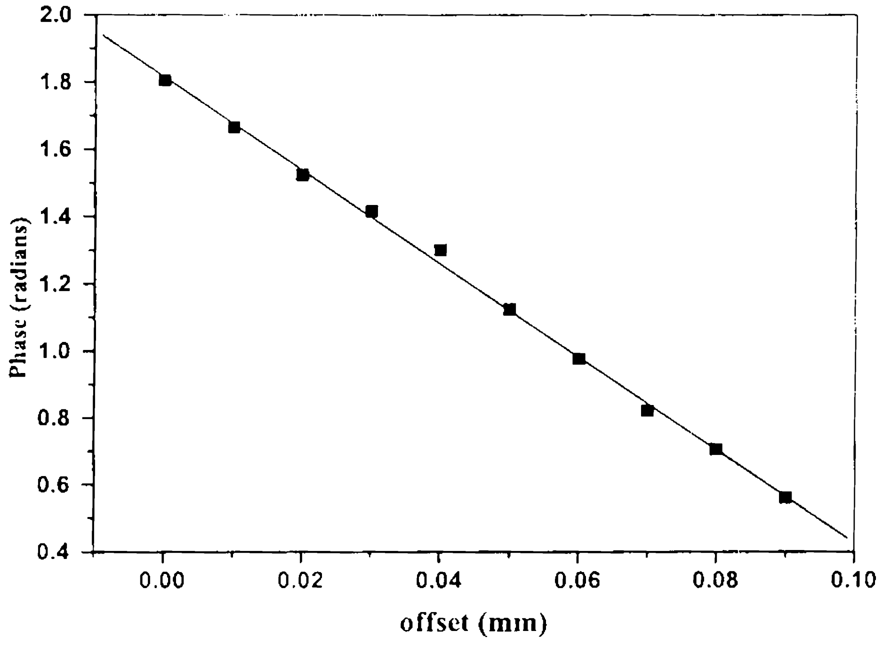

Figure (4) phase vs. the pump-probe offset for 10 Hz CCl_4 for poly o toluidine properties [29] and are basically insulators. The high direct and indirect band gap compared to the pump beam energy (1.95eV since a He-Ne laser having wavelength 632.8 nm is used) rules out the possibility of photo-excited carrier generation. Hence, any heat diffusion in these samples are solely due to the lattice vibrations without any contribution from electron diffusion or carrier recombination.

Two basic factors that need to be considered in the photothermal beam deflection technique are the effects of coupling media and substrate on which the samples are coated. In order to have an idea about the influence of the thermal properties of coupling media to the deflection signal, the experiments were repeated using liquid paraffin as the coupling medium instead of carbon tetrachloride. The Phase vs. offset plot and *ln*[amplitude] vs. offset plot for poly o toluidine, poly m toluidine and poly diethylaniline are shown in figures (16) to (27) for

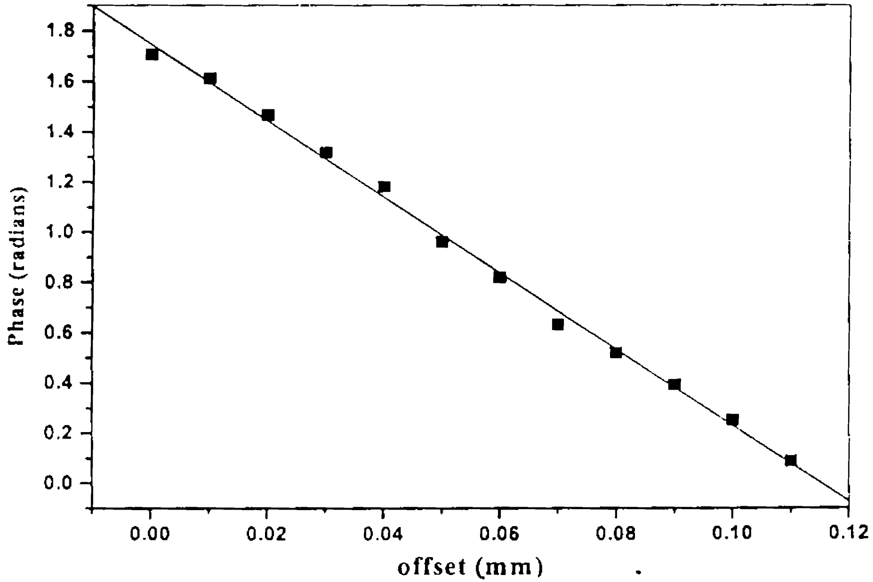

Figure (5) phase vs. the pump-probe offset for 12 Hz in CCl_4 for poly o toluidine

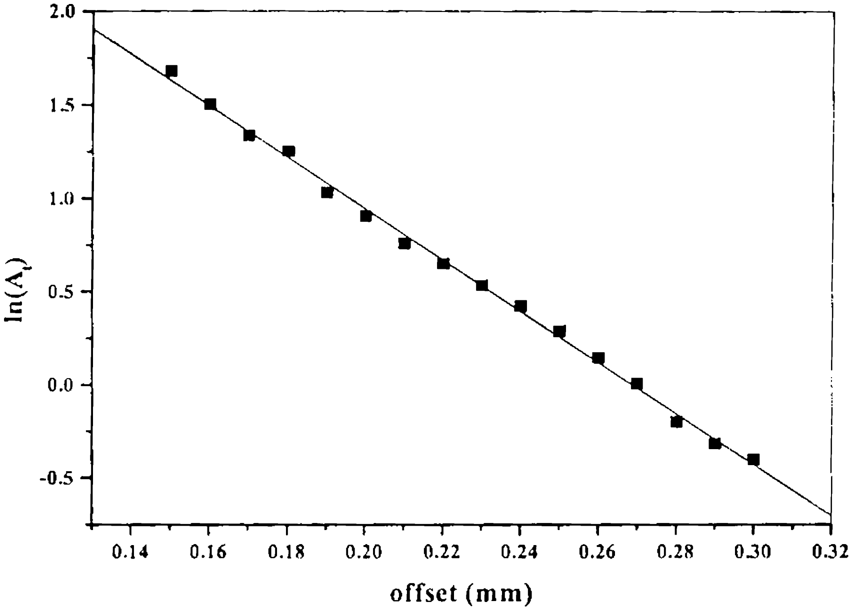

Figure (6) ln(Amplitude) vs. the pump-probe offset for 10 Hz CCl_4 for poly o toluidine

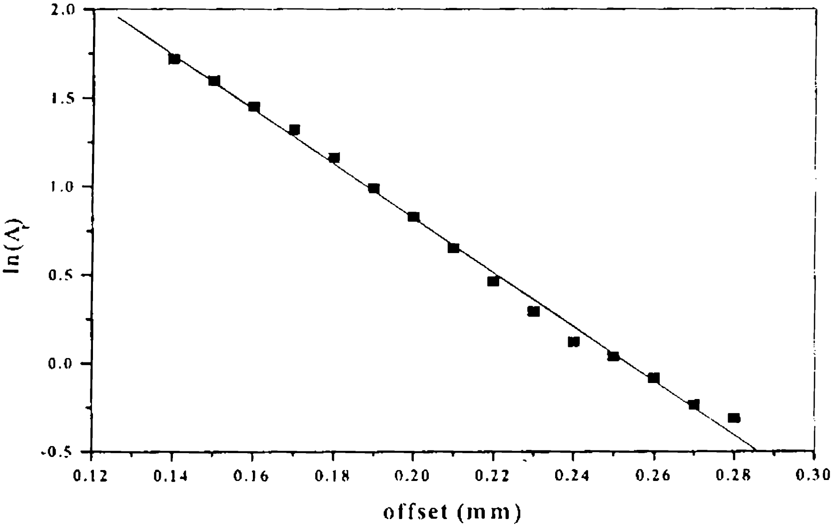

Figure (7) ln(Amplitude) vs. the pump-probe offset for 12 Hz CCl_4 for poly o toluidine

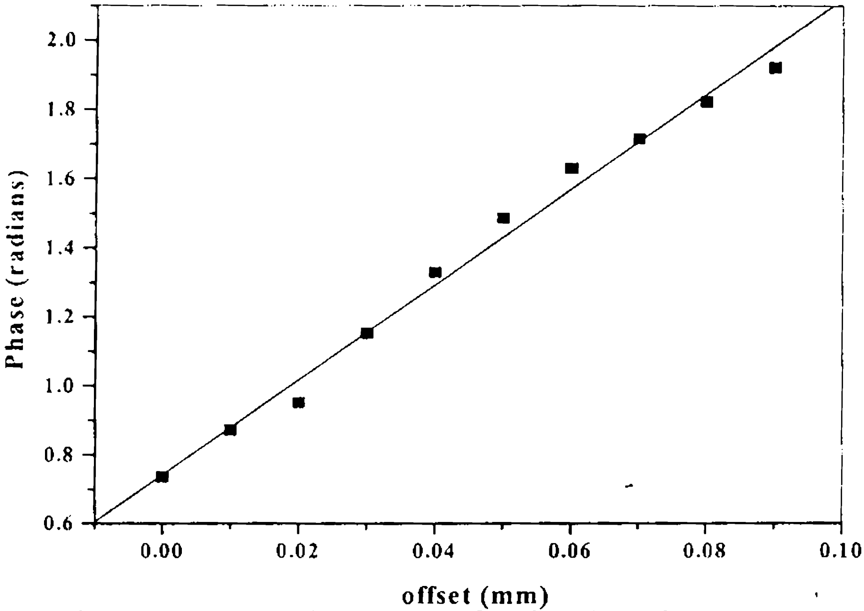

Figure (8) phase vs. offset at 8 Hz in CCl_4 for poly m toluidine

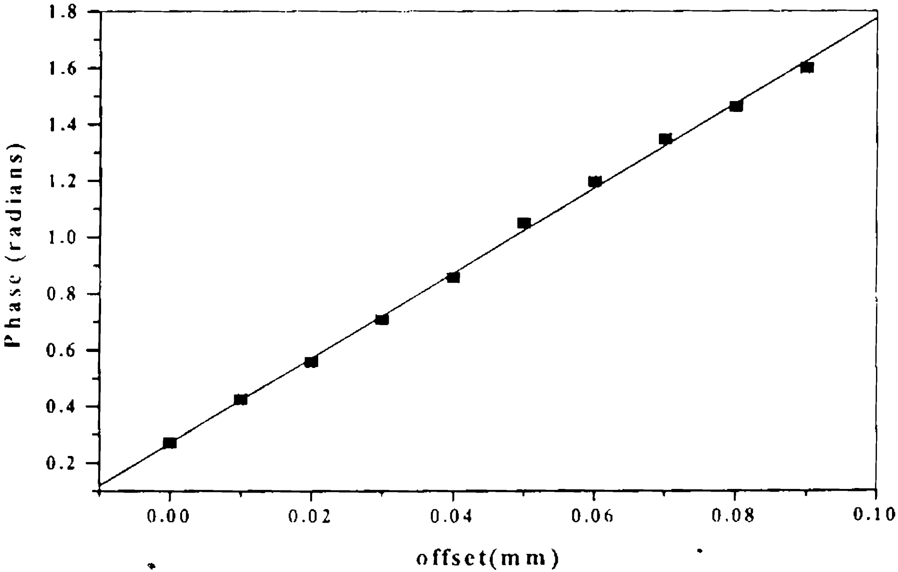

Figure (9) phase vs. offset at 10 Hz in CCl_4 for poly m toluidine

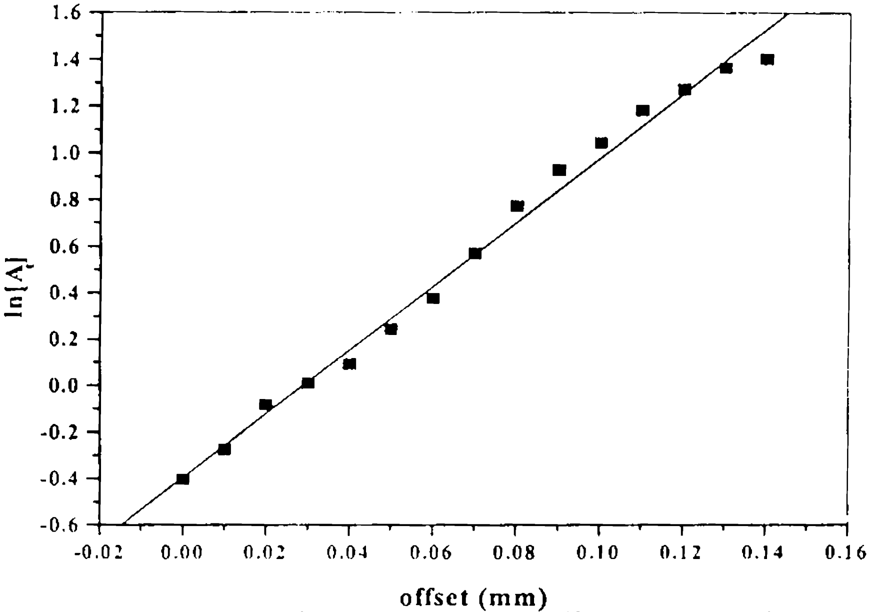

Figure (10) ln(amplitude) vs. offset at 8 Hz in CCl_4 for poly m toluidine

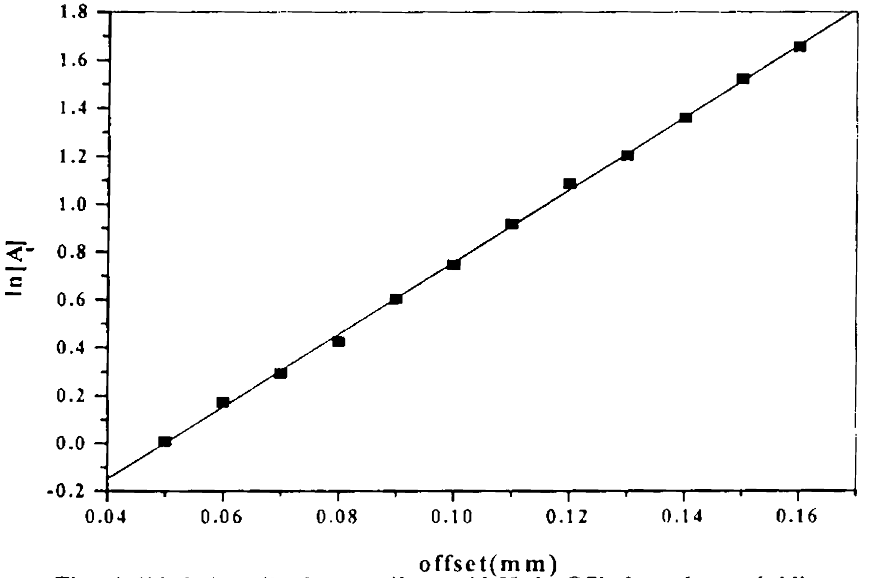

Figure (11) ln(amplitude) vs. offset at 10 Hz in CCl_4 for poly m toluidine

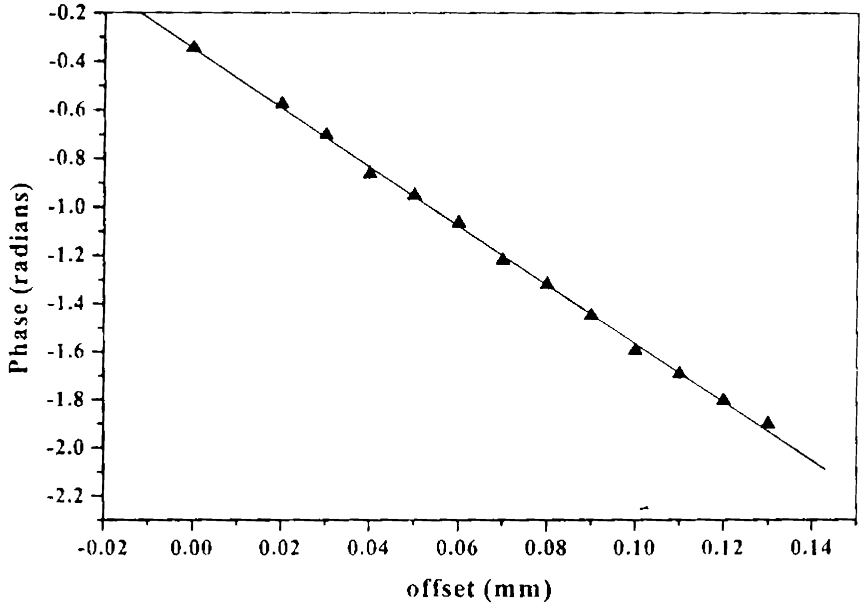

Figure (12) phase vs. pump-probe offset for 10 Hz in CCl_4 for poly diethylaniline

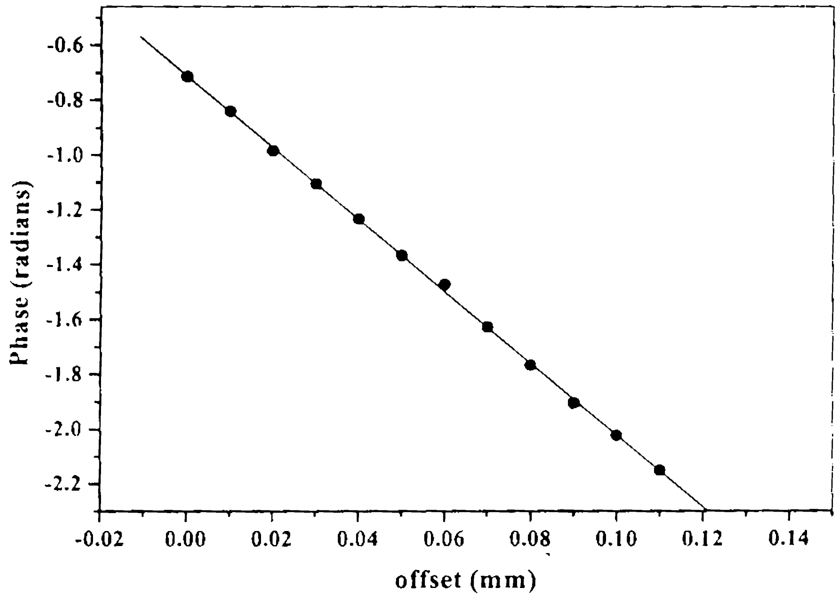

Figure (13) phase vs. pump-probe offset for 12 Hz in CCl_4 for poly diethylaniline

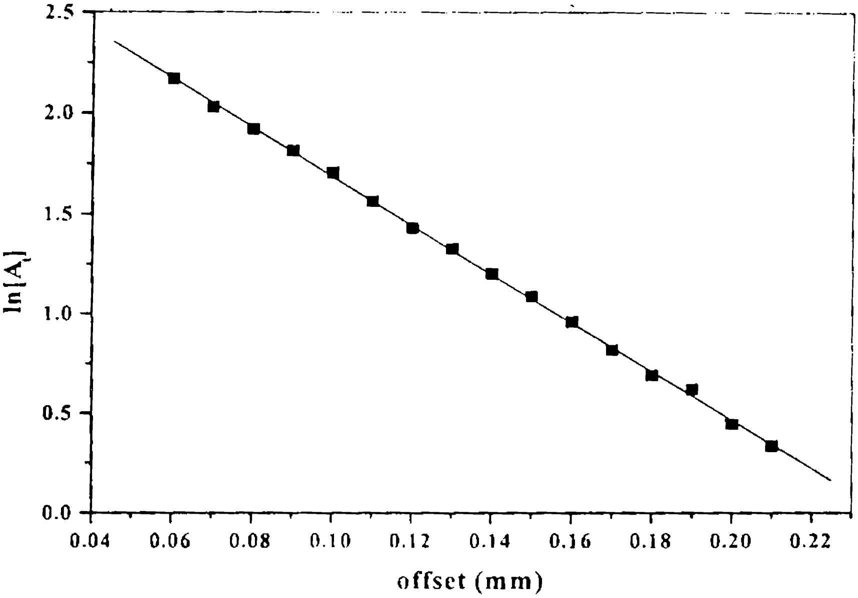

Figure (14) ln(amplitude) vs. pump-probe offset for 10 Hz in CCl_4.for poly diethylaniline

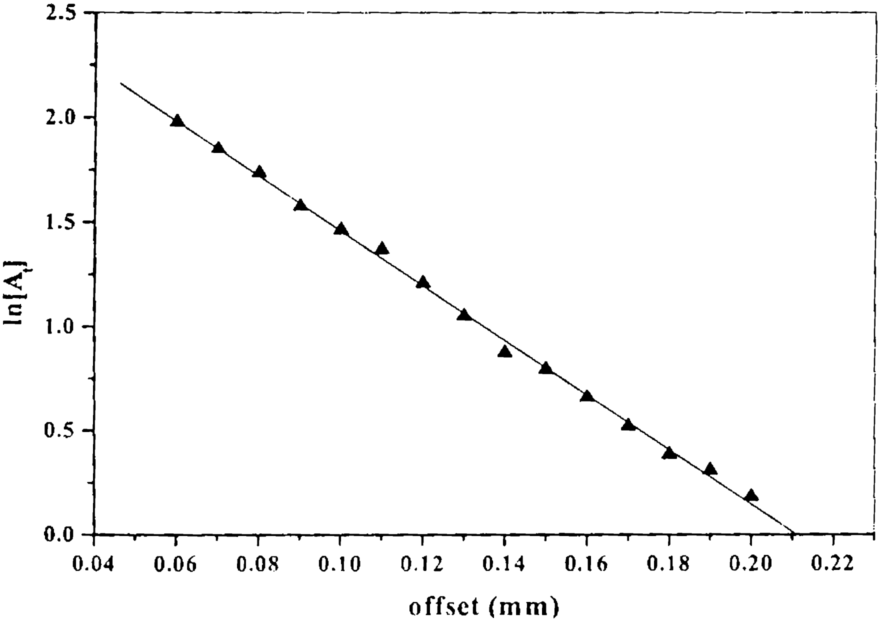

.Figure (15) ln(amplitude) vs. pump-probe offset for 12 Hz in CCl_4.for poly diethylaniline

Sample	Method of Analysis	Frequency (Hz)	Thermal Diffusivity ($10^{-2}cm^2s^{-1}$)
Poly o Toluidine	Phase Method	10	0.163 ± 0.005
		12	0.164 ± 0.006
	Amplitude Method	10	0.166 ± 0.005
		12	0.160 ± 0.005
Poly m toluidine	Phase Method	8	0.132 ± 0.009
		10	0.139 ±0.004
	Amplitude method	8	0.132 ±0.007
		10	0.139 ±0.003
Poly ditheylaniline	Phase Method	10	0.211 ±0.001
		12	0.210 ±0.002
	Amplitude Method	10	0.211 ±0.003
		12	0.222 ±0.004

Table I shows the thermal diffusivity values obtained for the three plasma polymerized samples with carbon tetrachloride as the coupling medium

different modulation frequencies. All the graphs are linear and thermal diffusivity values are calculated from the slopes, which are tabulated in Table II. It is found that Table I and

Table II are in good agreement. Moreover, the measurement carried out at a different modulation frequency also yielded the same value. If there were any contribution from the coupling media, then the thermal diffusivity value calculated would have been different for different modulation frequencies [26] and also the two coupling media with different thermal properties would have yielded different results. The contribution from the coupling fluid to the photothermal signal becomes dominant in the skimming configuration only when the thermal diffusivity of the coupling fluid is greater than that of the sample. In the present work, although the thermal

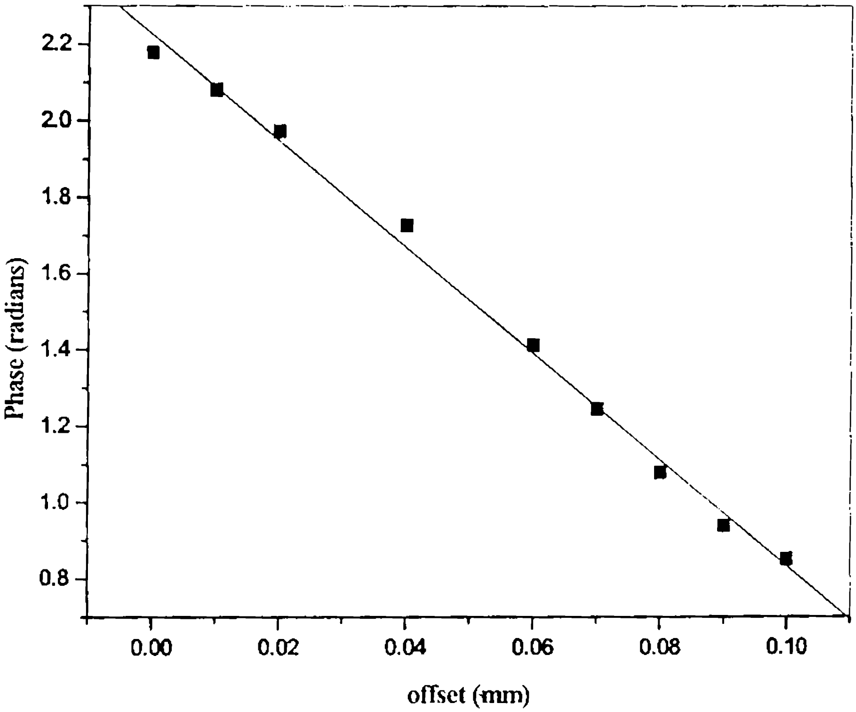

Figure (16) phase vs. the pump-probe offset for 10 Hz in liquid paraffin for poly o toluidine

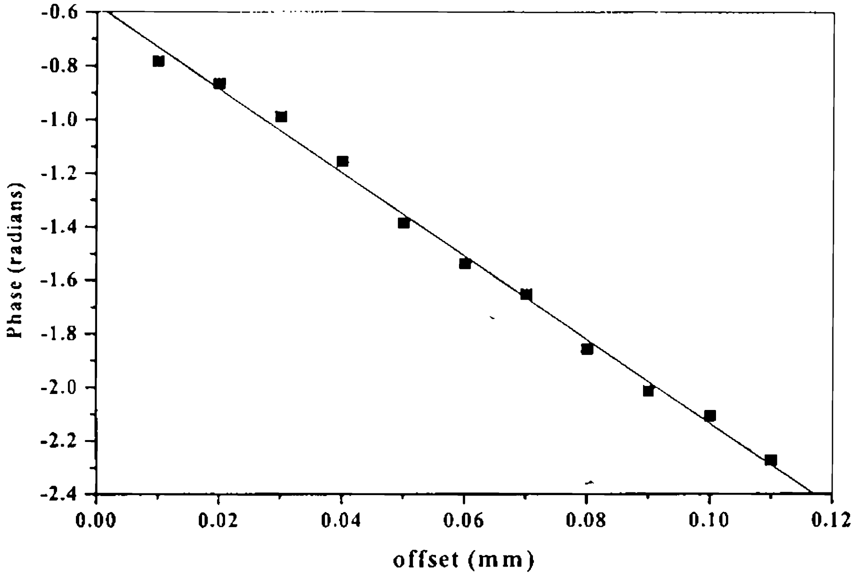

Figure (17) phase vs. the pump-probe offset for 12 Hz in liquid paraffin for poly o toluidine

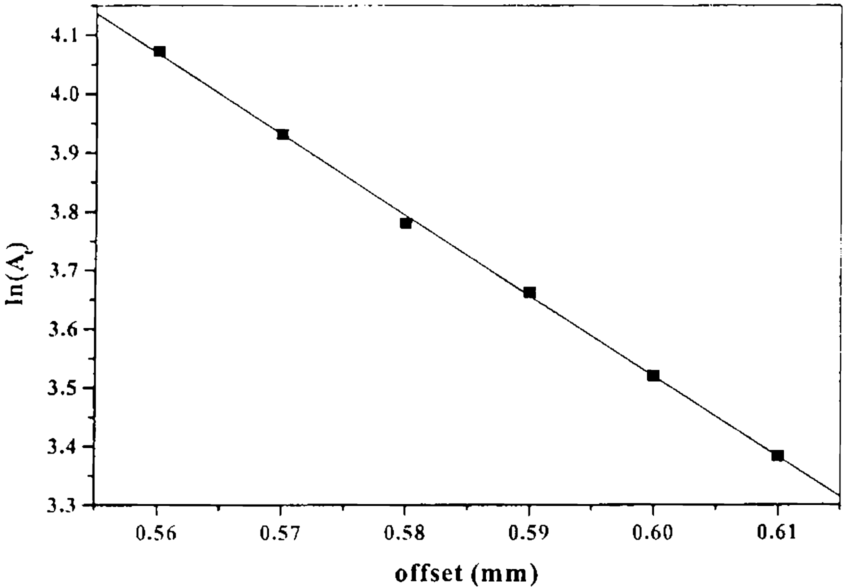

Figure (18) ln(Amplitude) vs. the pump-probe offset for 10 Hz in liquid paraffin for poly o toluidine

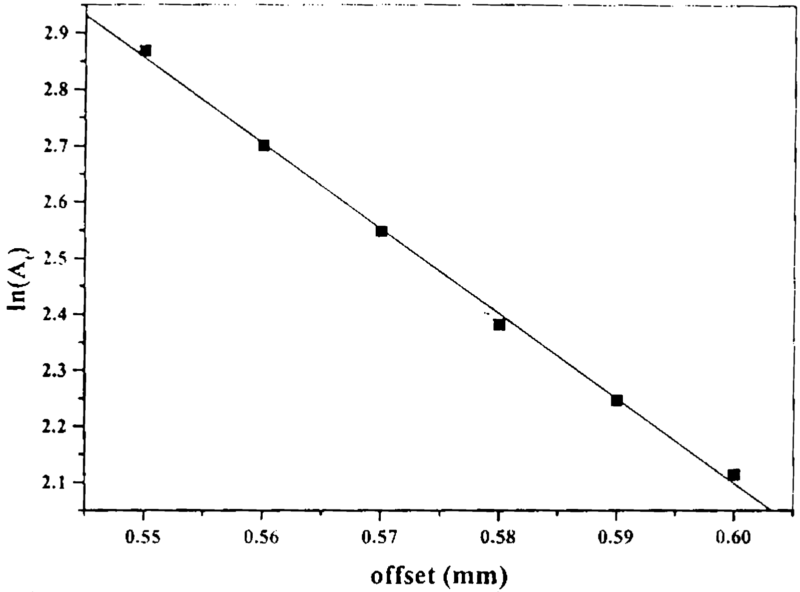

Figure (19) ln(Amplitude) vs. the pump-probe offset for 12 Hz in Liquid Paraffin for poly o toluidine

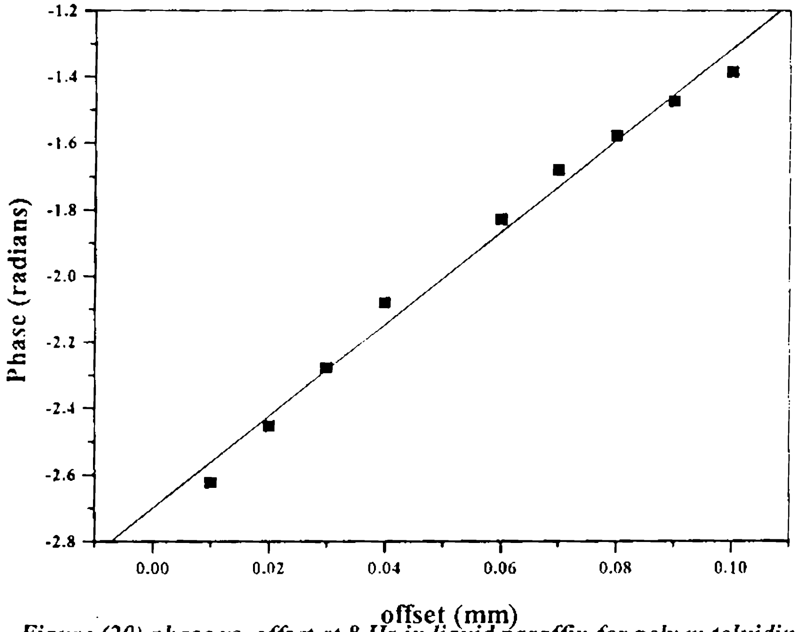

Figure (20) phase vs. offset at 8 Hz in liquid paraffin for poly m toluidine

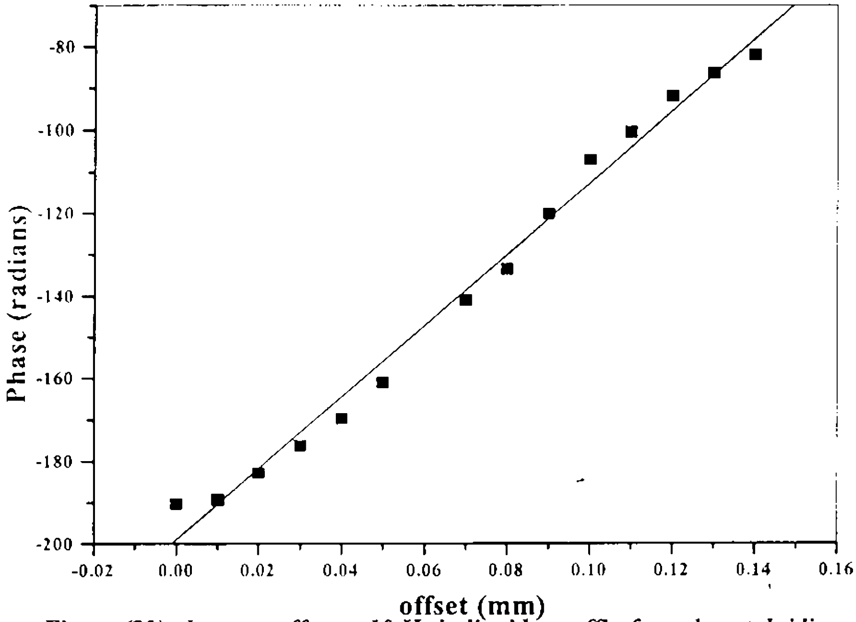

Figure (21) phase vs. offset at 10 Hz in liquid paraffin for poly m toluidine

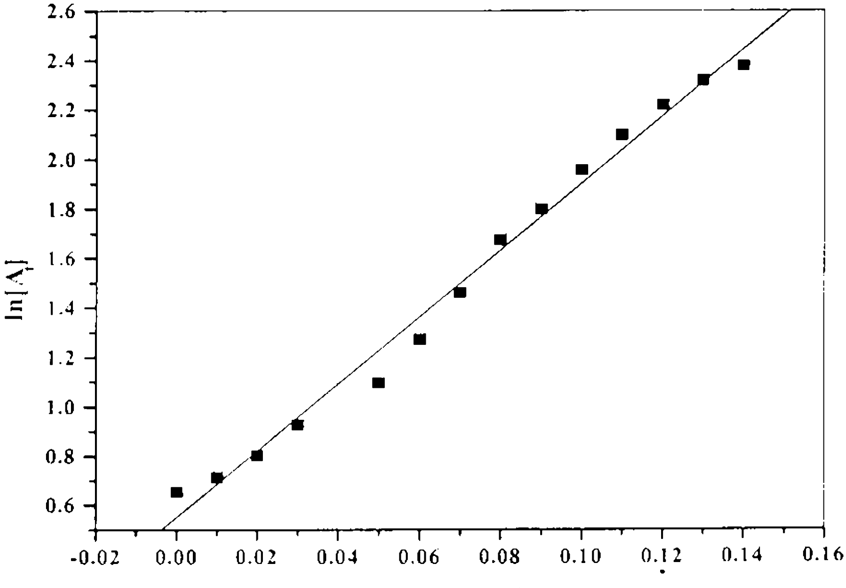

Figure (22) ln(amplitude) vs. offset at 8 Hz in liquid paraffin for poly m toluidine

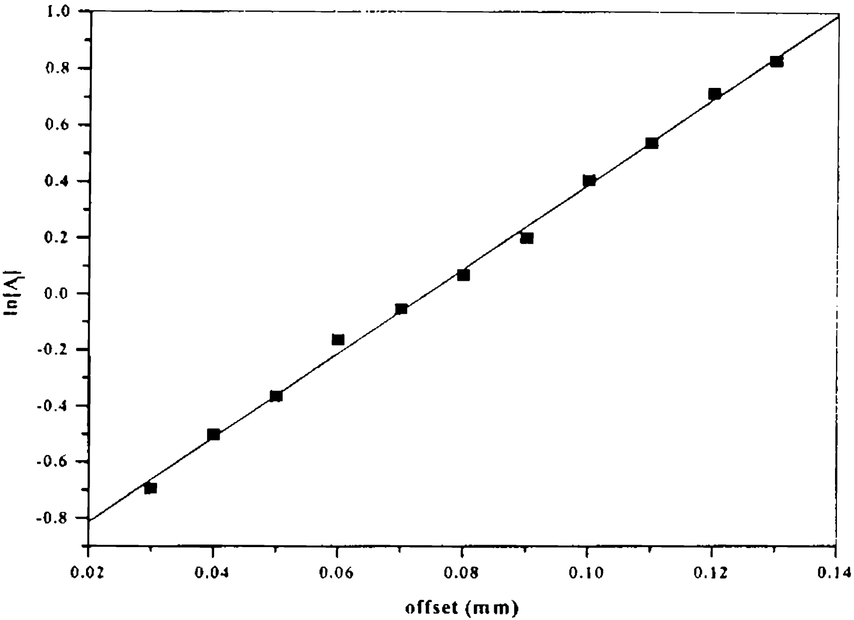

Figure (23) ln(amplitude) vs. offset at 10 Hz in liquid paraffin for poly m toluidine

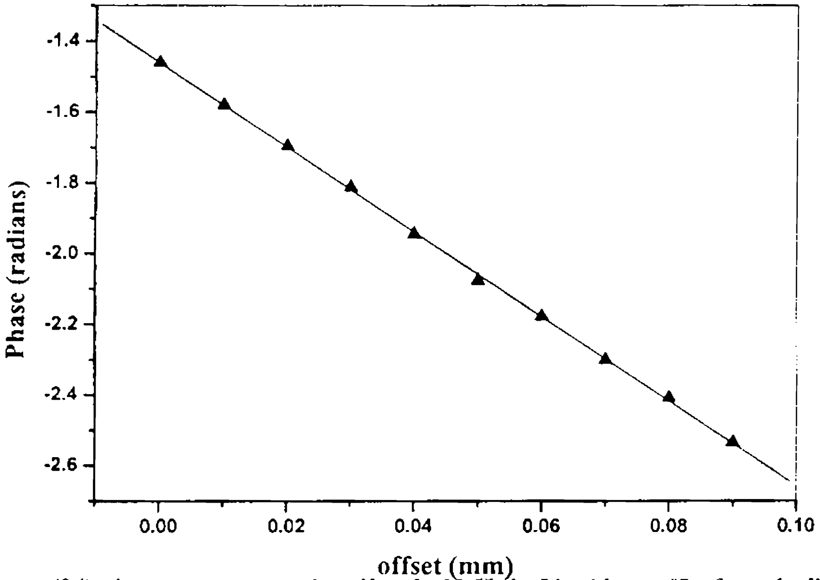

Figure (24) phase vs. pump-probe offset for10 Hz in Liquid paraffin for poly diethylaniline

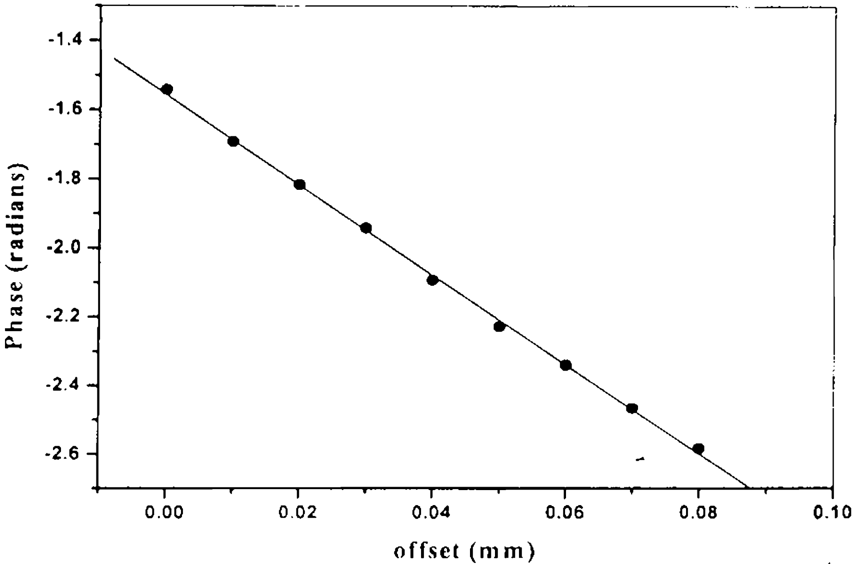

Figure (25) phase vs. pump-probe offset for12 Hz in Liquid paraffin for poly diethylaniline

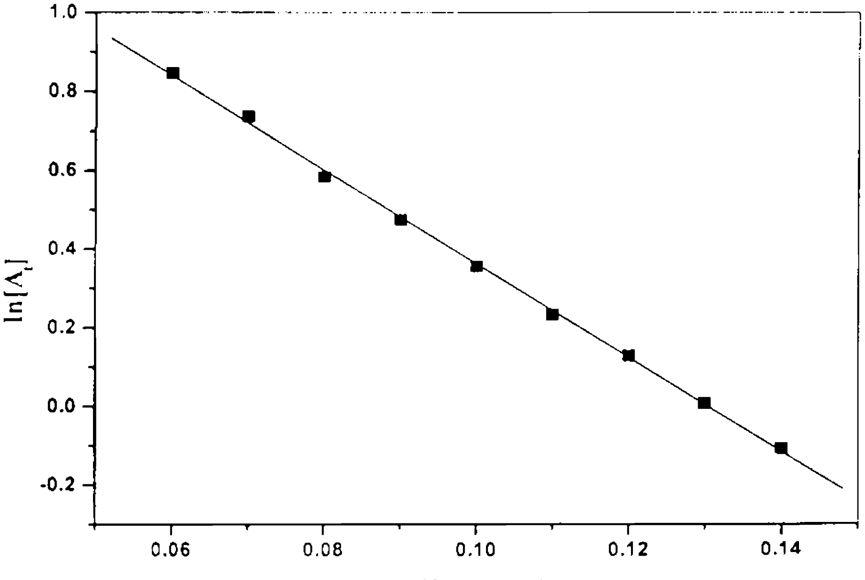

Figure (26) ln(Amplitude) vs. pump-probe offset for10 Hz in Liquid paraffin for poly diethylaniline

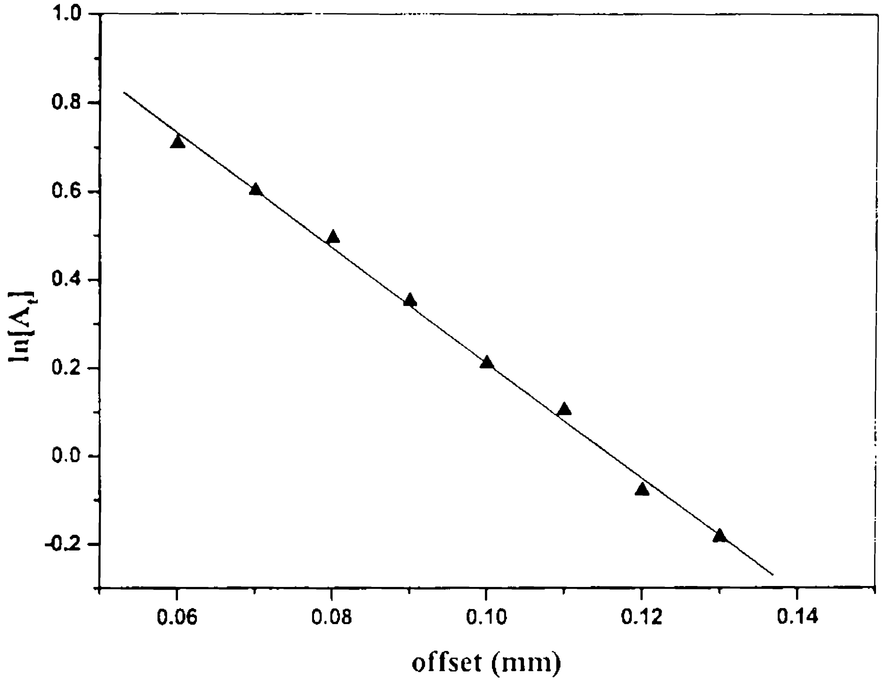

Figure (27) ln(Amplitude) vs. pump-probe offset for12Hz in Liquid paraffin for poly diethylaniline

diffusivity of the samples under study are low, the coupling media chosen in our measurements carbon tetrachloride (D_{CCl_4} ~ 0.731 x 10^{-3} cm^2s^{-1})and liquid paraffin ($D_{liquid\ paraffin}$ ~ 0.3 x 10^{-3} cm^2s^{-1}) have still lower diffusivity values. In conclusion, the thermal properties of the coupling media do not influence the photothermal measurements.

As verified from their absorption spectra, all the samples under investigation shows very low absorption at the pump laser wavelength, and are thermally thin at the modulation frequencies used in the experiment. In such circumstances, substrate absorption can play non-negligible role in the photothermal measurements. As a result, the samples must now be treated as layered one and we have to relax the assumption that the backing or substrate is non-absorbing. However, in the present work, the samples are coated on to a glass substrate, which is perfectly non-absorbing at the pump beam wavelength. Hence, the effect of substrate on the photothermal measurements can be neglected [30].

While dealing with the polymer samples, another important factor to be dealt with is the effect of the temperature rise on the expansion of the samples. However, the temperature rise in the heated area is estimated to be approximately 1 degree, which can cause a surface deformation of only <1nm. This expansion can affect the photothermal measurements only when the bouncing configuration is employed. In the present work, skimming configuration is used where the probe beam skims the sample surface and the height of the probe beam above the sample surface is limited by the spot size of the probe beam. Due to the large spot size of the probe beam compared to the surface deformation, any error in the photothermal measurements caused by the thermal expansion of polymers is completely eliminated.

In conclusion, the thermal diffusivity values of r.f plasma polymerized poly *o*-toluidine, poly *m*- toluidine and poly diethyl aniline thin films are measured using a compact and simple photothermal beam deflection experimental setup. The analysis of the deflection signal for thermal diffusivity is done using the Phase method and is verified using the Amplitude method. The measurements are repeated for different modulation frequencies and for two different coupling media, all of which are found to lead to similar results.

Sample	Method of Analysis	Frequency (Hz)	Thermal Diffusivity ($10^{-2}cm^2s^{-1}$)
Poly *o* toluidine	Phase Method	10	0.162 ± 0.008
		12	0.155 ± 0.005
	Amplitude Method	10	0.167 ± 0.005
		12	0.164 ± 0.005
Poly *m* toluidine	Phase Method	8	0.132 ±0.006
		10	0.139 ±0.004
	Amplitude method	8	0.137 ± 0.004
		10	0.138 ± 0.005
Poly diethylaniline	Phase Method	10	0.219 ± 0.003
		12	0.221 ± 0.004
	Amplitude Method	10	0.220 ±0.001
		12	0.221 ± 0.007

Table II shows the thermal diffusivity values of the three plasma-polymerized samples with liquid paraffin as the coupling fluid.

REFERENCES:

1) Jeffrey A Sell, *Photothermal Investigations on Solids and Fluids*, Academic Press Inc, New York (1989)
2) A.Rosencwaig, A.Gersho, *J.Appl.Phys.* **47,** (1976) 64
3) A. Rosencwaig, *Photoacoustics and Photoacoustic Spectroscopy*, John Wiley & Sons, New York, (1980)
4) C. Garcia-Segundo, M.Villagran-Muniz, S.Muhi, *J.Phys.D: Appl.Phys* **31**, (1988) 165.
5) J.A.Balderas lopez, D.Acosta-Avalos, J.J.Alvarado, O.Zelaya-Angel, F.Sanchez-Sinencio, C.Falcony, A.Cruz-Orea, H.Vargas, *Meas.Sci.Technol.* **6** (1995) 1163
6) A.Rosencwaig, T.W.Hindley, *Appl.Opt.* **20(4)** (1981) 606.
7) E.Marin, H.Vargas, P.Diaz, I.Riech *Phys.stat.sol (a)* **179** (2000) 387.
8) J.C.Murphy, L.C.Aamodt, *J.Appl.Phys.* **51(9)** (1980) 4580.
9) L.C.Aamodt, J.C.Murphy, *J.Appl.Phys.* **52(8)** (1981) 4903.
10) M.A.Schweitzer, J.F.Power, *Appl.Spectro.*, **48(9)** (1994) 1054.
11) M.A.Schweitzer, J.F.Power, *Appl.Spectro.*, **48(9)** (1994) 1076
12) P.K.Kuo, M.J.Lin, C.B.Reyes, L.D.Favro, R.L.Thomas, D.S.Kim, Shu-Yi-Zhang, L.J.Inglehart, D.Fournier, A.C.Bocarra, N.Yacoubi, *Can.J.Phys.*, **64** (1986) 1165.
13) P.K.Kuo, E.D.Sendler, L.D.Favro, R.L.Thomas, *Can.J.Phys.* **64** (1986) 1168.
14) A.Mandelis, Martin M.Zver, *J.Appl.Phys.* **57(9)** (1985) 4421.
15) C.Preethy Menon, J.Philip, *Meas.Sci.Technol.*, **11**(2000) 1744.
16) M.A.Sheikh, S.C.Taylor, D.R.Hayhurst,R.Taylor *J.Phys.D:Appl.Phys.***33**(2000) 1536.
17) F.Charbonnier, D.Fournier, *Rev.Sci.Instrum* **57(6)** (1986) 1126.
18) E.Legal Lasalle, F.Lepoutre, J.P.Roger, *J.Appl.Phys.* **64(1)** (1988) 1.

19) M.Bertolotti, V.Dorogan, G.Liakhou, R. Li Voti, S. Paoloni, C.Sibilia, *Rev.Sci.Instrum* **68(3),** 1521 (1997)

20) Turner RH, Segall I, Boerio FJ, Davis GD. *J Adhesion* **62** (1997) 1.

21) Alexander MR, Duc TM. *Polymer* **40(20)** (1999) 5479

22) Alexander MR, Duc TM. *J Mater Chem* **8(4)** (1998) 937.

23) S. Kurosawa, N. Kamo, D. Matsui, Y. Kobatake, *Anal. Chem.* **62** (1990) 353

24) S. Kurosawa, E. Tawara-Kondo, N. Kamo, *Anal. Chim. Acta* **43** (1997) 175.

25) Y. Segui, Bui Ai, *Thin Solid Films* **50** (1978) 321.

26) M.Bertolotti, R.Li Voti, G.Liakhou, C.Sibilia, *Rev.Sci.Instrum* **64(6)** (1993) 1576

27) X.Quelin,B.Perrin, G.Louis, P.Peretti, *Phys.revB* **48 (6)** (1993)3677

28) D.Fournier, C.Boccara, A.Skumanich, N.M.Amer *J.Appl.Phys* **59(3)** (1986) 787.

29) H. Yasuda, *Plasma Polymerization*, Academic Press, New York, 1985

30) G.Amato, G.Benedetto, M.Maringelli and R.Spagnolo, *Appl. Phys A* **52** (1991) 280

CHAPTER V

PHOTOACOUSTIC INVESTIGATIONS ON CERTAIN COPPER DELAFOSSITES

5.1 INTRODUCTION:

Substances exhibiting high electrical conductivity, optical transparency and which can be efficiently grown into thin films are essential for the next generation photovoltaics, energy efficient windows, flat panel displays, organic LED's and other optoelectronic applications. Though certain transparent conductors like ITO and F-doped SnO_2 are extensively studied and used, they are insufficient for many future applications. It is seen that the best p-type materials have much poorer properties than their n-type analogues [1]. Majority of the transparent conducting oxides exhibit only n type electrical conductivity. This limits their application to transparent electrodes and coating films for IR reflection. The full potential of transparent conducting oxides (TCO's) can be realized only if p-type is developed. For instance, a combination of two types of transparent conducting oxides namely a **p** type and **n** type in the form of a **pn** junction would lead to a functional window that transmits visible light and yet generates electricity in response to the absorption of ultraviolet photons [2, 3]. Transparent conducting oxides like ZnO and SnO_2 are transparent similar to glass but conductive like metal. The traditional TCO's can be readily doped to form n type but never p type. Bipolar doping, namely n type and p type doping is even more difficult. Moreover, in the case of oxides the valence band is generally the 2p band of Oxygen. Though it is not difficult to produce holes in this band through doping, the mobility of these holes is low. The electronic conductivity of such p type oxides is highly activated and can be generally measured at temperatures well above room temperature. The solution suggested to overcome the problem of low mobility holes is the use of a valence band that is not the 2p band of oxygen but d or s band of a cation. However recent discovery [3] of a p type delafossite oxide thin film, $CuAlO_2$, is an important step in that they even provide a mechanism for equilibrium bipolar doping [4].

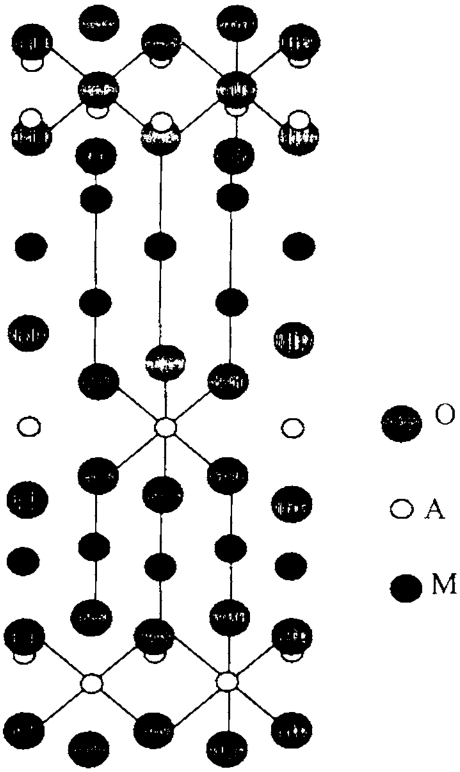

Figure (1): Structure of delafossite

Delafossite type compounds have a general formula ABO_2 where A is a monovalent metal ion (Cu, Ag, Pd, Pt) and B is a trivalent ion (Al, In, Ga, Cr, Co, Fe etc.). The trivalent B ions are octahedrally surrounded by oxygen ions and the octahedral are connected to form sheet, perpendicular to the c-axis, of net composition $[MO_2]^-$. The A ions are also in layers perpendicular to the c-axis and sandwiched between the $[MO_2]^-$ layers. Each A ion forms two collinear A-O bonds with oxygen ions in neighboring layers. These compounds crystallize in a simple structure built of infinite one-octahedron thick sheets of close packed MO_6 octahedra. These layers are linked together by the A-atoms, forming linear O-A-O units, which are appropriate for A^+ cations. The stacking of successive layers of MO_6 octahedra can result in different polytypes of which two common ones are 3R and 2H delafossites. The electrical properties of the delafossites depend on which ion occupies the A site: Pd and Pt (d^9 ions) result in conductivity while Cu and Ag (d^{10} ions) produce semiconductivity [5]. Delafossites are being employed as catalysts, for flat panel displays, organic LEDs and various other optoelectronic applications in addition to their recent solar applications [3, 6]. In copper delafossites, the monovalent metal ion is Cu. The electronic, optical and structural properties of certain delafossites are studied extensively by several workers [2,4,7,8,9,10,11]. However, the thermal properties like thermal conductivity (related to thermal diffusivity), which is equally important to electrical conductivity, remains relatively unexplored. In the present chapter, the results of a photoacoustic study of the thermal diffusivity and transport properties like carrier diffusion coefficient and surface recombination velocity of certain polycrystalline copper delafossites, $CuGa_{1-x}Fe_xO2$ (x = 0 to 1) is reported.

Polycrystalline $CuGa_{1-x}Fe_xO_2$ powders are prepared from a mixture of 99.9% pure Cu_2O, Ga_2O_3 and Fe_2O_3. The mixture was pelletised and heated at 1100°C for 24 hours in argon atmosphere. The solid solution of $CuGa_{1-x}Fe_xO_2$ in delafossite structure can be formed for x=0 to x=1. The X-ray diffraction patterns of $CuGa_{1-x}Fe_xO_2$ (x=0 to 1) do not show any peaks of impurity phases. The $CuGa_{1-x}Fe_xO_2$ crystallizes as the 3R delafossite poly type (space group R3m). The powdered samples are again pelletised and sintered at 1200°C in nitrogen atmosphere.

The versatility and potential of the photoacoustic (PA) technique in the characterization of materials has been well established [12-18]. Photoacoustic technique generally consists in a closed cavity detection of the energy liberated by atoms or molecules through non-radiative de-excitation mechanism subsequent to the light absorption by a sample. In the PA technique, the sample to be studied is placed in a closed cell or chamber. For gases and liquids the sample generally fills the chamber [18]. However in the case of solids, the sample fills only a portion of the chamber and the rest of the chamber is filled with non-absorbing gas such as air. In the present work, we deal only with the PA studies on solid samples.

When the sample is irradiated with modulated electromagnetic radiation, absorption of the intermittent radiation and subsequent non-radiative de-excitation takes place in the sample material. This results in an acoustic signal in the gas medium with which the sample surface is in contact within the cell or chamber. The acoustic signal thus generated can be detected by a sensitive transducer (microphone) kept inside the cell. The theoretical explanation to this effect in condensed media formulated by Rosencwaig and Gersho [19] is given in chapter I of the thesis. The photoacoustic cells are designed depending upon the sample (solid, liquid or gas) and also on the purpose of measurement (trace gas detection, optical absorption, thermal characterization, temperature varying measurements etc.). In any case, PA cells are broadly classified into two: resonant and non-resonant cells. A phase transition measurement, where the sample temperature has to be varied, requires a resonant cell, where the microphone is separated from the sample chamber by a long narrow tube. In non-resonant cells, the microphone is placed in close proximity of the sample so that the gas volume can be minimized which in turn provides better signal. In the present work, an open photoacoustic cell (OPC) in the transmission detection configuration is used for measuring the thermal and transport properties of the copper delafossites.

5.2 OPEN PHOTOACOUSTIC CELL CONFIGURATION:

Open photoacoustic cell configuration is a modified and convenient form of the conventional photoacoustic cell. This technique has been successfully applied for the study of optical spectra of liquids [20], discrimination of bulk and surface optical absorption coefficients [21], determination thermal and transport properties [22,23] etc. The open cell photoacoustic theory was developed by Helander *et al* [24, 25] and was later modified by McQueen *et al* [26]. The OPC technique does not require additional transducer medium like air chamber in the case of conventional PA cells and may be called minimal volume PA detection. The solid sample is mounted directly on to the top of microphone leaving a small volume of air in between the sample and the microphone. OPC detection has been widely employed in thermal characterization of samples. A schematic representation of the open photoacoustic cell is shown in figure (2). The periodic pressure variation in the air chamber can be derived using the R-G theory. The sample is assumed to be optically opaque so that whole energy is absorbed at the sample surface itself and the heat flux into the surrounding air is negligible.

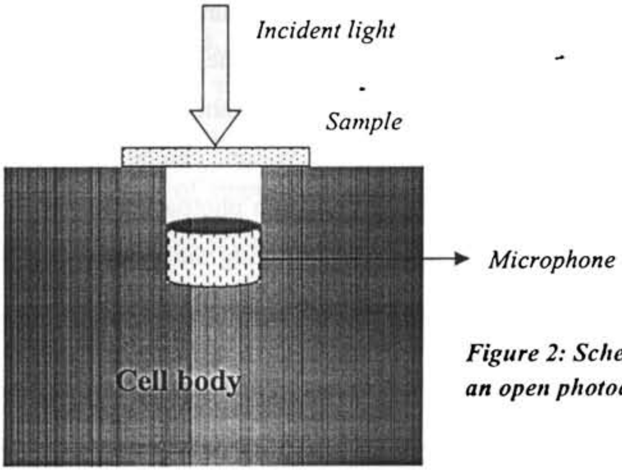

Figure 2: Schematic representation of an open photoacoustic cell.

The expression for the PA signal from the 1-D heat flow model of Rosenwaig and Gersho [27] is obtained as

$$\delta P = \frac{\gamma P_0 I_0 \left(\alpha_g \alpha_s\right)^{1/2}}{2\pi l_g T_0 k_s f \sinh\left(l_s \sigma_s\right)} \exp\left[j\left(\omega t - \pi/2\right)\right] \qquad (1)$$

where γ is the air specific heat ratio, $P_0(T_0)$ is the ambient pressure (temperature), I_0 is the absorbed light intensity, f is the modulation frequency, and l_i, k_i and α_I are the length, thermal conductivity and thermal diffusivity of material I respectively. Here i subscript denotes the sample (s) and gas (g) media respectively and $\sigma_g = (1+j)a_g$, $a_g = \left(\pi f/\alpha_g\right)^{1/2}$ is the complex thermal diffusion co-efficient of the material i.

If the sample is optically opaque and thermally thick then equation (1) reduces to

$$P \cong \frac{\gamma P_0 I_0 \left(\alpha_g \alpha_s\right)^{1/2}}{\pi l_g T_0 k_s} \frac{\exp - l_s \left(\pi f/\alpha_s\right)^{1/2}}{f} \exp\left[j\left(\omega t - \pi/2 - l_s a_s\right)\right] \qquad (2)$$

where l_s and a_s are the thickness and thermal diffusion coefficient of the sample. Thus, according to equation (3) the amplitude of the PA signal varies with modulation frequency as $\left(1/f\right)\exp\left[-l_s\left(\pi f/\alpha_s\right)^{1/2}\right]$ and phase varies as $-l_s\left(\pi f/\alpha_s\right)^{1/2}$. Hence, thermal diffusivity can be obtained either from the phase data or amplitude data. However in the case of plate shaped solid samples surrounded by air, the contribution of the photoacoustic signal from the thermoelastic bending of the sample cannot be neglected, especially in the case of thermally thick samples [28]. This effect is mainly due to the temperature gradient inside the sample along the z-axis as shown in figure (3).

Since the temperature gradient exists in a direction parallel to the z-axis, thermal expansion depends on the z. This z dependence of the displacement along the radial direction induces a bending of the plate in the z direction (drum effect) [29].

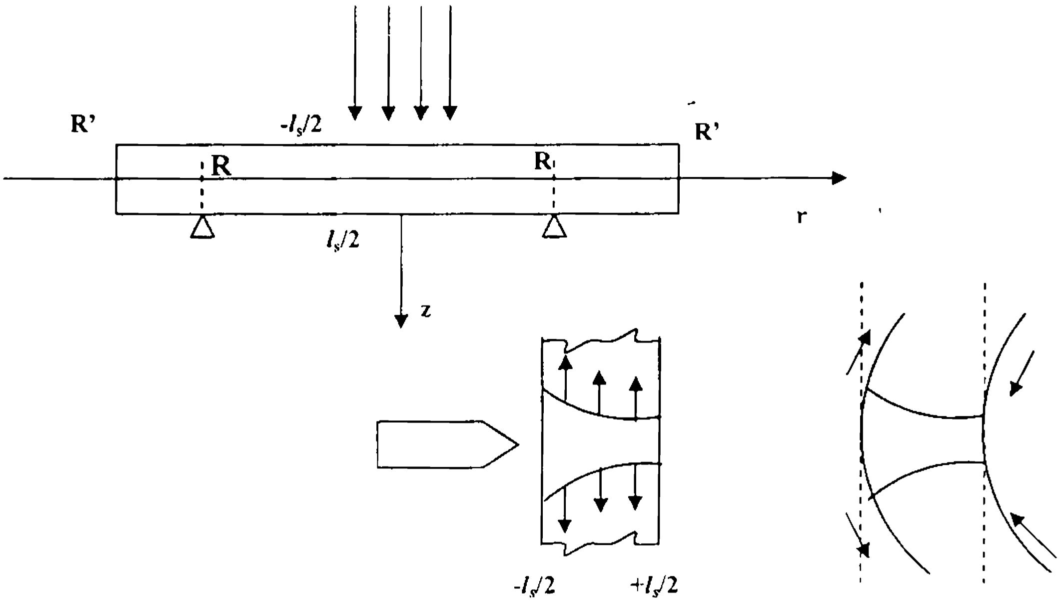

Figure (3): Geometry and sources of surface strain for the thermoelastic bending. R' and R are the microphone inlet hole radii

The contribution from the sample bending is described by a coupled set of equations. The heating caused by the surface displacement (elastic waves) is neglected. For the configuration shown in figure 3, assuming that all the light is absorbed at the surface,

$$T_s(z) = \frac{I_0}{k_s\sigma_s}\frac{\cosh\{[z-(l_s/2)]\sigma_s\}}{\sinh(l_s\sigma_s)}e^{j\omega t} \tag{3}$$

neglecting the inertial term also since the experiment is performed at low frequencies. Assuming that the sample is cylindrically symmetric and thin enough such that $l_s << R'$. In this condition the stress condition is applicable i.e. one has $\sigma_{zz} = \sigma_{rz} = 0$ along z direction where σ_{ij} is the stress tensor. Then on solving the set of thermoelastic equations for the sample displacement u_r and u_z along the radial and z directions subjected to the boundary conditions that the sample is simply supported at r=R and $z=l_s/2$ and that at the edges r=R' it is free of forces and moments, one gets

$$u_z(r,z) = \alpha_T\left\{\frac{6(R^2-r^2)}{l_s^3}M_T + \frac{1+v}{1-v}\int_{l_s/2}^{z}dzT_s - \frac{v}{1-v}\times\left[\frac{12M_T}{l_s^3}\left(z^2-\frac{l_s^2}{4}\right)+\frac{2N_T}{l_s}\left(z-\frac{l_s}{2}\right)\right]\right\} \tag{4}$$

with

$$M_T = \int_{-l_s/2}^{l_s/2}dzzT_s \quad N_T = \int_{-l_s/2}^{l_s/2}dzT_s \tag{5}$$

The first term in equation (5) represents the bending of the sample and the other ones are due to the thickness dilation. The thermoelastic contribution P_{el} to the pressure fluctuation in the PA chamber can be calculated if the sample displacement along the z direction is known using the piston model as

$P_{el} = \gamma P_0 {}^{\Delta V}\!/\!{}_{V_0}$ where ΔV is the volume change due to the sample surface displacement.

$$\text{Hence } P_{el} = \frac{\gamma P_0 2\pi}{V_0} \int_0^R dr\, r u_z\left(r, \frac{l_s}{2} \right) \tag{6}$$

Combining equations 3, 4 & 5,

$$P_{el} = \frac{3\alpha_T R^4}{R_c^2 l_s^2} \times \frac{\gamma P_0 I_0}{l_g K_s \sigma_s^2} \left(\frac{\cosh(l_s\sigma_s) - \left(\left({}^{l_s\sigma_s}\!/\!{}_2 \right) \sinh(l_s\sigma_s) \right) - 1}{l_s\sigma_s \sinh(l_s\sigma_s)} \right) e^{j\omega t} \tag{7}$$

where R_c is the radius of the PA chamber in front of the diaphram. It follows from equation (7) that fro a thermally thin sample $(l_s\sigma_s) << 1$, the thermoelastic contribution to the PA signal reduces to

$$P_{el} \approx \frac{\alpha_T R^4 \gamma P_0 I_0}{8 R_c^2 l_g k_s} e^{j(\omega t + \pi)} \tag{8}$$

This means that the PA signal becomes independent of the modulation frequency while its phase ϕ_{el} approaches 180^0. AT the same time for a thermally thick sample,

$$P_{el} = \frac{3\alpha_T R^4 \gamma P_0 I_0 \alpha_s}{4\pi R_c^2 l_s^2 l_g k_s f} \left[\left(1 - \frac{1}{x} \right)^2 + \frac{1}{x^2} \right]^{1/2} e^{j\left[\omega t + \left(\pi/2 \right) + \phi\right]} \tag{9}$$

where $x = l_s a_s = l_s\left(\pi f/\alpha_s\right)^{1/2}$ and

$$\tan\phi = 1/(x-1) \tag{10}$$

At high modulation frequencies such that x>>1, the thermoelastic contribution varies as f^{1} and its phase ϕ_{el} approaches 90^0 as

$$\phi_{el} = \pi/2 + \arctan\left(1/[x-1]\right)$$

(11)

Thus for a thermally thick sample, if the thermoelastic contribution is dominant then the thermal diffusivity can be evaluated from the modulation frequency dependence of either the signal amplitude or its phase.

5.3 EXPERIMENTAL

The main components of the experimental setup are 1) pump laser for exciting the sample 2) chopper to provide an intensity modulation for the incident beam 3) a photoacoustic cell (which in the present case is an open photoacoustic cell) with an electret microphone attached to it for detecting the acoustic (pressure) wave. Necessary biasing must be given to the microphone depending upon the specifications of the one used. The important criteria to be met with the electret microphone used is that it should have high sensitivity and flat response in the frequency range chosen for the experiment.4) Lock-in amplifier for obtaining the amplitude and phase of the pressure wave.

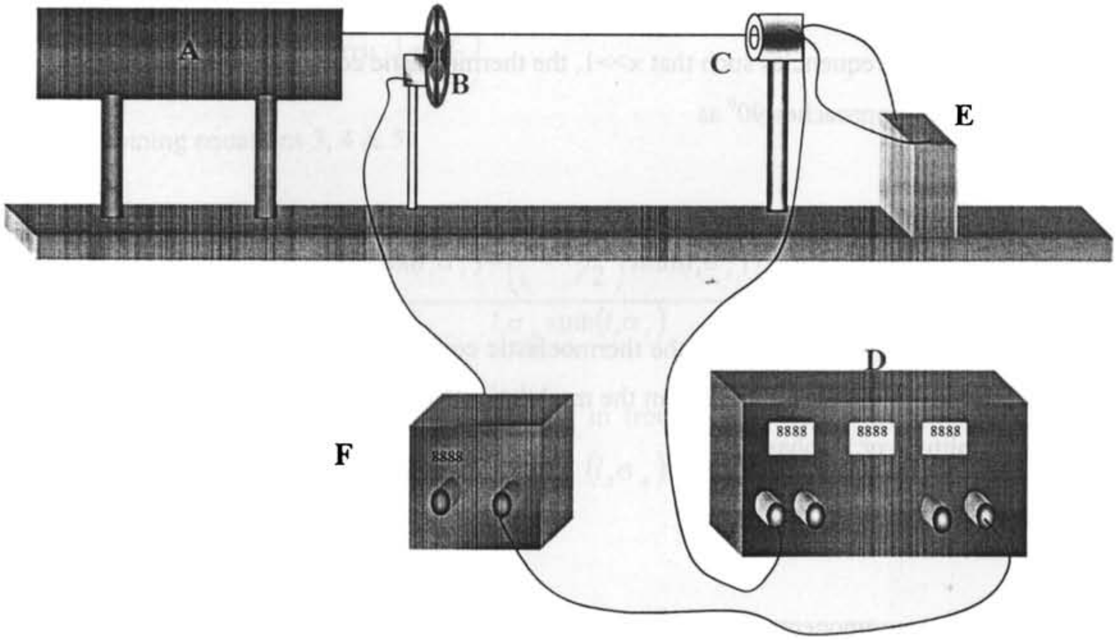

Figure 4: A: ***He-Ne laser*, B: *Mechanical Chopper*,**
C: *OPC*, D: *Lock-in-Amplifier* E: *Battery* F: *Chopper control*

A schematic diagram of the experimental setup used is given by figure 4. A He-Ne laser (632.8 nm, 20 mW) is used as the excitation source and is intensity modulated using a mechanical chopper (Stanford SR 540). The samples in the form of discs are pressed directly on to the top of the OPC using vacuum grease The laser beam is used without focusing in order to minimize the lateral heat flow. The pressure fluctuations as a result of thermal waves produced are detected using an electret microphone (Knowles FG 3392). The amplitude and phase of the PA signal is obtained from the lock-in-amplifier (Stanford SR 830). Varying the modulation frequency and noting the phase and amplitude of the PA signal perform the experiment. The measurements are taken for samples of different thickness. The experimental setup is standardized using silicon wafer and InP of thickness 414 micrometers and 350 micrometers respectively. We obtained the thermal diffusivity values of 0.92 ± 0.007 cm^{2}s^{-1} for silicon and 0.414 ± 0.002 cm^{2}s^{-1} for InP. These values are in good agreement with the earlier results [30,31]. Figures (6) & (7) show the plots of phase vs. frequency$^{1/2}$ of silicon wafer and InP wafer.

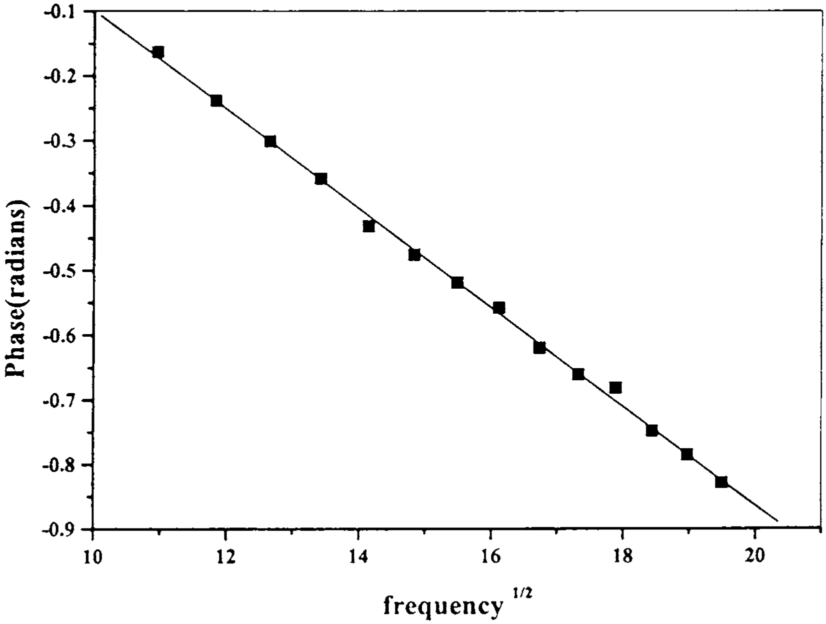

Figure (5): Plot of phase vs.frequency$^{1/2}$ for silicon wafer.

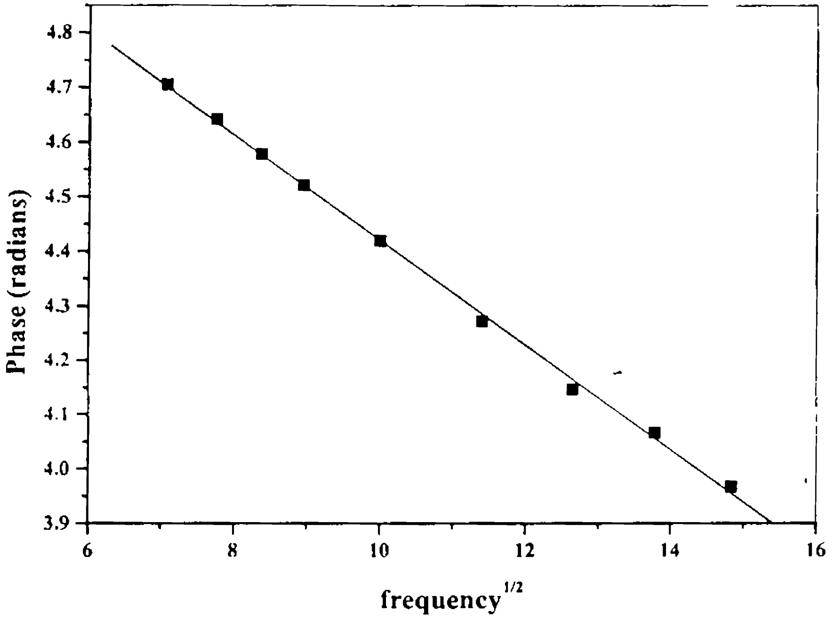

Figure (6): Plot of phase vs. frequency$^{1/2}$ for InP wafer

5.4 RESULTS AND DISCUSSION:

Figure (7) to (10) shows the variation of the PA signal amplitude with modulation frequency. It is observed that in each graph, at a particular frequency (f_{min}), the amplitude drops to a minimum and then increases. Furthermore, as thickness increases f_{min} decreases. This can be explained as follows: As frequency increases the thermal diffusion length (μ) decreases and at a low modulation frequency, the thermal diffusion length is large that it exceeds the thickness (l_s) of the sample. Hence, a point is reached when the thermal diffusion becomes smaller than the thickness or the thermal diffusion length falls inside the sample thickness as the frequency is increased. f_{min} thus corresponds to the frequency at which the sample changes from thermally thin ($\mu >> l_s$) to thermally thick ($\mu << l_s$) and has been reported by Qing Shen *et al* [32].

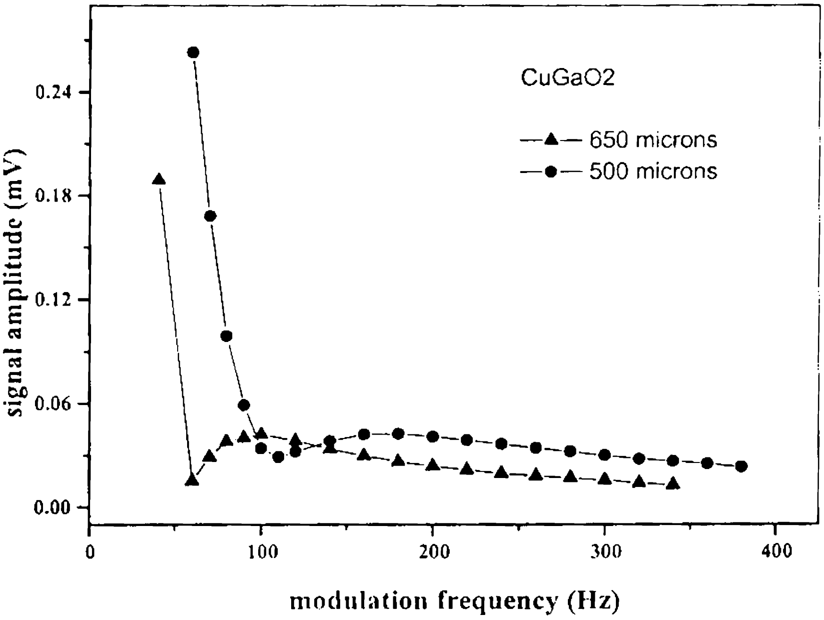

Figure (7): Variation of PA signal amplitude with modulation frequency.

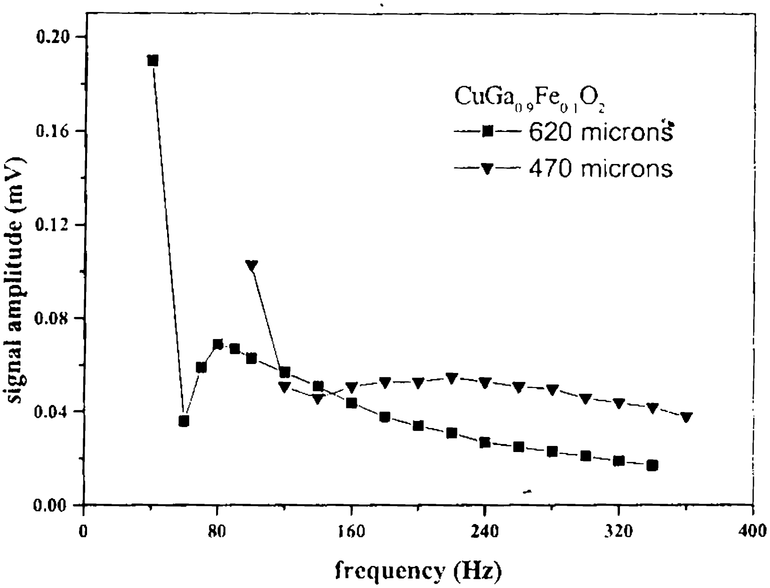

Figure (8): Variation of amplitude with frequency for $CuGa_{0.9}Fe_{0.1}O_2$

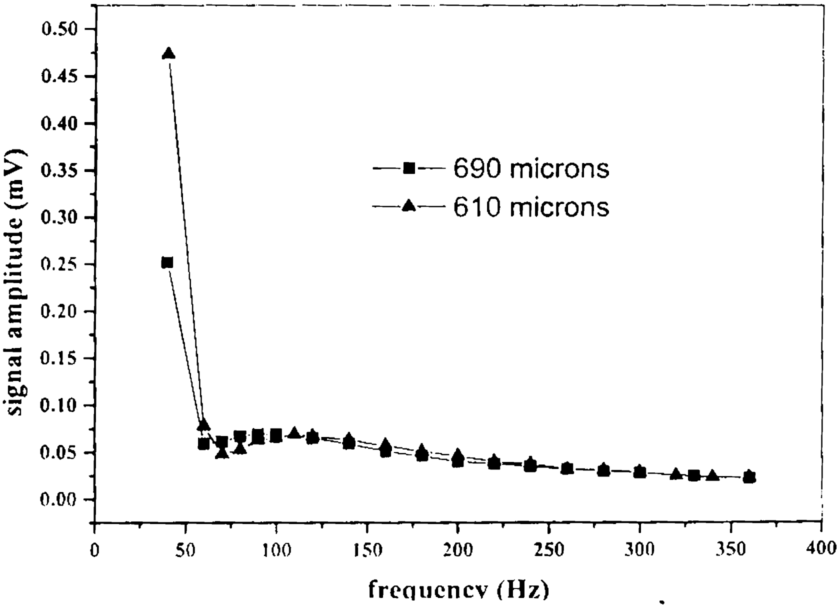

Figure (9): Variation of amplitude with frequency for $CuGa_{0.8}Fe_{0.2}O_2$

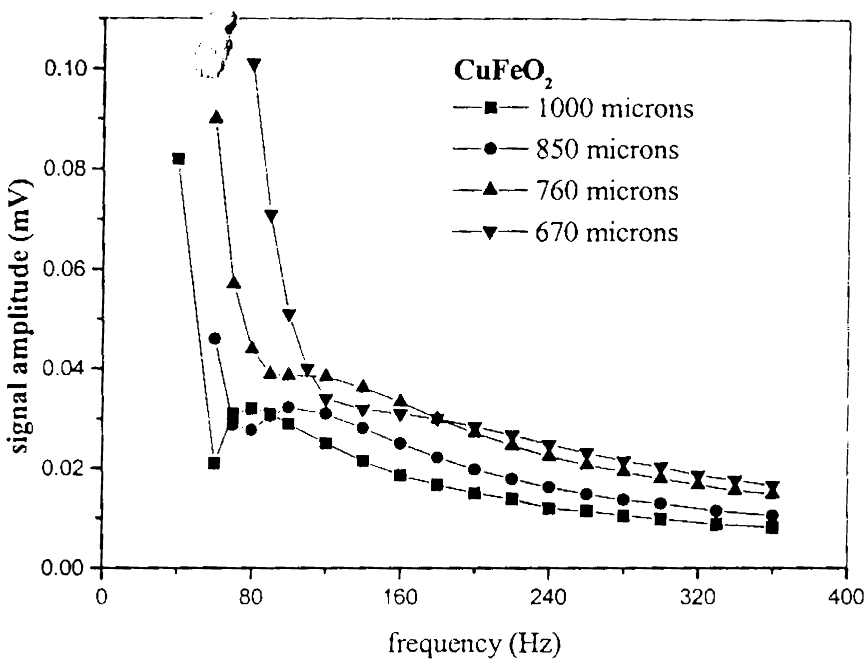

Figure (10): Variation of amplitude with frequency for CuFeO$_2$

The thermal diffusivity values are determined from the graph drawn between the phase and square root of modulation frequency. Figure (11) to (14) shows the plot of phase vs. square root of frequency for samples of different thickness.

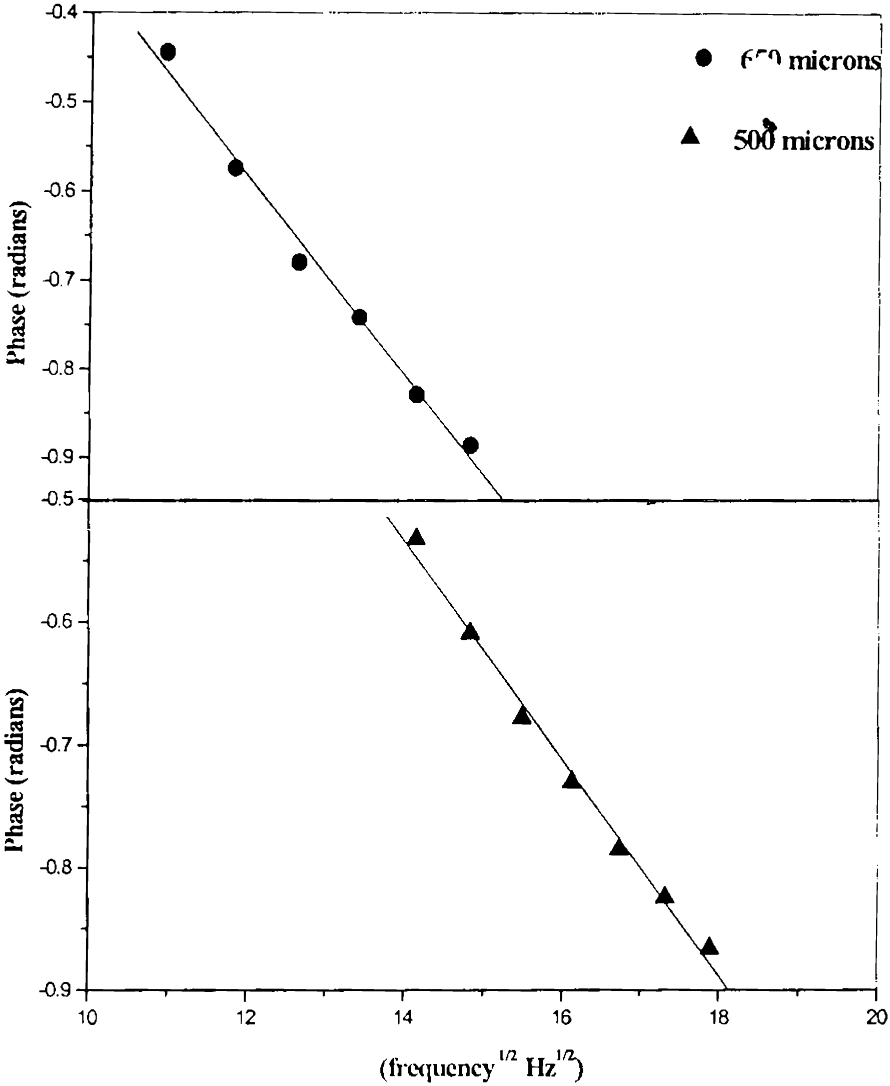

Figure (11): Plot of phase vs. square root of frequency for $CuGaO_2$

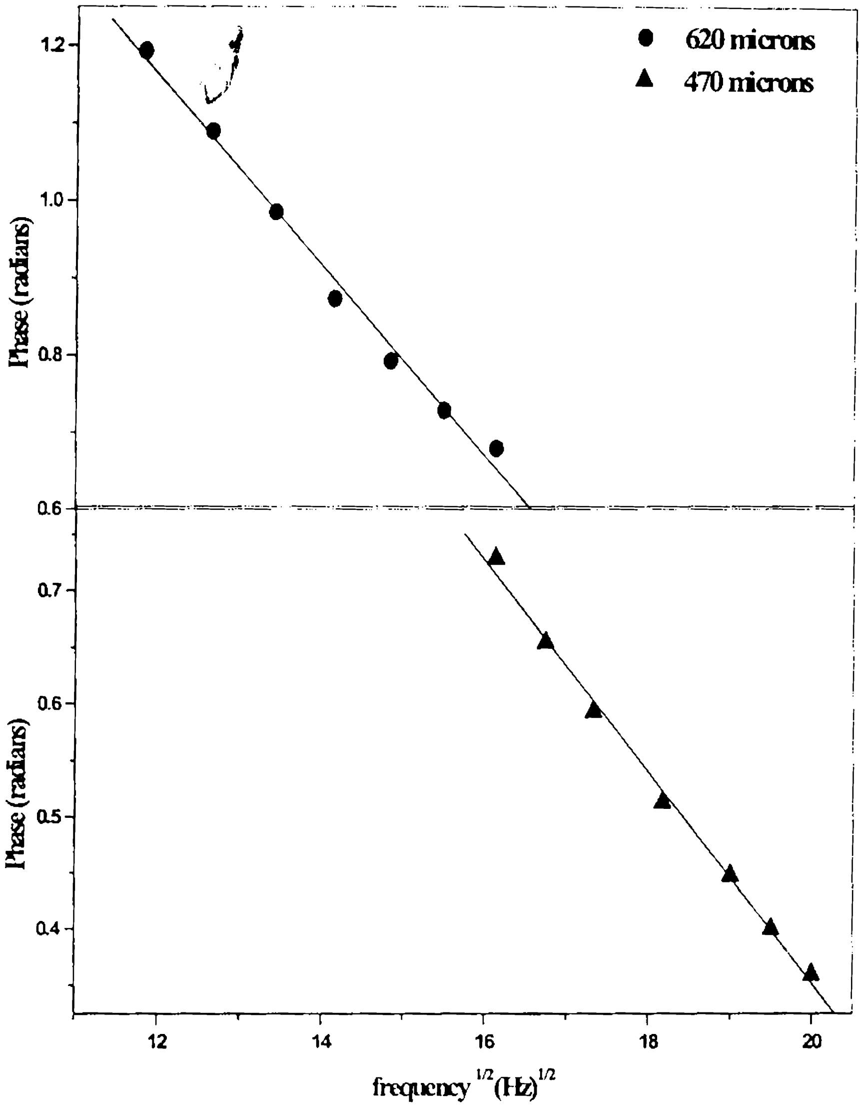

Figure (12): Plot of phase vs. square root of frequency for $CuGa_{0.9}Fe_{0.1}O2$

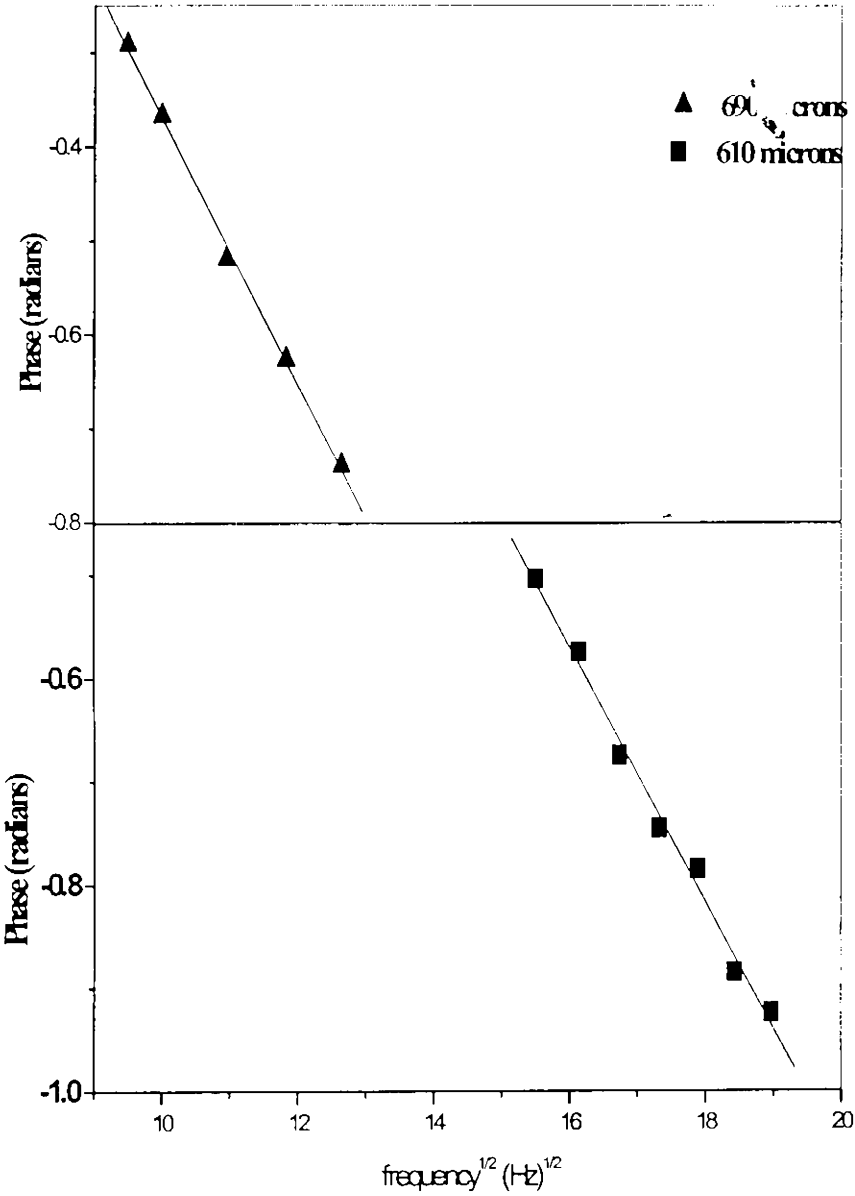

Figure (13): Plot of phase vs. square root of frequency for $CuGa_{0.8}Fe_{0.2}O_2$

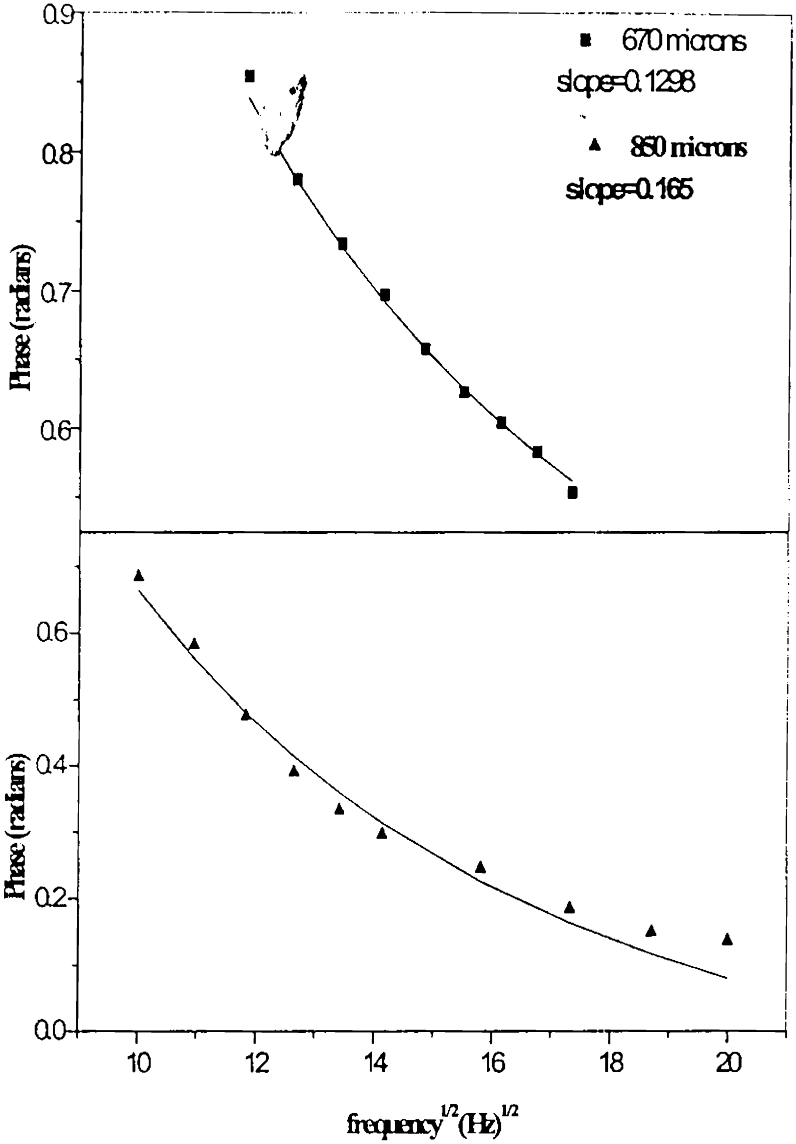

Figure (14): Plot of phase vs. square root of frequency for $CuFeO_2$

It is observed from figure (11) to (14) that the phase varies linearly with square root of frequency. Hence, the thermal diffusivity can be directly obtained However, figure (13) is not linear. This can be attributed to the thermoelastic bending, which the thermal diffusivity can be determined using equation (12). The thermal diffusivity values of the copper delafossite samples ($CuGa_{1-x}Fe_xO_2$, x = 0 to 1) is given in Table I

SAMPLE	THICKNESS (μm)	THERMAL DIFFUSIVITY (cm^2s^{-1})
$CuGaO_2$	**650**	**1.041 ± 0.004**
	500	**1.011 ± 0.005**
$CuGa_{0.9}Fe_{0.1}O_2$	**620**	**0.794±0.003**
	470	**0.790± 0.002**
$CuGa_{0.8}Fe_{0.2}O_2$	**610**	**0.744 ± 0.006**
	690	**0.745 ± 0.005**
$CuFeO_2$	**850**	**0.833± 0.004**
	670	**0.837 ±0.002**

TABLE I gives the thermal diffusivity values of $CuGa_{1-x}Fe_xO_2$ with x varying from 0 to 1 for different thickness

Figure (15) shows the variation of thermal diffusivity of the $CuGa_{1-x}Fe_xO_2$ samples with varying composition. It is observed that the mixtures have thermal diffusivity lower than that of the pure samples. This is due to the fact that on the substitution of solute atoms, phonons are scattered as a result of difference in atomic masses, atomic binding forces and lattice distortion introduced by the presence of solute atoms[33]. The scattering of phonon reduces the thermal conductivity (thermal diffusivity). In the present case, in mixture samples, Fe^{3+} replaces some of the Ga^{3+} ions. Even though the charge remains the same, Fe has a larger ionic radius than Ga and hence the substitution will result in a lattice distortion. This can be the reason for the reduced thermal diffusivity in the case of mixtures than that of pure samples.

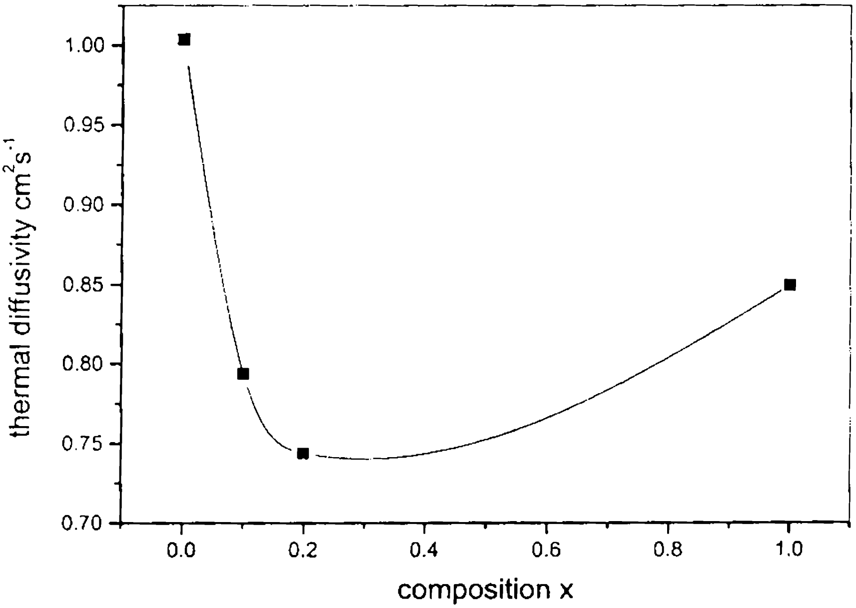

Figure (15) shows the variation in thermal diffusivity of $CuGa_{1-x}Fe_xO_2$ with composition 'x'

In semiconductors, the heat is generated in the sample following optical absorption via three different process [34,35]: 1) an instantaneous intraband non-radiative thermalisation with energy greater than E_g. This process is due to the electron-phonon collisions within the conduction band and occurs in a time scale of picoseconds. The heat power density due to this process is denoted by

$$Q_D = \frac{\beta\left(h\nu - E_g\right)}{h\nu} I_0 e^{\beta(x+l_s)} e^{j\omega t} \qquad (12)$$

where β is the optical absorption coefficient for photons of energy $h\nu$ incident at the surface with an intensity of I_0 (W/cm^2). 2) Nonradiative bulk recombination due to the recombination of the excess electron-hole pairs after diffusing through a distance $(D\tau)^{1/2}$, where D is the carrier diffusion coefficient, and τ is the band-to-band recombination time. The power density for this process denoted by Q_{NRR} is given by

$$Q_{NRR} = \frac{E_g}{\tau} n(x,t) \qquad (13)$$

where n (x,t) is the density of the photo excited carriers. 3) Non-radiative surface recombination: The heat power density Q_{SR} is given by

$$Q_{SR} = E_g\left[\upsilon\delta\left(x\right) + \upsilon_0\delta\left(x + l_s\right)\right]n(x,t) \qquad (14)$$

Hence, the periodic temperature distribution in the PA cell should be the sum of contributions due to the three components above mentioned. However, the periodic variation of the sample temperature and consequently the PA signal has a complex dependence on the modulation frequency. In the case of a thermally thin sample or when the sample thickness (l) is less than the thermal diffusion length (μ) then the amplitudes of thermalisation and bulk recombination components are dominant and in this frequency range all the three components decrease with slope ω^{-1}. As the thickness of the sample is greater than the thermal diffusion length (thermally thick sample); then the slopes of the thermalisation and bulk recombination components change to $\omega^{-1}\exp\left[-l(\omega/2D)^{1/2}\right]$ where D is the thermal diffusivity. Nevertheless, the bulk recombination component again changes slope with increasing frequency because the carrier diffusion length ($L_\omega > \mu$). Therefore, the bulk and surface recombination components become dominant. This implies that the electronic components determine the behavior of the rear surface temperature vs. the modulation frequency at higher frequencies [36]. Taking into account the three heat sources, the pressure fluctuation for thermally thick sample is obtained as [34,35]

$$\delta P = \frac{2\varepsilon I_0 P_0}{T_0 l_g \sigma_s k_s \sigma_g}\left[\left[\frac{\varepsilon - 1}{\varepsilon}\right]\exp\left(-l_s \sigma_s\right) + \frac{F\sigma_s}{D\gamma\tau}\left[\frac{1}{\sigma_s^2 - \gamma^2} + \frac{v\tau}{\sigma_s}\right]\right] \qquad (15)$$

where $\sigma_s = (1+j)a_s$, $a_s = \left(\pi f/\alpha_s\right)^{1/2}$ is the thermal diffusion coefficient of the sample,

$\gamma = \left(1/D\tau\right)^{1/2}(1+j\omega\tau)^{1/2}$ $\quad \varepsilon = E_g/h\nu$, $\quad r = v/D\gamma$, $\quad r_0 = v_0/D\gamma$ and

$$F = \frac{1}{(1+r_0)(1+r)\exp(\gamma l) - (1-r)(1-r_0)\exp(-\gamma l)}$$

I_0 is the intensity of the incident optical beam, D is the carrier diffusion coefficient, τ is the band to band recombination time, v_0 is the carrier surface recombination velocity at the (back) heating surface and v is the surface recombination velocity at the sample-gas interface. The first term of equation (15) varies with modulation frequency as $\frac{1}{f}\exp\left(-a\sqrt{f}\right)$ where $a = l_s(\pi/\alpha_s)$ and corresponds to the thermalisation component while the second term which is in the high frequency regime such that $\sigma_s^2 > \gamma^2$ scales as $f^{1.5}$ corresponding to the non Radiative bulk recombination and finally the lat term of the equation varying as f^1 corresponds to the non radiative surface recombination.

In figures (11) to (14) we have chosen the low frequency range corresponding to the first term of equation (15) in order to obtain the thermal diffusivity due to the thermalisation process only. The transport properties of the copper delafossites ($CuGa_{1-x}Fe_xO_2$, x= 0 to 1), namely the carrier diffusion coefficient and surface recombination velocity are determined by studying the variation of the amplitude and phase of the PA signal at high modulation frequencies.

In the case of $CuGaO_2$, it is observed that in the frequency range 450Hz to 1400Hz, the amplitude varies with frequency as $f^{1.499}$. Similarly for $CuGa_{0.9}Fe_{0.1}O_2$, the variation of amplitude with frequency in the range 450-750 is $f^{1.44}$ and $f^{1.43}$ in the range 800-1400 Hz. The sample, $CuGa_{0.8}Fe_{0.2}O_2$, shows a variation $f^{1.4}$ in the range 600-130Hz. Finally for $CuFeO_2$, the frequency variation is $f^{1.28}$ in the frequency range 500- 800 Hz and $f^{1.3}$in the frequency range 850- 1400 Hz. These facts are depicted in figures (16) to (19).

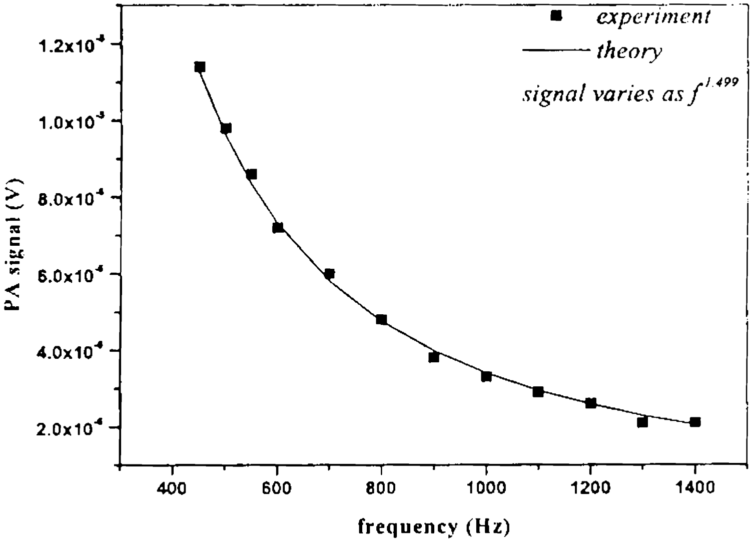

Figure (16): Plot of PA signal amplitude vs. frequency for $CuGaO_2$

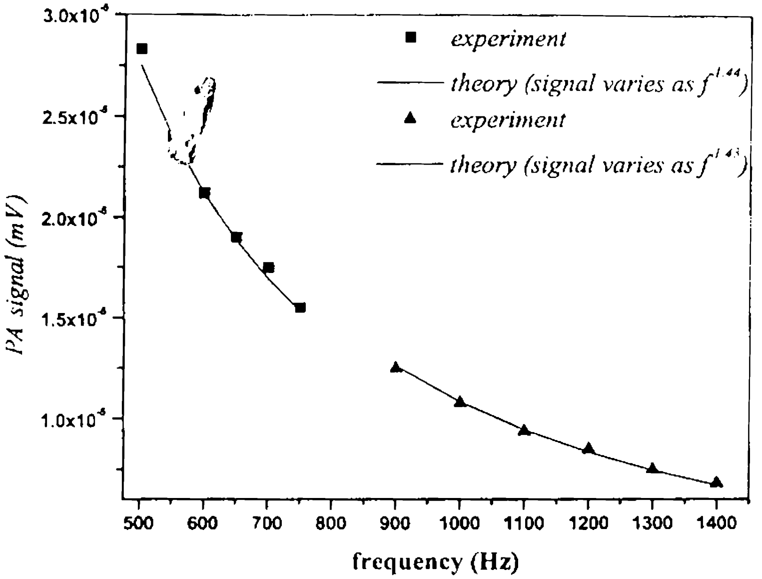

Figure (17): Plot of PA signal amplitude vs. frequency for $CuGa_{0.9}Fe_{0.1}O_2$

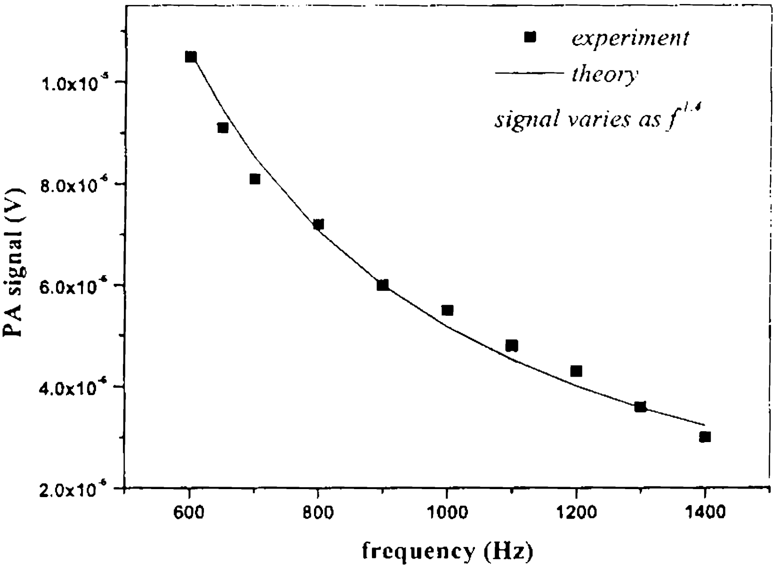

Figure (18): Plot of PA signal amplitude vs. frequency for $CuGa_{0.8}Fe_{0.2}O_2$

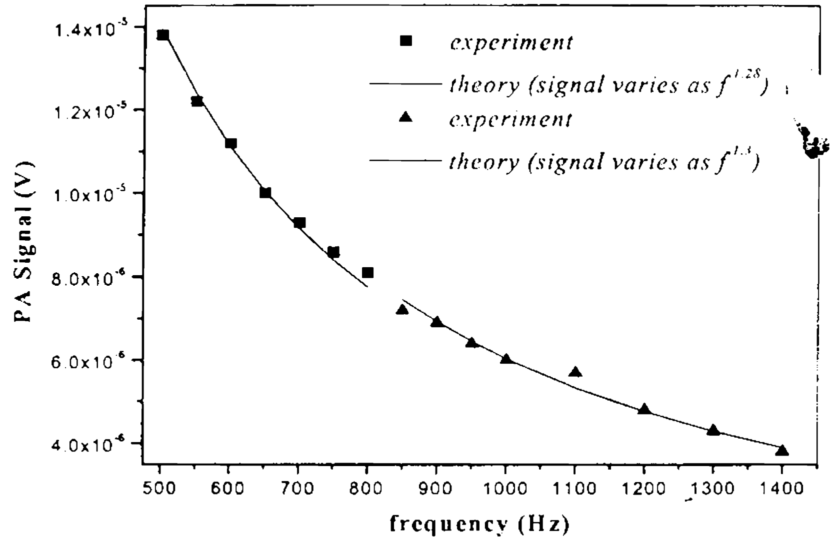

Figure (19): Plot of PA signal amplitude vs. frequency for $CuFeO_2$

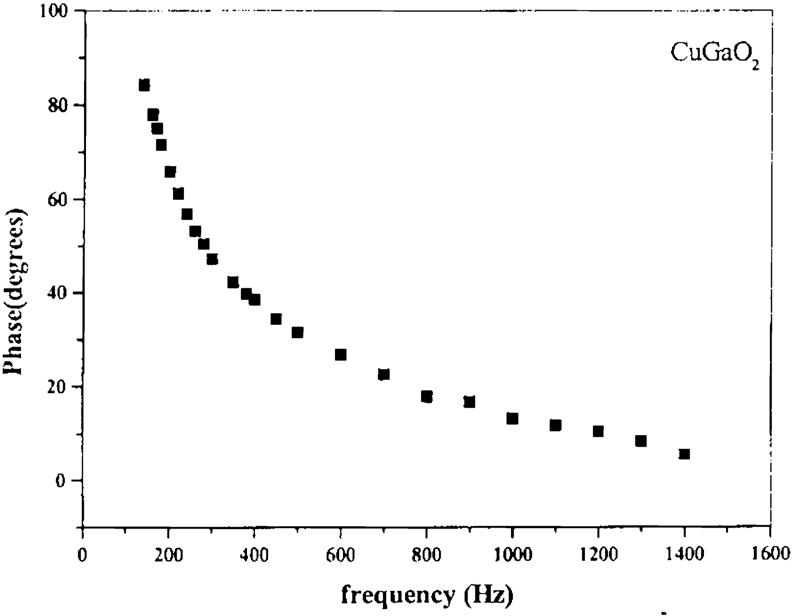

Figure (20): Plot of phase vs. frequency for $CuGaO_2$

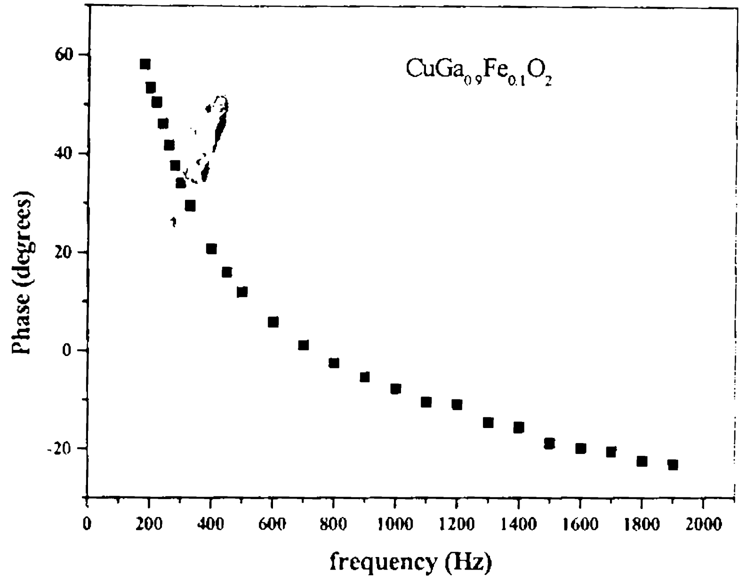

Figure (21): Plot of phase vs. frequency for $CuGa_{0.9}Fe_{0.1}O_2$

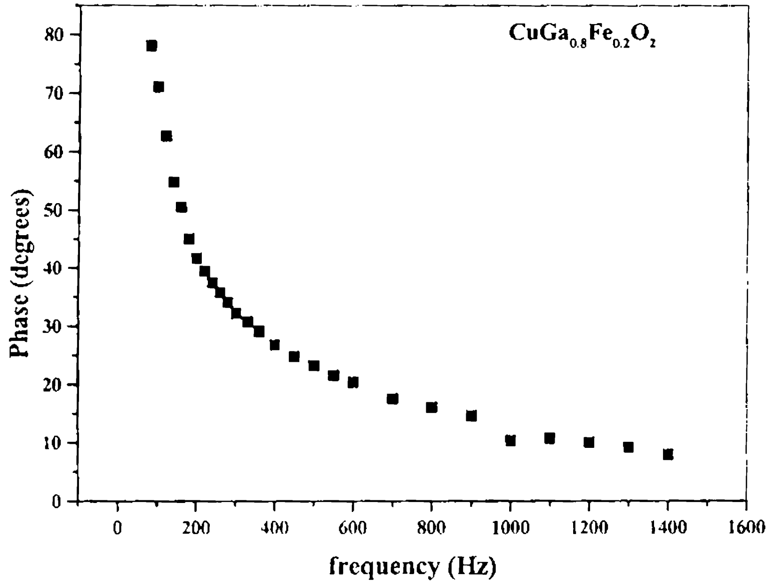

Figure (22): Plot of phase vs. frequency for $CuGa_{0.8}Fe_{0.2}O_2$

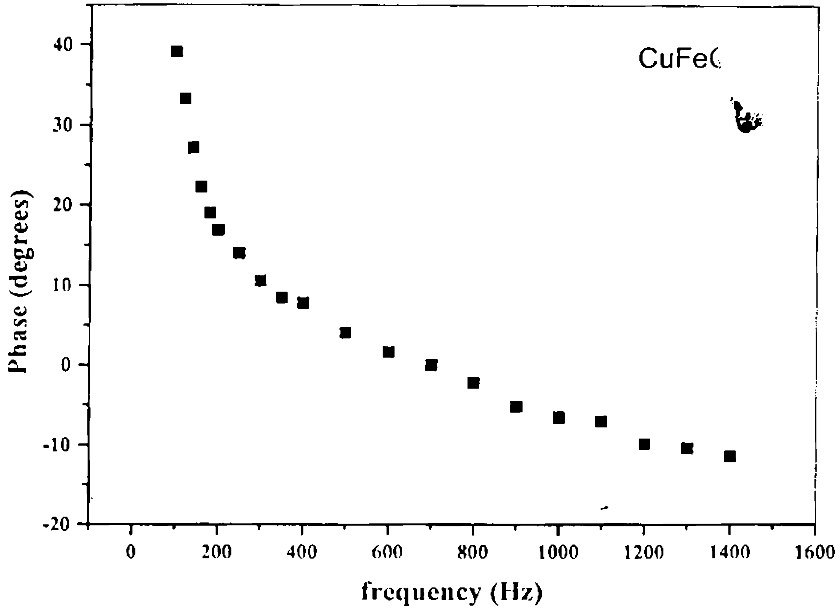

Figure (23): Plot of phase vs. frequency for $CuFeO_2$

The variation of phase with modulation frequency fro the same set of samples is shown in figures (20) to (21). From figures (16) to (19), it is observed in the high frequency regime, there is no region where the frequency varies as $f^{1.0}$ that comes from the non-radiative surface recombination, and the frequency dependence of the PA signal amplitude for the non-radiative recombination region is the same throughout. This dependence is similar to that observed for silicon [34,35]. Moreover, it is also expected that the phase should initially decrease reach a minimum and then increase as the signal amplitude changes from $f^{1.5}$ to $f^{1.0}$. This minimum is exhibited for only those samples where $\omega\tau<<1$ [35]. This is also not observed for the samples under study (figures (19) to (22)). Hence, in all the samples, it is concluded that PA signal is dominated by the non-radiative bulk recombination. Considering only the non-radiative bulk recombination and assuming that ω [illegible] the band-to band non-radiative bulk recombination signal amplitude is expressed as

$$|\delta P| = \frac{\varepsilon P_0 I_0 D \alpha_g{}^{1/2} \alpha_s}{(2\pi)^{3/2} T_0 l_g k_s \tau} \frac{1}{f^{1.5}\left[a^2 + (bf)^2\right]^{1/2}} \qquad (16)$$

where

$a = D(v + v_0) + l v v_0$ and $b = 2\pi l D$.

From the best theoretical fit obtained using equation (16), carrier diffusion coefficient and surface recombination velocity are determined. Figures (24)-(27) show the variation of signal amplitude with modulation frequency for the $CuGa_{1-x}Fe_xO_2$ samples with the square points showing the experimental values obtained and the line showing the theoretical fit of equation (16). Since the pellets under study are not polished, both the surfaces are rough so that $v=v_0$. The carrier diffusion coefficient and the surface recombination velocity obtained are given in Table II.

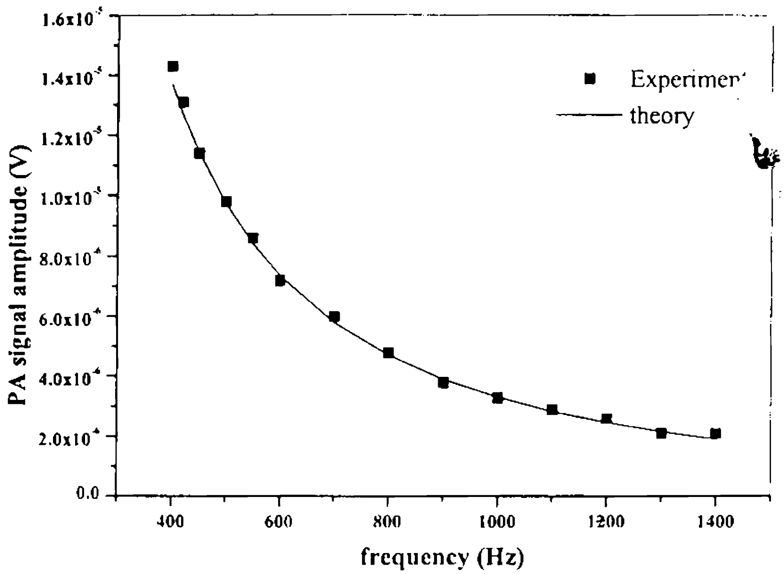

Figure (24): Plot of PA signal amplitude vs. frequency for $CuGaO_2$

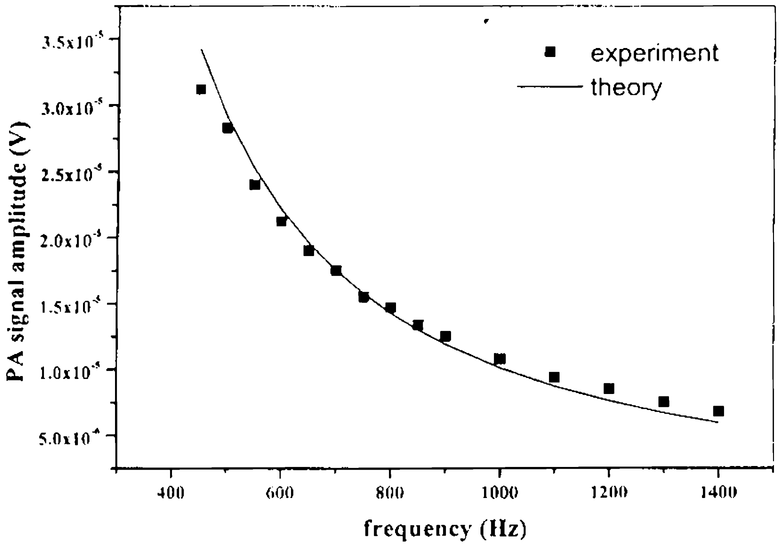

Figure (25): Plot of PA signal amplitude vs. frequency for $CuGa_{0.9}Fe_{0.1}O_2$

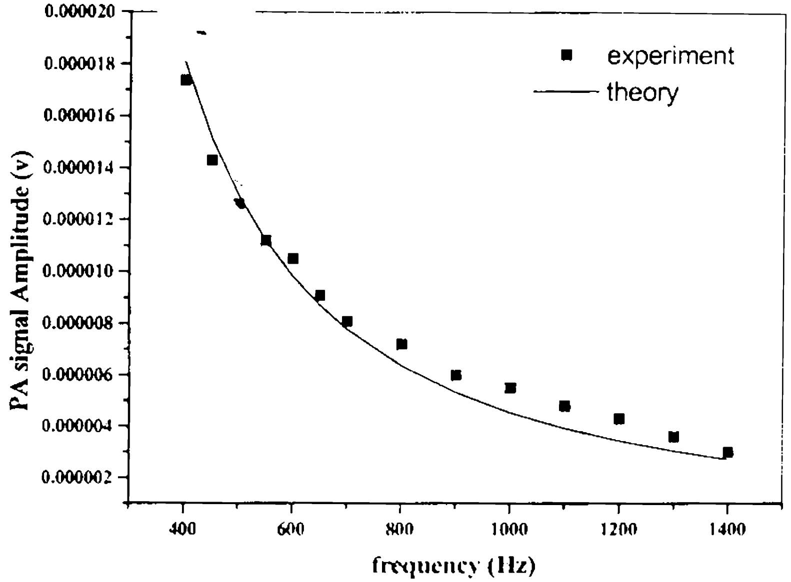

Figure (26): Plot of PA signal amplitude vs. frequency for $CuGa_{0.8}Fe_{0.2}O_2$

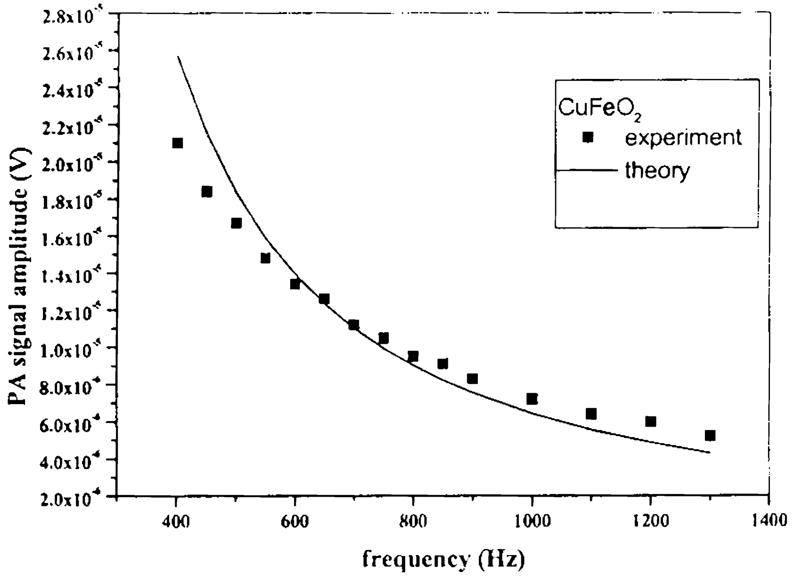

Figure (27): Plot of PA signal amplitude vs. frequency for $CuFeO_2$

SAMPLE	CARRIER DIFFUSION COEFFICIENT (cm^2s^{-1})	SURFACE RECOMBINATION VELOCITY (cms^{-1})
$CuGaO_2$	16.5	233.5
$CuGa_{0.9}Fe_{0.1}O_2$	19.9	416
$CuGa_{0.8}Fe_{0.2}O_2$	11.5	541
$CuFeO_2$	27	703.8

TABLE II shows the carrier diffusion coefficient and surface recombination velocity values obtained for $CuGa_{1-x}Fe_xO_2$ *with x varying from 0 to 1*

In conclusion, the thermal diffusivity and transport properties (carrier diffusion and surface recombination velocities) of four copper delafossite samples, $CuGa_{1-x}Fe_xO_2$ with x varying from 0 to 1 are successfully determined using the open cell photoacoustic technique. The detailed analysis of the dependence of amplitude and phase of PA signal on the modulation frequency suggests that in the high frequency region, non-radiative bulk recombination mechanism dominate the non-radiative surface recombination in the heat transport process.

REFERENCES.

1. N.Duan, A.W.Sleight, M.K.Jayaraj, J.Tate, *Appl.Phys.lett.*77 **(9)** (2000) 1325.
2. K.Ueda, T.hase, Yanagi, H.Kawazoe, H.Hosono, H.Ohta, M.Oritha, M.Hirano, *J.appl.Phys.* **89**[illegible] (2001) 1790.
3. H.Kawazoe, [illegible] yasukawa, H.Hyodo, M.Kuritha, H.Yanagi, H.Hosono, *Nature* **389**, (1997) 9[illegible].
4. Antonio Buljan, Pere Alemany, Eliseo Ruiz, *J.Phys.Chem B* **103** (1999) 8060
5. D.B.Rogers, R.D.Shanon, C.T.Prewitt, J.L.Gilson, *Inorg.Chem.* **10** (1971) 723.
6. J.R. Monnier, M.J.Hanrahan, G.Apai, *J.catal.* **92**, (1985) 119
7. F.A.Benko, F.P.Koffyberg, *Phys.stat.sol.(a)* **94**, (1986) 231
8. Xiliang Nie, Su-Huai Wei, S.B. Zhang *Phy.Rew.letts.*88 **(6)** (2002) 66405-1
9. H.Yanagi, H.Kawazoe, A.Kudo, M.Yasukawa, H.Hosono, *J.electroceramics,* **4:2/3**, (2000). 407.
10. M.V.Lalic, J.Mestnik-Filho, A.W.Carbonari, R.N.Saxena, M.Moralles *J.Phys: condens.matter* **14** (2002) 5517
11. R.Nagarajan, N.Duan, M.K.Jayaraj, J.Li, K.A.Vanaja,A. Yokochi, A.Draeseke, J.Tate, L.W.Sleight, *Int.J.inorg.materials* 3 (2001) 265.
12. A.Rosencwaig, J.B.Willis, *J.Appl.Phys.*51**(8)** (1980) 4361.
13. J.C.Murphy, L.C.Aamodt, *J.Appl.Phys.* **48(8)** (1977) 3502.
14. F.Scudieri, M.Marinelli, U.Zammit, S.Martellucci, *J..Phys.D Appl. Phys.* **20** (1987) 1045.
15. Nibu A.George, C.P.G Vallabhan, V.P.N. Nampoori, A.K. George P.Radhakrishnan *J.Phys.D. Appl.Phys* **33** (2000) 3228.
16. J.Bernal-Alvarado, M.Vargas, J.J.Alvarado-Gil,I.Delgadillo,A.Cruz-Orea,H.Vargas, A.Tufino-Velazquez, M.L.Albor-Aguilera, M.A.Gonzalez-Trujillo, *J.Appl.Phys.* **83(7)** (1998) 3807.

17. O.Delgado-Vasallo. E.Marin, *J.Phys.D:Appl.Phys.* **32** (1999) .
18. A.Rosencwaig. *Photoacoustics and Photoacoustic Spectroscopy*, John Wiley &Sons, New York (1980)
19. A. Rosenwaig, A.Gersho,*J.Appl.Phys* **47**, (1975) 64
20. P.Helander, *J.Photoacoust.*1 (1982) .103
21. P.Helander, I.Lundstrom. *J.Appl.Phys.* **54** (1983) 5069.
22. M.D.Dramicanin,Z.D.Ristovski,P.M.Nikolic,D.G.Vasiljevic,D.M.Todorovic, Phy.Rev.B.**51(20)** (1995) 14226
23. E.Marin, H.Vargas, P.Diaz, I.Riech, *Phys.stat.sol (a)* **179** (2000) 387.
24. P.Helander, *J.Photoacoust.*1. (1982) 251
25. J.Helander*J.Appl.Phys.* **59** (1986) 3339.
26. D.H.McQueen, *J.Phys.E.* **16** (1983) 738.
27. A. Rosenwaig, A.Gersho,*J.Appl.Phys* **47**, 64 (1975)
28. G.Rousset, F.Lepoutre, L.Bertrand, *J.Appl.Phys.* **54,** (1983), 2383.
29. L.F.Perondi, L.C.M.Miranda, *J.Appl.Phys.* **62** **(7)** (1987) 2955.
30. E.Marin, H.Vargas, P.Diaz, I.Riech, *Phys.stat.sol. (a)* **179**, (2000) 387
31. M.Bertolotti, V.Dorogan, G.Liakhou, R.LiVoti, S. Paoloni, C.Sibilia, *Rev.Sci.Instrum* 68(3), (1997) 1521
32. Quin Shen, Taro Toyoda, *Jpn.J.Appl.Phys* **39**, (2000) 511.
33. N. P. Padture, P.G.Klemens, J.Am.Ceram.Soc.8 (14) (1997) 1018.
34. A.Pinto Neto, H.Vargas, N.F.Leite, L.C.M.Miranda, *Phy.Rev B.* **40(6),** (1989) 3924.
35. A.Pinto Neto, H.Vargas, N.F.Leite, L.C.M.Miranda, *Phy.Rev B.* **41(14),** (1990) 9971.
36. D.M.Todorovic, P.M.Nikolic, A.I.Bojicic, *J.Appl.Phys.* **85(11)** (1999), 7716.

CHAPTER VI

SUMMARY AND CONCLUSIONS

Photothermal deflection technique and photoacoustic technique are two of the widely used non-destructive techniques for characterization of materials. The above-mentioned techniques utilize the refractive index gradient and pressure change respectively generated as a result of the absorption of intensity modulated electromagnetic radiation. In the present thesis the author has carried out photothermal deflection studies on certain plasma polymerized thin films and photoacoustic measurements on a few semiconducting samples. In addition, a new model for the analysis of photothermal deflection signal for determining low thermal diffusivity compared to that of the adjacent coupling medium, is proposed and is successfully applied.

Photothermal effects or the *light induced heating effects* are due to the excitation and subsequent de-excitation of the sample non-radiatively thereby transforming the absorbed radiant energy into thermal energy of the medium. Consequently, the optical as well as the thermal properties of the sample play a vital role in the photothermal signal generation. Photothermal deflection and photoacoustic techniques are based on the thermal wave propagation through the sample; these can be effectively used in the determination of thermal and transport properties of materials. Depending upon the nature of the sample under study (for eg. optically opaque or optically transparent, thermally thick or thermally thin) and the purpose of measurement, any of these methods are chosen and are suitably analyzed.

Though there are several methods available for analysis [illegible] photothermal deflection signal for thermal diffusivity, the situation becomes difficult when the thermal diffusivity of the sample is very low. This is mainly due to the fact that the thermal properties of coupling medium surrounding the sample will be dominant and hence will contribute to the photothermal signal. This can be reduced either by 1) the use of suitable configuration i.e. bouncing configuration in which the probe beam is directed on to the sample surface so that the height of the probe beam above the sample surface is zero. 2) the use of a coupling fluid with low thermal diffusivity compared to that of the sample. 3) eliminating the vertical offset dependence (z) of the characteristic length. The author has suggested a new model, which is an extension of the ***Amplitude Method*** for eliminating the offset dependence thereby allowing the determination of sample possessing very low thermal diffusivity compared to that of the sample. In the analysis, it was found that when the sample thermal diffusivity was higher than that of the coupling fluid ***Amplitude Method*** was sufficient for the analysis of the signal in determining the diffusivity. Moreover, the different modulation frequencies used also gave the same result as used in the computer simulation. On the contrary, when the sample thermal diffusivity was taken to be lower than that of the coupling medium, it was found that ***Amplitude Method*** did not yield the value used for computer simulation. The graphs obtained were similar to the ones obtained for high thermal diffusivity and were linear with the slopes increasing with frequency. However, for each modulation frequency the thermal diffusivity value obtained is different and did not agree with the value used for computer simulation. In the new method suggested the author eliminated the probe beam dependence by a graph between the characteristic length and inverse of the square root of frequency. The thermal diffusivity calculated from the slope of this graph gave the same value used in computer simulation.

Plasma [illegible]ized samples are well known for its adhesiveness as well as ability to form ultra thin films. They are being used in a wide range of applications starting from corrosion [illegible]evention to sensor technology and microelectronics. Though, the electrical and optical properties of these films are being studied from time to time, the thermal properties remained under the covers. The author prepared three plasma-polymerized films and determined direct band gap, Urbach energy and refractive index. The linkage in the polymerization process is also suggested form the FTIR spectra of the polymer and monomer. The thermal properties are determined by the probe beam deflection technique. A compact and cost effective probe beam deflection experimental setup is designed and fabricated. Measurements are taken in two different coupling media namely carbon tetra chloride and liquid paraffin for different modulation frequencies. The deflection signal is analyzed using two different methods of analysis: Phase Method and Amplitude Method. Both yielded similar results for the thermal diffusivity value of each sample. Similarly, thermal diffusivity values obtained using measurements with two different coupling fluids and for two different modulation frequencies also show very good agreement. These observations imply that the measured photothermal signals have no contribution from the thermal properties of the coupling fluid. The thermal diffusivity values of the coupling fluids, $D_{CCl4} \sim 0.731 \times 10^{-3}$ cm^2s^{-1} and $D_{liquid\ paraffin} \sim 0.3 \times 10^{-3}$ cm^2s^{-1} are small compared to that of the sample, the thermal properties of the sample dominate that of the coupling media.. Another factor to be taken into account is the surface deformation due to the thermal expansion of polymers. However, the temperature rise is estimated to be ~1 degree which will result in a surface deformation of few Angstroms. This will affect mirage measurements only if bouncing configuration is used. In present case, skimming configuration is used. i.e the probe beam just grazes the sample surface and travels at a finite height above the sample surface.

Photoacoustic technique is employed for the characterization of certain copper delafossites. An open photoacoustic cell in the heat transmission configuration is used for the determination of the thermal diffusivity and transport properties like the carrier diffusion coefficient and surface recombination velocity of $CuGa_{1-x}Fe_xO_2$ with x varying from 0 to 1. The variation of the signal amplitude with modulation frequency for different thickness are studied and observed a minimum in the signal amplitude at a frequency at which the sample changes from thermally thin to thermally thick. The thermal diffusivity of the samples are determined for various thickness and it is found that the thermal diffusivity of the mixture compounds are less than the pure ones. This is explained as the enhancement in phonon scattering due to the lattice distortion, difference in atomic mass, binding energy etc on the substitution of solute atoms into a lattice. The analysis for determining the transport properties like carrier diffusion coefficient and surface recombination velocity suggests that the non-radiative bulk recombination is the dominant mechanism compared to the non-radiative surface recombination.

To conclude, the author has successfully employed two of the powerful non-destructive characterization techniques for the thermal characterization of some polymer and semiconducting materials, leading to the first measurement of important thermal and transport parameters. In the case of PBD, a new method is proposed and applied for the analysis of the deflection signal for samples of low thermal diffusivity compared to that of the adjacent coupling medium. This method can be applied to both optically transparent and optically opaque materials and no knowledge of the thickness of the sample is required for the successful evaluation of thermal diffusivity.

Further refinements in the methodology of these two important photothermal methods can of course be made, the exploitation of which could contribute tremendously to various fields of science and technology.